ФЕДЕРАЛЬНОЕ ГОСУДАРСТВЕННОЕ
БЮДЖЕТНОЕ УЧРЕЖДЕНИЕ НАУКИ

ИНСТИТУТ ПРОБЛЕМ МЕХАНИКИ им. А. Ю. ИШЛИНСКОГО
РОССИЙСКОЙ АКАДЕМИИ НАУК

С. Д. Алгазин

ЧИСЛЕННЫЕ АЛГОРИТМЫ КЛАССИЧЕСКОЙ МАТФИЗИКИ.

XXXIX. Numerical algorithms of classical mathematical physics.

Препринт № 1034

Москва 2013 г.

Аннотация.

В этой обзорной статье рассматривается новый подход к конструированию алгоритмов математической физики. Кроме спектральных задач для обыкновенных дифференциальных уравнений, уравнения Лапласа (три краевых задачи) и бигармонического уравнения (две краевые задачи), рассматривается флаттер пластин и пологих оболочек.

Для двумерных задач громоздкие вычисления затабулированы в таблицах небольшого объёма, что позволяет разработать компактные алгоритмы решения поставленных задач.

Статья представляет интерес для студентов и аспирантов физико-технических и математических специальностей, специалистов по численным методам, а также для научных сотрудников и инженеров, интересующихся новыми методами численного решения задач математической физики.

Ключевые слова: Численный алгоритм без насыщения, оценка погрешности в задачах на собственные значения, обыкновенные дифференциальные уравнения, уравнение Лапласа, Бигармоническое уравнение, пластина переменной толщины, флаттер пластин и пологих оболочек.

ISBN 978-5-91741-068-5
055(02)2

To my parents,
Dmitriy Alexandrovich Algazin
and Nadezhda Nikolaevna Algazina

Foreword

In 1973 I graduated from the Faculty of Mechanics and Mathematics of M.V.Lomonosov Moscow State University and started to work at the 12th Division of the Institute of Applied Mathematics of the USSR Academy of Sciences; later, I moved to the 4th Division headed by Konstantin Ivanovich Babenko. Konstantin Ivanovich suggested that I work on novel algorithms (non-saturating numerical algorithms) for the classical problems of mathematical physics. First, we considered one-dimensional problems (Sturm-Liouville problem, Bessel equation and others), after which we focused on the eigenvalue problem for the Laplace equation. When analyzing the matrices of the discrete problem, I noticed that the matrix in question has the following block structure:

$$H = \left\| \begin{matrix} h_{11}\ h_{12} \ldots h_{1m} \\ h_{21}\ h_{22} \ldots h_{2m} \\ \ldots\ldots\ldots\ldots\ldots \\ h_{m1}\ h_{m2} \ldots h_{mm} \end{matrix} \right\|$$

where $h_{\mu\nu}$, $\mu,\nu = 1,2,\ldots,m$ are symmetric circulants of dimension $N\times N$, where $N = 2n + 1$, i. e. the first row of these matrices have the form $b_0,b_1,\ldots,b_n,b_n,\ldots,b_1$, while all other rows are obtained from the first one by cyclic permutation. For brevity, we refer to the matrices of this form as вида h-matrices. Here, m is the number of circular grid lines, while $N = 2n + 1$ is the number of nodes on each circular line. It took me an evening to prove a theorem on the properties of this matrix. Later, it became clear that matrices of this form and some their generalizations are encountered in many problems of mathematical physics. They can be in such a way that discretization of two-dimensional problem is reduced to discretization of one-dimensional problem, and three-dimensional discretization is reduced to two-dimensional. The practical application of this approach is the essense of the current book.

Each chapter contains references to additional literature, citations in the text are given in brackets.

The work was supported by the Russian Foundation for Basic Research under the grants No. 95–01–00407, 97–01–00923, 05–01–00250, 06–08–08169-ofi, 08–01–00207-a, 09–08–00011-a.

Introduction

In this book, the classical boundary-value and spectral problems for the Laplace operator are considered in one, two, and three-dimensional formulation. Also considered are the

spectral problems for the biharmonic operator, plate and shell flutter, transient Navier-Stokes problems etc.
The two-dimensional spectral and boundary-value problems for the Laplace operator are considered only on smooth domains. Solutions to these problems (eigenfunctions) are infinitely differentiable, or even analytical, and this outstanding a-priori information on the solution properties has to be taken into account to develop efficient numerical algorithms. The traditional finite-difference and finite-element methods almost never take into account the solution smoothness, i.e., these methods suffer from saturation. The term "saturation" was introduced by K.I.Babenko [1]. To elucidate its meaning in our case, consider the abstract scheme of the algorithms described in this book.
Let T be a closed linear operator in the Banach space $\boldsymbol{B}$ defined on a domain $D(T)$, and P_n be a projector onto a finite-dimensional subspace $L^n \subset D(T)$. We call the operator P_nTP_n the discretization of operator T. Suppose we consider an eigenvalue problem for the operator T:

$$Tu = \lambda u, \ \|u\| = 1. \qquad \text{(B1)}$$

If H is the matrix of the finite-dimensional operator P_nTP_n in some basis $l_1, l_2, ..., l_n \subset L^n$, the exact eigenvalue Λ of the operator T satisfies the equation

$$Hu = \lambda u + r. \qquad \text{(B2)}$$

Here, H is a $n \times n$ matrix, $u = (u_1, u_2, ..., u_n)'$ is a vector of eigenfunction values at the grid nodes; $r = (r_1, r_2, ..., r_n)'$ is the discretization error. Note that (B2) is a strict relation, i.e., Λ is the eigenvalue of problem (B1), while u_i, $i = 1,2,...,n$ are the exact values of the corresponding eigenfunction of problem (B1) at the grid nodes. Discarding in (B2) the discretization error, we obtain an approximate finite-dimensional eigenvalue problem

$$H\tilde{u} = \tilde{\lambda}\tilde{u}.$$

It will be shown in Chapter 1 that, generally speaking, $|\lambda - \tilde{\lambda}|$ is of the order of the discretization error $\|r\|$. Thus, the accuracy with which the approximate eigenvalues of operator T are obtained depends on the rate at which $\|r\| \to 0$ as $n \to \infty$. Note that $r = r(u, \lambda)$, i. e. it has some value for each eigenfunction and corresponding eigenvalue. In the algorithms considered in this book, the rate at which $\|r(u, \lambda)\|$ tends to zero depends on the smoothness of the eigenfunction, and, the more smooth is the function u, the faster $\|r\| \to 0$ as $n \to \infty$. This exactly means that the algorithms described are non-saturating. The finite-difference methods also give rise to relations of the form (B2). However, in this case $\|r\| = O(h^p)$, where h is the grid cell size, and p is the numerical scheme order. Therefore, the rate at which $\|r\|$ tends to zero does not increase if the smoothness of the eigenfunction is increased. Similar reasoning is valid for the finite-element methods.
The principal aim of this book is the development and study of non-saturating algorithms for the above-mentioned classical problems.
The foundations of theory of non-saturating numerical methods were developed in the first edition of book by K.I.Babenko [1]. Note that the advances in the computational mathematics in this direction gained little publicity in Russia and abroad, and are still unknown to foreign researchers.

This is confirmed by the fact that, in our days, we see a "rediscovery" (seemingly, independent) of the same computational methods in the West, under the name of "spectral" methods (S. Orszag, D. Gotlieb [2], E. Tadmor*, USA), as well as modern ($h - p$) specializations of the finite-element method (O. Widlund [3], USA and S. Schwab[4, 5], Switzerland), in which with the grid refinement (i. e. as h → 0) is accompanied by the increase in the order p of the polynomials used for the function approximation within one finite element. It is very sad that works by K.I.Babenko and his colleagues became almost forgotten by now.

Solution of the eigenvalue (or boundary-value) problems consists in two stages: firstly, we have to reduce the inifinite-dimensional problem to a finite-dimensional one, and secondly, a solution method to the algebraic eigenvalue problem (system of linear equations) has to be chosen. For two and three-dimensional problems, this is a complicated task. However, deeper study of the structure of finite-dimensional problem enables us to overcome these difficulties. For example, in case of two-dimensional problems on disc domains it turned out that the matrices of the corresponding finite-dimensional problems have the following block structure

$$H = \begin{Vmatrix} h_{11} & h_{12} & \dots & h_{1m} \\ h_{21} & h_{22} & \dots & h_{2m} \\ \dots & \dots & \dots & \dots \\ h_{m1} & h_{m2} & \dots & h_{mm} \end{Vmatrix}, \qquad \text{(B3)}$$

where $h_{\mu\nu}$, $\mu, \nu = 1,2,\dots,m$ are symmetric circulants of dimension $N{\times}N$, where $N = 2n + 1$, i. e. the first row of these matrices have the form $b_0,b_1,\dots,b_n,b_n,\dots,b_1$, while all other rows are obtained from the first one by cyclic permutation. For brevity, we refer to the matrices of this form as вида h-matrices. Therefore, in the array H there are only $m^2(n + 1)$ different elements. Here, m and N are parameters of the grid introduced on the disc domain for the discretization of the corresponding spectral problems (m is the number of circular grid lines, N is the number of nodes on each circular line), i. e. the total number of grid nodes is $M = mN$. The properties of the matrices of the form (B3) are studied in Chapter 3. It turns out that they inherit the properties of the corresponding infinite-dimensional problems. Despite large sizes of these matrices (up to 1230), all their eigenvalues can be computed even on a rather modest PC.

For an arbitrary domain, the problem is reduced to a problem on a disc domain by appropriate conformal mapping, therefore, the matrix of discrete problem still has a simple structure. As a result, the method of simple iteration in combination with the elimination method [6] can be applied. As an example, the first five eigenfrequencies of a simply supported plate bounded by an epitrochoid having the curvature of about 10^3 at 12 points are calculated with 7–8 decimal places.

The study of the structure of finite-dimensional problem enabled us to develop an efficient algorithm for the solution of Poisson's equation. Note that a fast method for the solution of Poisson's equation is necessary for the calculation of the beam of charged particles (plasma) is self-consistent electric field, because the electric field potential must be reevaluated at each time step by solving appropriate Poisson's equation.

---

* **Eitan Tadmor Distinguished University Professor** – Department of Mathematics Institute for Physical Science & Technology Director, Center for Scientific Computation and Mathematical Modeling (CSCAMM). Email: tadmor@cscamm.umd.edu.

References

1. Babenko K. I. Foundations of numerical analysis. Moscow, Nauka, 1986, 744 p.; 2nd-Ed. (revised): A. D. Bruno (Ed.), Moscow, Izhevsk, RChD, 2002, 847 p.
2. Orszag S. A., Gotlib D. Numerical Analysis of Spectral Methods. Theory and Applications. Society for industrial and applied mathematics, 1977, 169 pp. Philadelphia, pennsylvania 19103.
3. Andrea Toselli, Olof Widlund. Domain Decomposition Methods – Algorithms and Theory. Springer Series in Computational Mathematics. Springer-Verlag Berlin Heidelberg, 2005, 450 pp.
4. Cristoph Schwab. p – and Hp – Finite Element Methods theory and application to solid and fluid mechanics. Oxford University, 1998.
5. C. Schwab, M. Suri, M. Suri, C. Xenophontos, C. Xenophontos,... The hp finite element method for problems in mechanics with boundary layers (1996).
6. D. K. Fadeev, V. N. Fadeeva. Numerical methods of linear algebra. Sankt-Petersburg, Lan', 2002, 736 p.

Chapter 1. Formal description of algorithms and error estimate

In this chapter, the regular perturbation theory [1] is applied to the proof of theorems on the localization of eigenvalues of a closed linear operator in Banach space. Necessary details from functional analysis are formulated in Sect. 1.1. The theorems enable us to develop an abstract error estimate scheme for the methods of approximate evaluation of eigenvalues of linear operators.

1.1. Formalization

Let X be a Banach space. Denote by $B(X)$ the set of linear operators bounded in X. If $P,Q \in B(X)$ is a pair of projectors $(P^2 = P, Q^2 = Q)$ and $\|P-Q\|<1$, then the images PX and QX are isomorphic. In particular, $dimP = dimQ$.

Theorem 1

Let $P(t)$ be a projector continuous with respect to a parameter t spanning a (simply-connected) domain on the real axis or complex plane. Then the images $P(t)X$ are isomorphic for any t. In particular, $dimP(t)X$ is a constant-valued function.

To prove the theorem, it is sufficient to note that

$$\|P(t')-P(t'')\|<1$$

for close enough t' and t'', therefore the above results are applicable to the pair of projectors $P(t')$ and $P(t'')$. The operator-valued function

$R(\zeta) = R(\zeta,T) = (T-\zeta I)^{-1}$

is called resolvent of operator T (where I is the identity operator), it satisfies the resolvent identity

$$R(\varsigma_1)-R(\varsigma_2)=(\varsigma_1-\varsigma_2)R(\varsigma_1)R(\varsigma_2),$$

from which, in particular, we obtain that $R(\zeta)$ is a holomorphic function of parameter ζ. The singular points of $R(\zeta)$ are the eigenvalues λ_ν, $\nu = 1,2,...$ of operator T. The residue of resolvent

$$P_\nu = -\frac{1}{2\pi i}\int_{\Gamma_\nu} R(\varsigma)d\varsigma$$

is a projecting operator, i.e., $P_\nu^2 = P_\nu$. If a closed contour Γ_ν contains no other eigenvalues of operator T except λ_ν, then $P_\nu X$ is referred to as algebraic eigen subspace, while its dimensionality $dimP_\nu X$ is called algebraic multiplicity of eigenvalue λ_ν. Projector P_ν is commutative with operator T: $TP_\nu = P_\nu T = P_\nu TP_\nu$.

Among the unbounded operators, there exists an operator class referred to as closed operators. Denote by $D(T)$ the domain of operator T. Operator T is called closed if, for any ordered sequence $u_n \in D(T)$ such that $u_n \to u$ and $Tu_n \to v$, the vector u belongs to $D(T)$ and $Tu = v$. A bounded operator is closed when and only when the subspace $D(T)$ is closed. If operator T is invertible, then closeness of T is equivalent to closeness of T^{-1}.

1.2. Localization theorems

Let **B** be Banach space and T a closed linear operator. Denote by $\rho(T)$ the resolvent set of operator T, i.e., the set of points ζ of the complex plane, for which there exists the bounded operator $(T-\zeta I)^{-1}$, with domain of definition dense in **B**. If the operator T is closed, then $R(\zeta)$ is not defined in the whole of **B**. For a bounded operator T we denote its spectral radius by

$$Spr\,T = \lim_{n\to\infty}\left\|T^n\right\|^{1/n}$$

Theorem 2

Let T be a closed operator in Banach space **B** defined on a domain $D(T)$, and let T_n be a bounded operator. Let Γ be a rectifiable closed contour (or a finite set of pairwise nonintersecting contours of this type), containing inside it m eigenvalues of operator T, counted so as to take account of their algebraic multiplicities, and let the following condition hold:

$$\sup_{\varsigma\in\Gamma} Spr(R(\varsigma)(T_n - \varsigma I) - I) < 1, \qquad (1.2.1)$$

then there are exactly m eigenvalues of operator T_n inside Γ, counting each as many times as its algebraic multiplicity.

The proof is based on the classical perturbation theory [1]. We introduce the family of operators $T(\kappa) = T + \kappa T^{(1)}$, $T^{(1)} = T_n - T$, where κ is a complex-valued number. Let $\zeta \in \rho(T)$, then $T(\kappa)-\zeta I = (T-\zeta I)(I + \kappa R(\zeta)T^{(1)})$, where $R(\zeta)$ is the resolvent of operator T. We observe that $R(\zeta)T^{(1)} = R(\zeta)(T_n - \zeta I) - I$ is a bounded operator, and we denote

$$r_0 = \left[\sup_{\varsigma\in\Gamma} Spr(R(\varsigma)(T_n - \varsigma I) - I)\right]^{-1} > 1. \qquad (1.2.2)$$

With $|\kappa| < r_0$ we obtain

$$(T(\kappa) - \varsigma I)^{-1} = R(\varsigma) + \sum_{k=1}^{n}\kappa^k R^k(\varsigma),\ \ R^k(\varsigma) = (-1)^k (R(\varsigma)T^{(1)})^k R(\varsigma), \qquad (1.2.3)$$

i. e., $\varsigma \in \rho(T(\kappa))$ и $(T(\kappa) - \varsigma I)^{-1}$ can be represented uniformly with respect to $\varsigma \in \Gamma$ by the convergent series (1.2.3). The coefficients of this series are also bounded operators, and,

hence, $(T(\kappa)-\varsigma I)^{-1}$ is also a bounded operator, defined in the whole of **B**. Integrating (1.2.3) term by term, we obtain that the natural projector $P(\kappa)$ of operator $T(\kappa)$ is defined by a series, convergent for $|\kappa|<r_0$:

$$P(\kappa)=-\frac{1}{2\pi i}\int_\Gamma R(\varsigma,\kappa)d\varsigma = P+\sum_{k=1}^{n}\kappa^k P^{(k)},\ \ P^{(k)}=-\int_\Gamma R^{(k)}(\varsigma)d\varsigma,\ P=-\frac{1}{2\pi i}\int_\Gamma R(\varsigma)d\varsigma.$$

In particular, $P(\kappa)$ is continuous with respect to κ, and, hence, there are in general m eigenvalues $\lambda_1(\kappa),\ldots,\lambda_m(\kappa)$ of operator $T(\kappa)$ inside Γ for $|\kappa|<r_0$. But $r_0>1$. QED.

Notes

1) Instead of condition (1.2.1) we can introduce a cruder condition

$$\sup_{\varsigma\in\Gamma}\left\|R(\varsigma)(T_n-\varsigma I)-I\right\|<1. \qquad (1.2.4)$$

If operator T is bounded, relations (1.2.1) and (1.2.4) hold, provided that

$$\|R(\varsigma)\|\ \|T_n-T\|<1,\quad \forall\varsigma\in\Gamma,$$

where $\|R(\varsigma)\|$ is a continuous function in a compact subset of the complex plane.

2) If $\varsigma\in\rho(T)$ and $Spr(R(\varsigma)(T_n-\varsigma I)-I)<1,$ then $\varsigma\in\rho(T_n)$.

3) Condition (1.2.1) implies that the resolvents of operators T and T_n are closely similar.

If we additionally assume in Theorem 2 that operator T is bounded, then T and T_n can be interchanged in condition (1.2.1). For instance, if the interior of $\Gamma_{\tilde\lambda}$, where $\tilde\lambda$ is a simple eigenvalue of operator T_n (we can find $\tilde\lambda$ and the corresponding isolating neighborhood by numerical calculations), contains no other eigenvalues of T_n, and we have the condition

$$\sup_{\varsigma\in\Gamma_{\tilde\lambda}} Spr(R_n(\varsigma)(T-\varsigma I)-I)<1,\ \ R_n(\varsigma)=(T_n-\varsigma I)^{-1},$$

then the interior of $\Gamma_{\tilde\lambda}$ contains a unique eigenvalue of operator T. In other words, by using the results of calculations, we can prove a strict theorem on localization of the eigenvalues of a bounded operator T. We are faced with a task of this kind in Gauss's problem [2].

Let us exemplify the application of Theorem 2 in the finite-dimensional case. Let A be an $n\times n$ matrix with complex-valued elements a_{ij}. Denote $A_1 = diag(a_{11},\ldots,a_{nn})$, $A_2 = A-A_1$, $A_3(\zeta) = (A_1-\zeta I)^{-1}A_2$, i. e.

$$A_3(\varsigma)=\begin{pmatrix} 0 & \frac{a_{12}}{a_{11}-\varsigma} & \cdots & \frac{a_{1n}}{a_{11}-\varsigma} \\ \frac{a_{21}}{a_{22}-\varsigma} & 0 & \cdots & \frac{a_{2n}}{a_{22}-\varsigma} \\ \cdots & \cdots & \cdots & \cdots \\ \frac{a_{n1}}{a_{nn}-\varsigma} & \cdots & 0 & \end{pmatrix}, \qquad (1.2.5)$$

where $\zeta\in\Gamma$ is a boundary point of the domain formed by the union of circles with centers a_{ii} and radii r_i (Γ can consist of several closed nonintersecting contours). Let $P_i=\sum_{i\neq j}|a_{ij}|$, $i = 1,\ldots,n$; then it was shown by Gershgorin [3] that all the eigenvalues of matrix A lie inside the domain formed by the union of circles with centers a_{ii} and radii P_i. This widely known

result can easily be obtained as a corollary to Theorem 2. Indeed, let $|A|_\infty = \max_i \sum_j |a_{ij}|$ be the Chebyshev matrix norm; then

$$|A_3(\varsigma)|_\infty = \max_i \sum_{i \neq j} \frac{|a_{ij}|}{|a_{ii} - \varsigma|} \le \max_i \frac{P_i}{r_i}. \qquad (1.2.6)$$

If $\max_i \frac{P_i}{r_i} < 1$, then all eigenvalues of matrix A lie inside Γ. From this, Gershogin's result follows. Let $r_i = P_i + \varepsilon$, $\varepsilon > 0$, then the right-hand side of (1.2.6) is less than unity, but s > 0 is arbitrary and, hence, with $r_i = P_i$, all the eigenvalues of matrix A lie inside or on the boundary of the corresponding domain. In fact, this is Gershgorin's theorem.

Notice that condition (1.2.4) has been utilized in these considerations; if the finer condition (1.2.1) is used, we arrive at the following theorem.

Theorem 3

Let A be an $n \times n$ matrix with complex elements a_{ij}, and let Γ be a rectifiable contour (or a finite set of such contours that are pairwise nonintersecting), which contains inside it the diagonal elements a_{ii}, $i = 1,2,\ldots,n$ of matrix A; then, if we have the condition

$$\sup_{\varsigma \in \Gamma} Spr\, A_3(\varsigma) < 1$$

[see (1.2.5) for the notation], all the eigenvalues of matrix A lie inside Γ.

The result of Theorem 3 is thus a generalization of Gershgorin's result. By using Theorem 2, other results of a similar type can easily be obtained. Notice that on eigenvalue localization theorems are of great importance for practical evaluation of eigenvalues [4].

1.3. A Priori Error Estimate in Eigenvalue Problems

Theorem 4

Assume that the hypotheses of Theorem 2 hold, except that Γ is a convex contour Γ_λ, which contains in its interior an eigenvalue λ of operator T of algebraic multiplicity m, and contains no other spectral points of this operator. Denote $\rho = \max_{\varsigma \in \Gamma_\lambda} |\lambda - \varsigma|$, while $\hat{\lambda} = \frac{1}{m}(\lambda_1 + \ldots + \lambda_m)$ is the arithmetic mean of the eigenvalues of operator T_n, lying inside Γ_λ, then we have

$$|\lambda - \hat{\lambda}| \le \rho \frac{r_0^{-1}}{1 - r_0^{-1}},$$

where r_0 is defined in (1.2.2).

Proof. Function $\hat{\lambda}(\kappa) = \frac{1}{m}\ \lambda_1(\kappa) + \ldots + \lambda_m(\kappa)$ (see proof of Theorem 2) is holomorphic for $|\kappa| < r_0$, i. e.,

$$\hat{\lambda}(\kappa) = \lambda + \kappa\hat{\lambda}_1 + \kappa^2\hat{\lambda}_2 + \ldots, \qquad (1.3.1)$$

while, since Γ_λ is a convex contour, $\hat{\lambda}(\kappa)$ lies inside Γ_λ, and for the coefficients of series (1.3.1) we have the Cauchy formulas:

$|\hat{\lambda}_k| \le \rho r_0^{-k}, \quad k = 1, 2, \ldots,$

But $r_0>1$, and hence series (1.3.1) is majorized by a convergent geometric progression with ratio $q = r_0^{-1}$. Hence follows the theorem.

Corollary. Let T be a bounded operator; then the operator $T^{(1)} = T_n - T$ is likewise bounded. Assume that we have

$$\|R(\varsigma)\|\|T^{(1)}\| < 1,\ \varsigma \in \Gamma_\lambda,$$

then we have the inequality

$$|\lambda - \hat{\lambda}| \le C_n \|T^{(1)}\|, \qquad (1.3.2)$$

where $C_n = \rho\|R(\varsigma_0)\|(1 - \|R(\varsigma_0)\|\|T^{(1)}\|)^{-1}$, while $\zeta_0 \in \Gamma_\lambda$ is the point at which $\|R(\varsigma)\|$ reaches its maximum for $\zeta \in \Gamma_\lambda$.

We should probably be not far wrong in saying that the existing methods for calculating the eigenvalues of operator (differential, integral, etc.) equations amount in the long run to a finite-dimensional problem of the type $Av = \mu v$ obtained from the relation

$$Au = \lambda u + r, \qquad (1.3.3)$$

where A is a $n\times n$ matrix, while u and r are n-dimensional vectors. Notice that λ is an exact eigenvalue of the corresponding operator T. Further, $u = (u_1 \ldots u_n)'$, where u_i are the exact values at the interpolation nodes (grid nodes, coefficients of series expansion, etc.) of the eigenfunction of the initial operator, corresponding to eigenvalue λ; $r = (r_1 \ldots r_n)'$is the discretization error. Here, $r = r(u,\lambda)$, i.e., the discretization error has its own value for each eigenfunction.

Let λ be a simple eigenvalue of operator T, and P_n the projector onto the finite-dimensional subspace $L_n \subset \mathbf{B}$. We shall call operator $T_n = P_nTP_n$ the discretization of operator T, and denote by A the matrix of the finite-dimensional operator $P_nTP_n\big|_{L_n}$ in a basis $l_1, \ldots, l_n \in L_n$. Let condition (1.2.1) be satisfied, where Γ is the contour Γ_λ, satisfying the conditions of Theorem 2. Thus, there is one eigenvalue of operator T_n. inside the contour Γ_λ. Hence, there is one eigenvalue of matrix A inside Γ_λ. The exact eigenvalue of the initial operator T satisfies a relation of type (1.3.3). We introduce the matrix $B = A-(u,u)^{-1}ru^*$, where $u^* = (\bar{u}_1, \ldots, \bar{u}_n)$ is the matrix adjoint to column matrix u, while $(u,v) = (u_1\bar{v}_1 + \ldots + u_n\bar{v}_n)$ is the scalar product in $\mathbf{C}^n$. It is easily seen that $Bu = \lambda u$, i. e., λ and u are an eigenvalue and an eigenvector of matirx B. Denote by $\|.\|_2$ the matrix norm subordinate to the vector norm in $\mathbf{C}^n$; then $\|A - B\|_2 \le \|r\|_2$.

We recall that there is one eigenvalue of matrix A inside contour Γ_λ. If we have the condition

$$\sup_{\varsigma\in\Gamma_\lambda} Spr(A - \varsigma I)(B - \varsigma I) - I) < 1, \qquad (1.3.4)$$

then there are no eigenvalues of matrix B apart from λ inside Γ_λ. Notice that condition (1.3.4) holds provided that

$$\|R(\varsigma, A)\|_2 \|r\|_2 < 1,\ \ \forall\varsigma \in \Gamma_\lambda.$$

Hence, if the discretization error is sufficiently small, then there are no "parasitic" eigenvalues of matrix B inside Γ_λ, i.e., eigenvalues other than λ. It now remains to apply the corollary to Theorem 4 in order to obtain the error estimate

$$|\lambda - \tilde{\lambda}| \le C_n \|r\|_2,$$

$$C_n = \rho \|R(\varsigma_0, A)\|_2 (1 - \|R(\varsigma_0, A)\|_2 \|r\|_2)^{-1},$$

where $\zeta_0 \in \Gamma_\lambda$ is the point at which the maximum of $\|R(\varsigma, A)\|_2$ is reached for $\zeta \in \Gamma_\lambda$.

Now let λ be a semisimple eigenvalue of the closed operator T of multiplicity m, while $\underline{M}$ is the corresponding m-dimensional geometric eigensubspace, and $dimP_nM = m$ for sufficiently large n. As a result of discretization of the eigenvalue problem for operator T, we in general obtain m finite-dimensional problems of type (1.3.3):

$$Au_i = \lambda u_i + r_i, \ \ i = 1,2,\dots,m,$$

where $(u_i,u_j) = \delta_{ij}$. If the contour Γ_λ satisfies the conditions of Theorem 2, while condition (1.2.1) holds, then there are m eigenvalues $\lambda_1,\dots,\lambda_m$ of operator T_n (of matrix A) inside Γ_λ, counting each eigenvalue as many times as its multiplicity. We introduce the matrix

$$B = A - r_1u_1^* - \dots - r_mu_m^*.$$

It is easily seen that matrix B has λ its m-tuple eigenvalues, while $u_1,\dots,u_m$ are the corresponding eigenvectors. If condition (1.3.4) holds, then there are no other eigenvalues of matrix B inside Γ_λ. Denote $R = A\text{-}B$; then $\|R\|_2 \le m \max_i \|r\|_2$. Relation (1.3.4) holds provided that

$$\|R(\varsigma, A)\|_2 \|R\|_2 < 1, \ \ \forall\varsigma \in \Gamma_\lambda.$$

Now, in the same way as for a simple eigenvalue, we obtain the estimate

$$|\lambda - \hat{\lambda}| \le C_n \|R\|_2,$$

$$C_n = \rho \|R(\varsigma_0, A)\|_2 (1 - \|R(\varsigma_0, A)\|_2 \|R\|_2)^{-1}.$$

Here, $\hat{\lambda} = \frac{1}{m}(\lambda_1 + \dots + \lambda_m)$, $\zeta_0 \in \Gamma_\lambda$ is the point at which the maximum of $\|R(\varsigma, A)\|_2$ is reached for $\zeta \in \Gamma_\lambda$.

1.4. A Posteriori Error Estimate in Eigenvalue Problems

The theorems proved in Sections 1.2 and 1.3 can also be used for obtaining an a posteriori error estimate in the eigenvalue problem for a bounded operator T. In fact, let T_n be a sequence of bounded operators (discretization of operator T), for which the eigenvalues can be calculated directly. For example, if $T_n = P_nTP_n$ (see Sec. 1.2), then calculation of the eigenvalues of operator T_n is equivalent to calculation of the eigenvalues of an $n \times n$ matrix A, for which reliable algorithms are available [4].

Let $\tilde{\lambda}$ be a simple eigenvalue of operator T_n, and let $\Gamma_{\tilde{\lambda}}$ be a closed contour containing the point $\tilde{\lambda}$ inside it and not containing other spectral points of operator T_n. To see the accuracy to which $\tilde{\lambda}$ is an eigenvalue of operator T, we have to calculate the quantity

$$r_0^{-1} = \sup_{\varsigma \in \Gamma_{\tilde{\lambda}}} Spr(R_n(\varsigma)(T - \varsigma I) - I) < 1, \quad R_n(\varsigma) = (T_n - \varsigma I)^{-1}.$$

If $r_0^{-1} < 1$, then the unique eigenvalue λ of operator T lies inside $\Gamma\tilde{\lambda}$, and we have an inequaity

$$|\lambda - \tilde{\lambda}| \le \rho \frac{r_0^{-1}}{1 - r_0^{-1}}, \ \ \rho = \max_{\varsigma \in \Gamma_{\tilde{\lambda}}} |\tilde{\lambda} - \varsigma|.$$

It is important to observe that the eigenvalue of maximum modulus of the bounded operator $R_n(\zeta)(T - \zeta I) - I$ can be calculated roughly. We only have to see that $Spr(R_n(\zeta)(T - \zeta I) - I) < 1$ and to note the order of this quantity.

1.5. Generalization for bundle of operators

Let **B** be a Banach space, and let A and B be a pair of bounded operators. We denote by $P(A,B)$ the resolvent set, i.e., the set of complex numbers $\zeta \in \mathbf{C}$, for which a bounded operator $(A - \zeta B)^{-1}$ exists. The complement $\Sigma(A,B) = \mathbf{C} - P(A,B)$ is called the spectrum of the operator pair A,B. If for some number $\lambda \in \mathbf{C}$ there is a solution $u \neq 0$ of the equation $Au = \lambda Bu$, then λ is called the eigenvalue corresponding to the eigenvector u for the operator pair A,B. The eigenvalues of the operator pair A,B lie in the spectrum $\Sigma(A,B)$. The notation $R(\zeta) = (A - \zeta B)^{-1}$ is used below. Let λ be an eigenvalue of the operator pair A,B, and let $\Gamma \subseteq P(A,B)$ be a rectifiable contour enclosing only this eigenvalue. Denote

$$E = -\frac{1}{2\pi i}\int_{\Gamma} R(\varsigma)\, d\varsigma.$$

Operator $P = EB$ is a projector. If the space $P(\mathbf{B})$ is finite-dimensional, then the algebraic multiplicity of the eigenvalue λ is $\dim P = \dim P(\mathbf{B})$ [1].

Theorem 5

Let A,B be a pair of bounded operators in the Banach space **B**, and A_n, B_n be another pair of bounded operators. Let Γ be a rectifiable closed contour (or finite set of such contours, which are pairwise non-intersecting), which encloses m eigenvalues of the operator pair A,B counted with their algebraic multiplicity, and let

$$r_0^{-1} = \sup_{\varsigma \in \Gamma} Spr(R(\varsigma)(A_n - \varsigma B_n) - I) < 1, \qquad (1.5.1)$$

Then, there are exactly m eigenvalues of the operator pair A_n,B_n inside Γ, each eigenvalue being counted as many times as its algebraic multiplicity.

The proof is similar to that of Theorem 2, except that now, unlike the classical theory of resolvents, the projection operator on the algebraic characteristic subspace is the operator $P = EB$ (see Sect. 1.2).

Theorem 6

Under the conditions of Theorem 5 but taking the contour Γ as a convex contour Γ_λ which encloses the eigenvalue λ of the operator pair A,B of algebraic multiplicity m and does not enclose any other points of the spectrum of that operator, let $\rho = \max_{\varsigma \in \Gamma_\lambda} |\lambda - \varsigma|$, and $\hat{\lambda} = \frac{1}{m}(\lambda_1 + \ldots + \lambda_m)$ be the arithmetic mean of the eigenvalues of the operator pair A_n,B_n, which lie inside Γ_λ. Then

$$|\lambda - \hat{\lambda}| \leq \rho \frac{r_0^{-1}}{1 - r_0^{-1}},$$

where r_0 has been defined in (1.5.1).

The proof is a word-for-word repetition of Theorem 4 (see above). Theorem 5 means that the resolvents of the operator pairs A,B and A_n,B_n are fairly close.

References

1. T. Kato, Perturbation Theory for Linear Operators, Springer-Verlag (1966).
2. K. I. Babenko and S. P. Yur'ev, "On discretization of a Gauss problem," Dokl. Akad. Nauk SSSR, 240, No. 6, 1273-1276 (1978).
3. S. Gershgorin, Uber die Abgrenzung der eigenwerte einer Matrix // Izv. Akad. Nauk SSSR, Ser. 7, No. 6, 749-754 (1931).
4. J. H. Wilkinson, Algebraic Eigenvalue Problem, Oxford Univ. Press (1965).

Chapter 2. Ordinary Differential Equations

2.1. Introduction

There are a number of competing methods for the numerical solution of the eigenvalue problem. These are primarily projection methods, such as those of Ritz. and of Bubnov and Galerkin, among others. Quite a lot is known on the accuracy of these techniques. For instance, the approximations for the eigenvalues of self-conjugate problems given by Ritz`s method are greater than the exact values. Several results have been obtained concerning convergence, and error estimates have been established for projection methods in some special cases [1].

Difference methods are also widely used [2]. However, the importance of a number of factors which considerably reduce their effectiveness is not taken into account in these methods. We usually have a large amount of *a priori* information at our disposal when solving an eigenvalue problem. The solutions that are sought are most often infinitely differentiable, or even analytic. They are, therefore, elements of functional compact sets which are fairly simply organized. As a rule, the asymptotic of the width of these compact sets is known.

On the other hand, all projection methods are based on the choice of a set of finite-dimensional subspaces and, thus, a certain method for the approximation of the required solution, which, as a rule, is not compatible with the optimal methods discussed above. This naturally results in the numerical algorithm based on such a projection method being far from optimal. However, if an appropriate method for the approximation of a required element is used, a nearly optimal algorithm can be obtained. This approach, which is based on the ideas of work [3], will be followed below. The difference methods have serious deficiencies (see the review in [3]) including, in particular, the fact that they are featured by saturation (of the fairly large amount of work which has been done on the accuracy of these methods, we would mention only [2, 4]). Moreover, even with the difference method for solving the eigenvalue problem, *a priori* information on the smoothness of the solution is ignored, and if the inherent loss of smoothness of difference methods is taken into account, the algorithms obtained are far from optimal. The problem of building numerical methods for the solution of eigenvalue problem can be divided into two stages: i) the infinite-dimensional problem must first be reduced to a finite-dimensional problem, and ii) a method of solving the resulting algebraic eigenvalue problem must be chosen. Only the first stage is considered here; the resulting algebraic problem is solved by the QR-method.

Abstract theorems on error estimation in the eigenvalue problems have been presented in [5, 6]. It is worth noting that only compact operators are considered in [6], while and arbitrary closed operators are dealt with in [5]. In Chapter 1, the results of [5] are presented together with their generalization to the case of a bundle of bounded operators.

To elucidate the difference between the proposed algorithms and classical approaches, consider the classical Sturm-Liouville problem

$$y''(x) - q(x)y(x) = \lambda\rho(x)y(x), \quad x \in (-1,+1), \tag{2.1.1}$$

$$y(-1) = y(+1) = 0. \tag{2.1.2}$$

Here, *q(x)* and ρ*(x)* are given functions, λ is the spectral parameter. It should be noted that problem (2.1.1) – (2.1.2) is trivial for numerical solution. The traditional approach is based on the finite-difference method. Its essence is the following: let *h* be the grid size; we take *n* nodes on the interval (-1, + 1) $x_i = -1 + hi$, $h = 2/(n + 1)$, $i = 1,2,\dots,n$, $x_0 = -1$, $x_{n+1} = 1$, i. e., total of (*n* + 2) nodes are chosen on the closed interval [-1,1].

If $y(x) \in C^3[-1,1]$, then

$$y(x+h) = y(x) + \frac{y'(x)}{1!}h + \frac{y''(x)}{2!}h^2 + \frac{y'''(x)}{3!}h^3 + O(h^4), \tag{2.1.3}$$

$$y(x-h) = y(x) - \frac{y'(x)}{1!}h + \frac{y''(x)}{2!}h^2 - \frac{y'''(x)}{3!}h^3 + O(h^4). \tag{2.1.4}$$

Summing up relations (2.1.3), (2.1.4), we obtain

$$y(x+h) + y(x-h) = 2y(x) + y''(x)h^2 + O(h^4),$$

then

$$y''(x) = \frac{y(x+h) - 2y(x) + y(x-h)}{h^2} + O(h^2). \tag{2.1.5}$$

Denote

$y(x_i) = y_i, \quad y''(x_i) = y_i'',$

Then we obtain from (2.1.5)

$$y_i'' = \frac{y_{i+1} - 2y_i + y_{i-1}}{h^2} + O(h^2), \quad i = 1,2,\dots,n. \tag{2.1.6}$$

The first term on the right-hand side of relation (2.1.6) is the finite-difference second-order derivative. Thus, the finite-difference derivative approximates y_i'' to the second order, i.e., with accuracy $O(h^2)$. Substitute (2.1.6) into (2.1.3) to obtain for each grid node

$$\frac{y_{i+1} - 2y_i + y_{i-1}}{h^2} - q_i y_i = \lambda\rho_i y_i + O(h^2), \quad i = 1,2,\dots,n,$$

$$y_0 = y_{n+1} = 0 .$$

Discarding the approximation error $O(h^2)$, we obtain an approximate finite-dimensional problem for a tridiagonal symmetric matrix. The perturbation (see Chapter 1) to the eigenvalues due to discarding the terms $O(h^2)$ is of the order of discretization error, with the proportionality coefficient depending on the distance between the eigenvalue in question λ to the remaining part of the spectrum of Sturm-Liouville problem. Thus, whatever smooth is the solution of Sturm-Liouville problem (2.1.1) – (2.1.2), the eigenvalues are obtained with the error $O(h^2)$. According to K. I. Babenko [3], the finite-difference method for the solution of Sturm-Liouville problem is featured by saturation. Similar deficiency is characteristic of

the finite-element method. We consider now an alternative method for the solution of eigenvalue problems which is free from the above limitations.

2.2. Discretization of classic spectral problems for ordinary differential equations

We will consider the eigenvalue problem for the zero-order Bessel equation, the Sturm-Liouville problem, and periodic and antiperiodic problems for the Sturm-Liouville operator. We first consider the boundary-value problem for the Bessel equation:

$$(xy')' + \lambda xy = 0, \quad x \in (0,1), \tag{2.2.1}$$

$$y(1) = 0, \tag{2.2.2}$$

$$|y(0)| < \infty. \tag{2.2.3}$$

This problem is suitable for testing the technique because its solution is known. The boundary-value problem (2.2.1) – (2.2.3) is equivalent to the integral equation

$$y\left(\frac{x+1}{2}\right) = \frac{\lambda}{2}\int_{-1}^{+1} G\left(\frac{x+1}{2}, \frac{\varsigma+1}{2}\right)\frac{\varsigma+1}{2} y\left(\frac{\varsigma+1}{2}\right)d\varsigma,$$

$$G(x,\xi) = -\ln[(x+\xi+|\xi-x|)/2].$$

For the function $[(\zeta + 1)/2]y[(\zeta + 1)/2]$ we will use an interpolation formula of the form

$$(P_n f)(x) = \sum_{k=1}^{n} f(x_k) l_k(x) + R_n(x; f), \tag{2.2.4}$$

where the fundamental interpolation functions are

$$l_k(x) = \frac{T_n(x)}{(x-x_k)T_n'(x_k)}, \quad k = 1, 2, ..., n,$$

$$T_n(x) = \cos(n \arccos x), \quad x_k = \cos[(2k-1)\pi / 2n],$$

and $R_n(x;f)$ is the interpolation error. Calculations give

$$y_j = \lambda \sum_{k=1}^{n} B_{jk} y_k + r_n(x_j; y), \tag{2.2.5}$$

$$B_{jk} = B_k(x_j), \quad y_k = y(x_k), \quad k, j = 1, 2, ..., n,$$

where

$$B_k(x) = \frac{\varsigma_k + 1}{4}\int_{-1}^{+1} G\left(\frac{x+1}{2}, \frac{\varsigma+1}{2}\right) l_k(\varsigma) d\varsigma,$$

$$r_n(x,y) = \frac{\lambda}{2}\int_{-1}^{+1} G\left(\frac{x+1}{2}, \frac{\varsigma+1}{2}\right) R_n\left(\varsigma; \left(\frac{\varsigma+1}{2}\right) y\right) d\varsigma,$$

Discarding the discretization error in (2.2.5), we obtain the approximate eigenvalue problem

$$\tilde{y} = \tilde{\lambda} B \tilde{y}.$$

Here, $\tilde{y}$ is the vector of approximate values of the required eigenfunction $y(x)$ at grid nodes, and $\tilde{\lambda}$ is the approximate eigenvalue. It is easy to see (cf. [3], p. 189, for instance), that

$$\max_{|x|\le 1} |r_n(x;y)| \le c|\lambda|(1+\omega_n)E_n(y),$$

where c is an absolute constant, ($\omega_n = O(\ln(n))$ is the Lebesgue interpolation constant, while $E_n(y)$ is the best approximation of the function y by a polynomial of degree not greater than $(n\text{-}1)$ in the norm C). Note further that the eigenfunctions of problem (2.2.1) – (2.2.3) are integers, and therefore (cf. [7], p. 254)

$$\lim_{n\to\infty} \sqrt[n]{E_n(y)} = 0,$$

that is, the discretization error tends rapidly to zero. The perturbation of the eigenvalues resulting from discarding the discretization error will be estimated below. Here we discuss the numerical results. For $n = 5$, the first eigenvalue is correct to four places, and the third eigenvalue is correct to one place after the decimal point. For $n = 20$, the first eigenvalue is calculated correct to 22 places, and the 14th to one place after the point. The last calculation was performed with double accuracy on the BESM-6 computer (mantissa of length 80 bits), The calculation time was 4 min 40 s, including calculation of the matrix. The BESSEL program used for these calculations and the results for the eigenfunctions of boundary-value problem (2.2.1) – (2.2.3) were published in [8].

We will now consider the eigenvalue problem for the equation

$$y''(x) - q(x)y(x) = \lambda\rho(x)y(x), \quad x \in (b_1, b_2), \tag{2.2.6}$$

with boundary conditions

$$\alpha y' + \beta y\big|_{x=b_1} = 0, \tag{2.2.7}$$

$$\alpha_1 y' + \beta_1 y\big|_{x=b_2} = 0, \tag{2.2.8}$$

$\alpha^2 + \alpha_1^2 \neq 0.$

The problem can be reduced to the interval (-1,1) by replacing the independent variable, and we will therefore assume from now on that $b_1 = -1$, $b_2 = 1$. We will also assume that the functions $q(x)$ and $\rho(x)$ in Eq. (2.2.6) are smooth.

We will reduce the boundary-value problem (2.2.6) – (2.2.8) to an integral equation. Let $G(x,\xi)$ be Green's function of the operator d^2/dx^2 with boundary conditions (2.2.7) and (2.2.8). Then

$$y(x) = \int_{-1}^{+1} G(x,\xi)[q(\xi) + \lambda\rho(\xi)y(\xi)]d\xi. \tag{2.2.9}$$

We discretize the integral equation (2.2.9) in the same way as before. Applying the interpolation formula (2.2.4) to the functions yq and $y\rho$, we obtain

$$y(x)q(x) = \sum_{k=1}^{n} y_k q_k l_k(x) + R_n(x; yq),$$

$$y(x)\rho(x) = \sum_{k=1}^{n} y_k \rho_k l_k + R_n(x; y\rho),$$

where

$$y_k = y(x_k), \quad \rho_k = \rho(x_k), \quad q_k = q(x_k), \quad k = 1, 2, \ldots, n.$$

Substituting these relations into (2.2.9), we have

$$y_j = \sum_{k=1}^{n} D_{jk} q_k y_k + \lambda \sum_{k=1}^{n} D_{jk}\rho_k y_k + r_n(x_j; yq) + \lambda r_n(x_j; y\rho), \quad j = 1, 2, \ldots, n$$

Here

$$D_{jk} = \int_{-1}^{+1} G(x_j, \xi) l_k(\xi) d\xi, \quad j,k = 1,2,...,n, \tag{2.2.10}$$

$$r_n(x_j; yq) = \int_{-1}^{+1} G(x_j, \xi) R_n(\xi, yq) d\xi, \quad j = 1,2,...,n, \tag{2.2.11}$$

$$r_n(x_j; y\rho) = \int_{-1}^{+1} G(x_j, \xi) R_n(\xi, y\rho) d\xi, \quad j = 1,2,...,n. \tag{2.2.12}$$

The resulting algebraic eigenvalue problem is

$$(A_n - \lambda B_n) y = r_a + \lambda r_b. \tag{2.2.13}$$

Here $A_n = I\text{-}DQ$ and $B_n = DP$ are $n \times n$ matrices; $Q = diag(q_1, ..., q_n)$ and $P = diag(\rho_1, \ldots, \rho_n)$ are diagonal matrices. The elements of the matrix D can be determined from (2.2.10). The components of the error vectors r_a and r_b can be determined from formulae (2.2.11) and (2.2.12), respectively. Note that λ in relation (2.2.13) is the exact eigenvalue, and y ·is a vector of length n, the components of which are the values of the corresponding eigenfunction at the grid nodes. Discarding the discretization errors r_a and r_b from (2.2.13), we obtain the approximate eigenvalue problem

$$(A_n - \tilde{\lambda} B_n) \tilde{y} = 0,$$

where $\tilde{\lambda}$ is an approximate eigenvalue, and $\tilde{y}$ is a vector of length n, the components of which are the approximate values of the required eigenfunction at the grid nodes. The perturbation of the eigenvalues resulting from discarding the discretization error will be estimated below, but we first examine some numerical results.

In [9], distant eigenvalues of the boundary-value problem

$$y''(x) + (\lambda - x^2) y(x) = 0, \; y(0) = y'(1) = 0$$

were calculated.

For the 100-th eigenvalue, we obtained the numerical value 97711.8842956852 using the asymptotic formula, and 97711.8846 by calculation. The calculations by the technique described in this section give the value 97711.884322 on a grid with n = 180 nodes. This is slightly more accurate than in [9]. Thus, the technique can be used to calculate the eigenvalues which are so distant that they can be obtained by asymptotic formula. Other results from [9] are presented in Table II (column (a) corresponds to the asymptotic formula, column (b) contains the results of calculations):

Table II

Eigenvalues corresponding to highly oscillatory egenfunctions of Weber's equation satisfying boundary condition (5.4) (ii)✓

λ_m		
m	***(a)***	***(b)***
100	97711.8842956852	97711.8846
200	392813.0560529779	392813.0561
300	885306.3153903790	885306.3152
400	1575191.6632255727	1575191.6632
500	2462469.0988021103	2462469.0989

✓ Eigenvalues Corresponding to Highly Oscillatory Eigcnfunctions of Weber's Equation Satisfying Boundary Condition (5.4) (ii).

600	3547138.6223169501	3547138.6223
700	4829200.2341860869	4829200.2342
800	6308653.9339494741	6308653.9340
900	7985499.7216152999	7985499.7215
1000	9859737.5974535981	9859737.5975

The results obtained by the technique described above on a grid with 3000 nodes are presented below:

100	97711.8843105742
200	392813.055899344
300	885306.315512695
400	1575191.66314519
500	2462469.09880420
600	3547138.62249124
700	4829200.23417049
800	6308653.93392193
900	7985499.72187408
1000	9859737.59750380

As a second example, consider the boundary-value problem

$$y''(x) + (\lambda x - x^4)y(x) = 0,\ y'(1) - y(1) = y'(2) - 4y\,(2) = 0.$$

The results of calculations for this example in Table VIII of [9] give the first eigenvalue 2.00000000. However, it is easy to see that the exact first eigenvalue is –2, corresponding to the eigenfunction $y(x) = c\cdot\exp(x^3/3)$. The next four eigenvalues are larger than the true eigenvalues by 6 units (the fractional part is correct). The correct eigenvalues obtained on a grid of n = 20 nodes are: $\lambda_1 = -2.000000000005$, $\lambda_2 = 7.4742107310$, $\lambda_3 = 27.637864542$, $\lambda_4 = 60.869801997$, $\lambda_5 = 107.37160421$. For n = 2, we obtained the eigenvalues -2.20 and 7.46, so that the first eigenvalue is calculated with 10% relative accuracy on a grid with two nodes. The calculations were carried out using the EIGVAL program [8]. Note that there is a bug in this program which only surfaces for odd n. The correct value of the sixth row (cf. [5. p. 54]) is *C*1 = *C*0*(1-(-1)***N*)/*N*. All the sample calculations given in [5] are correct.

ln connection with the results obtained here, note the following calculation given in [2, c. 335]: about 50 nodes are required in order to find the fifth eigenvalue to three correct places after the decimal point by a difference scheme of order six. For the method presented here, about 12–13 interpolation nodes are required.

Consider now the boundary-value problem for the Mathieu equation:

$$w'' + \{\lambda - 2q\cos 2x\}\,w = 0,$$
$$w(0) = w\,(\pi/2) = 0.$$

For this problem, the results presented in Table III were obtained in [9]:

Table III

	***q* = 1**	***q* = 10**	***q* = 25**	***q* = 100**
m	λ_m	λ_m	λ_m	λ_m
5	100.005050675	100.5067695	Notea	Notea
10	400.001253135	400.1253382	400.78419	Notea
15	900.00055617	900.0556195	900.34769	900.5836
100	40000.0000	40000.00	40000.0	40000.1
1000	4000000.000000	4000000.0000	4000000.000	4000000.00

The results obtained by the author on a grid containing 2000 nodes are given below in Table IIIa:

Table IIIa

	$q = 1$	$q = 10$	$q = 25$	$q = 100$
m	λ_m	λ_m	λ_m	λ_m
5	100.005050675217	100.506769462940	103.225680042440	126.442980323169
10	400.001253135554	400.125338231571	400.784185569627	412.796652012942
15	900.000556174255	900.055619516845	900.347693024637	905.583618703759
100	40000.0000125259	40000.0012500580	40000.0078127206	40000.1250033929
1000	3999999.99999857	3999999.99999750	4000000.00007584	4000000.00124503

Thus, in the above-cited work, the 15th eigenvalue for q = 100 was obtained with an error. This was established by comparison with the results of calculations carried out on a grid with 200 nodes, which gave the 15th eigenvalue equal to 905.583618703766.

As the next example, consider the equation of parabolic cylinder

$$y''(x) + \{\lambda + \gamma^2 x^2\}y(x) = 0,$$

$$y(0) = y(1) = 0.$$

In Table 2.1, the results obtained by the technique described above are presented for $\gamma = 50$ and $\gamma = 100$, together with the reference results from [9]. The number of nodes is $n = 40$ for $\gamma = 50$, and $n = 100$ for $\gamma = 100$.

Table 2.1

$\gamma = 50$			$\gamma = 100$		
m	λ_m		m	λ_m	
	Calculation by the present technique	*Results from [9] obtained on 100 grid points*		*Calculation by the present technique*	*Results from [9] obtained on 100 grid points*
9	121.0784681	121.0785	17	219.8930241	219.893
10	279.0426771	279.0427	18	483.3507150	483.351
11	465.1662800	465.1663			

The approach presented in [9] can be summarized in the following way. By the Prufer substitution, the problem is reduced to a system of two first-order equations. To find out the eigenvalues, one of these equations (having the right-hand side which depends on λ) is used. The left boundary condition provides the initial value. By the sixth-order Runge-Kutta scheme, one can solve the Cauchy problem for each λ. Applying the right boundary condition, we arrive at a transcendental equation for the eigenvalues. An important advantageous feature of this technique is that it enables high eigenvalues to be evaluated.

As a next example, we will consider for (2.2.6) with periodic potential $q(x)$, $q(x) = q(x + a)$ and $p = 1$ the periodic problem

$$y(0) - y(a) = y'(0) - y'(a) = 0, \qquad (2.2.14)$$

and the antiperiodic problem

$$y(0) + y(a) = y(0) + y'(a) = 0. \qquad (2.2.15)$$

Let κ be a real number. Then (2.2.6) can be rewritten in the form

$$d^2 y / dx^2 + \kappa^2 y = (\mu + q(x))y(x), \quad \mu = \lambda + \kappa^2.$$

Let $G(x,\xi)$ be Green`s function of the operator

$$d^2y/dx^2+\kappa^2$$

for boundary conditions (2.2.14) or (2.2.15). Then we obtain the integral equation

$$y(x)=\int_0^a G(x,\xi)(\mu+q(\xi)y(\xi))d\xi.$$

In the periodic case, we interpolate with the formula

$$P_n(x;y)=\frac{2}{2n+1}\sum_{k=0}^{2n} y(x_k)D_n(x-x_k;a),\quad x_k=\frac{ak}{2n+1},$$

where $D_n(x;a)$ is the Dirichlet kernel

$$D_n(x;a)=\frac{\sin[(n+0.5)2\pi x/a]}{2\sin(\pi x/a)}.$$

In the antiperiodic case we use the interpolation formula

$$P_n(x;y)=\frac{2}{2n+1}\sum_{k=0}^{2n} y(x_k)\cos\frac{\pi}{a}(x-x_k)D_n(x-x_k;a).$$

The subsequent considerations are similar to those for the Sturm-Liouville problem, and leads to the algebraic eigenvalue problem of the form (2.2.13). The approximate eigenvalue problem is obtained by discarding the discretization error:

$$y=\mu By,\qquad B=(I+AQ)^{-1}A. \tag{2.2.16}$$

Consider now in more details a finite-dimensional problem (2.2.16). For the periodic boundary conditions

$$G(x,\xi)=K(x-\xi),\qquad K(x)=\frac{2}{a}\left(\frac{1}{2\kappa^2}+\sum_1^{\infty}\frac{\cos\frac{2\pi\nu}{a}x}{\left(\frac{2\pi\nu}{a}\right)^2+\kappa^2}\right),$$

therefore

$$A_{ij}=\frac{2}{N}\sum_{k=0}^{n}{}'\frac{\cos\frac{2\pi k}{a}(x_i-x_j)}{\left(\frac{2\pi k}{a}\right)^2+\kappa^2} \tag{2.2.17}$$

where the prime on the summation sign means that the term for $k=0$ is taken with the coefficient ½; i.e. the matrix A is a symmetric circulant of dimension $N\times N$.

A symmetric circulants of dimension $N\times N$, $N=2n+1$, is a real-valued matrix with the first row taking the form $a_0a_1a_2\ldots a_na_{n-1}\ldots a_1$, while the remaining rows are obtained from the first one by the cyclic permutation. Therefore, such a matrix has $n+1$ different elements. The properties of circulants are well known [10]. In particular, all matrices of this class have the same eigenvectors $x_j=(1,\theta_j,\ldots,\theta_j^{N-1}),\ \ \theta_j=\exp(i\varphi_j),\ \ \varphi_j=\frac{2\pi j}{N},\ \ j=0,1,\ldots,2n,$

the corresponding eigenvalues are

$$\lambda_j=a_0+2\sum_{k=1}^{n}a_k\cos k\varphi_j,\quad j=0,1,\ldots,2n.$$

Evidently, λ_0 is an eigenvalue of multiplicity one, while $\lambda_1,\ldots,\lambda_n$ are of multiplicity two. It is straightforward to check that the class $\boldsymbol{L}$ of symmetric circulants of dimension $N\times N$ is closed with respect to algebraic operations, i. e. if $A,B\in\boldsymbol{L}$, then $A+B\in\boldsymbol{L}$, $AB\in\boldsymbol{L}$, $A^{-1}\in\boldsymbol{L}$,

provided that A^{-1} exists. Moreover, $AB = BA$. When algebraic operations are performed with matrices of class ***L*,** similar operations are performed with their eigenvalues. Note that here we consider only real-valued matrices, while the eigenvector x is written in the complex form just for convenience. It means that the eigenvectors corresponding to the eigenvalue Λ_j are Rex_j and Imx_j, respectively.

As a numerical example, consider Mathieu's equation ($q(x) = \cos 2x$) on the interval $[0,2\pi]$ in the periodic case, and on the interval $[0,\pi]$ in the antiperiodic case. Both these problems have common eigenfunctions (Mathieu's functions ce_{2n+1} and se_{2n}). The results obtained for $N = 21$ are presented in Table 2.2.

Table 2.2

Eigenvalues of Mathieu's equation λ_i		
i	***Periodic problem***	***Antiperiodic problem***
2	–0.11024881701	-0.11024881700
3	1.85910807252	1.85910807252
6	9.04773925990	9.04773925997
7	9.0783688477	9.0783688472
10	25.020840822	25.020840824
11	25.020854343	25.020854342
14	49.010413	49.010418
15	49.010413	49.010418
18	80.98	81.01
19	80.98	81.01

In Table 2.3, the results of calculations for $N = 101$ are presented (by the index i, the eigenvalues λ_i of the periodic problem are numbered in the ascending order, i.e., the eigenvalues corresponding to all Mathieu's functions). In Tables 2.2 and 2.3 only the coinciding digits are shown for the eigenvalues calculated by two approaches.

Table 2.3

Eigenvalues of Mathieu's equation λ_i		
i	***Periodic problem***	***Antiperiodic problem***
18	81.0062503	81.0062507
19	81.0062503	81.0062507
22	121.004167	121.004167
23	121.004167	121.004167
26	169.002976	169.002978
27	169.002976	169.002978
98	2400.995	2401.001
99	2400.995	2401.001

By considering the data presented in Table 2.3, the asymptotic law for the growth of eigenvalues of Mathieu's equation can be noted:

$$\lambda_{2k}, \lambda_{2k+1} \sim k^2. \qquad (2.2.18)$$

Thus, the approach described enables one, for the current problem, to calculate the eigenvalues which are distant enough for the asymptotic formula (2.2.18) to become valid.

2.3. Experimental determination of convergence rate

The second example for the Sturm-Liouville problem considered in Section 2.1 enables us to evaluate experimentally the convergence rate of the approach presented.

In this example, an eigenvalue exists which can be obtained analytically, equal to -2. The convergence rate of the proposed method was checked of the grids with 2 to 17 nodes. The following errors were obtained: 8*e*-1, 5*e*-1, 7*e*-2, 3*e*-2, 6*e*-3, 1*e*-3, 2*e*-4, 2*e*-5, 4*e*-6, 6*e*-7, 1*e*-7, 1*e*-8, 2*e*-9, 3*e*-10, 4*e*-11, 5*e*-12. This tabular dependency was approximated analytically by $\varepsilon = exp(a + bn^3)$, a = 0.013621586, b = -0.028013035.
Thus, in contrast to the classical finite-difference methods having power-law dependence of the approximation error on the number of grid points, here we have exponential decrease in the error. In Appendix 1, the subroutines and programming formulas are presented for the problems described in this chapter.

2.4. High-precision calculation of eigenvalues for the Bessel equation

The results presented in Section 2.2 were obtained by the author together with K. I. Babenko quite a while ago; here they are refined with the use of modern computational means. Currently, a FORTRAN compiler became available (Intel Visual Fortran 9.1), which enables calculations to be carried out with quadruple precision REAL*16. Using this compiler, calculations were performed for the number of grid points N = 3–23 and N = 110. The results obtained were compared with those in Table VI of [11]. In what follows, the values of $\sqrt{\lambda_i}$, i = 1,2,…,23 are presented which were obtained on a grid with N = 23 nodes:

N = 23
EPS = 0.33E-28
Eigenvalues
*2.4048255576957727686216318793*2315
*5.520078110286310649599*995531048766
*8.6537279129110122*9166741865684604
*11.791534439014*0843686267083669051
*14.930917708*4599940892731158995010
*18.071063*9711203998901712950375023
*21.211636*7066011374633859922408520
*24.3524*696616047016958823129522958
*27.4934*6013967059641870692581486 88
*30.634*7976897899335897734472259312
*33.775*9497154294753471218322997414
*36.9*231498885250203330212676349967
39.951027018872860268640302363 7232

The digits which coincide with Table VI [11] are given in italic. Thus, a grid with N = 23 nodes is sufficient to obtain the first eigenvalue with all digits given in the table mentioned (29 decimal places). Calculations on the grid with N = 110 give 32 eigenvalues (all first Table VI [11]) with all digits given in the table (28–29 decimal places):

N = 110
EPS = 0.17E-28
Eigenvalues
2.4048255576957727686216318793 2645
5.5200781102863106495966041128130 2
8.6537279129110122169541987126609 4

11.791534439014281613743044911925\u0035
14.930917708487785947762593997388\u0037
18.071063967910922543147882975618\u0032
21.211636629879258959078393350526\u0033
24.352471530749302737057944763178\u0037
27.493479132040254795877288234607\u0034
30.634606468431975117549578926854\u0030
33.775820213573568684238546346714\u0036
36.917098353664043979769493063273\u0032
40.058425764628239294799307373994\u0036
43.199791713176730357524072728743\u0030
46.341188371661814018685788879112\u0039
49.482609897397817173602761533177\u0036
52.624051841114996029251285380391\u0032
55.765510755019979311683492773463\u0032
58.906983926080942132834406634615\u0036
62.048469190227169882852500264652\u0037
65.189964800206860440636033742513\u0035
68.331469329856798270992303839985\u0031
71.472981603593732825063073856130\u0037
74.614500643701837883820540469336\u0038
77.756025630388055037739371891233\u0038
80.897555871137627863772143490870\u0038
84.039090776938190157879638348000\u0033
87.180629843641153651261805069052\u0039
90.322172637210480055717766777622\u0038
93.463718781944774171190591543970\u0039
96.605267950996268778121617323928\u0031
99.746819858680596470279979000082\u0035

Then, calculations were carried out on grids having N = 3 – 23 nodes. Below, the corresponding errors in the first eigenvalue are presented: 3) 0.11; 4) 0.53e-02; 5) 0.37e-03; 6) 0.54e-04; 7) 0.2e-05; 8) 0.23e-06; 9) 0.64e-08; 10) 0.68e-09; 11) 0.15e-10; 12) 0.14e-11; 13) 0.27e-13; 14) 0.23e-14; 15) 0.36e-16; 16) 0.28e-17; 17) 0.39e-19; 18) 0.28e-20; 19) 0.35e-22; 20) 0.23e-23; 21) 0.26e-25 ; 22) 0.15e-26; 23) 0.33e-28.

For these tabular data, analytical approximation $\varepsilon = \varepsilon(N)$ was found: $ln\varepsilon = a + bN + cN^2 + dN^3 + eN^4 + fN^5$; a = 0.39307047, b = 0.58615539, c = 0.40323914, d = –0.599229377, e = 0.12421718, f = –0.0076898089.

Thus, the error decreases exponentially. As was already mentioned, both the finite-difference and finite-element methods provide only power-law rate of error decrease.

References

1. Vayniko G. M. Asymptotic error estimates in the projection methods for eigenvalue problem. Zh. Vichisl. Matem. Mat. Fiz., 1964. V. 4, No. 3. pp. 405–425.
2. Prikazchikov V. G. Homogeneous high-order finite-difference schemes for the Sturm-Liouville problem. Zh. Vichisl. Matem. Mat. Fiz., 1964. V. 4, No. 3. pp. 687–698.

3. Babenko K. I. Foundations of numerical analysis. Moscow, Nauka, 1986, 744 p.
4. Hubbard B. E. Bounds for eigenvalues of the Sturm-Liouville problem by finite difference methods //Arch. Ration. Mech. and Anal. 1962. Vol. 10, № 2, P. 171–179.
5. Algazin S. D. Localization of eigenvalues of closed linear operators. Siberian Math. Journal. 1983. V. 24, No. 2. pp. 3–8.
6. Mersier B., Osborn J., Rappaz J., Raviart P. A. Eigenvalue aproximation by mixed and hybrid methods // Math. Comput. 1981, V. 36, № 154. P. 427–453.
7. Goncharov V. L. Theory of interpolation and approximation of functions. Moscow, Gostekhteorizdat, 1954. 328 p.
8. Algazin S.D., Babenko K.I., Kosorukov A.L. On the numerical solution of eigenvalue problems. Moscow, 1975. 57 p. (Preprint Inst. Applied Mathematics No. 108).
9. Hargrave B. A. Numerical Approximation of Eigenvalues of Sturm-Liouville Systems // J. Comput. Phys. 1976, V. 20. P. 381–396.
10. Bellman R. Introduction to theory of matrixes. Moscow, Nauka, 1969. 367 p.
11. Tables of zeroes of Bessel functions. Library of mathematic tables, Issue 44. Moscow, Comput. Center USSR Acad. Sci., 1967. 95 p.

Chapter 3.
Harmonic problem

3.1. Introduction

In this chapter, algorithms are developed for practical solution of three classical spectral and boundary-value problems: Dirichlet problem, Neumann problem, and mixed boundary value problem. Since the algorithms based on the local approximation methods suffer from saturation [1], the above-mentioned problems are discretized with the global interpolating formula for a function of two variables on a disc. For the Laplace equation, the problems formulated on a simply-connected domain Γ with a smooth boundary $\partial\Gamma$ can be reduced to those on a disc by an appropriate conformal mapping. In the algorithms considered below, the conformal map is considered known. Note also, that reliable algorithms to find out the conformal map are readily available [2].

The advantage of the classical discretization methods, including the finite-difference and finite-volume methods, is that the resulting discrete problem has a sparse matrix. The two-dimensional algorithms considered here result in full matrices. However, closer inspection of the matrix structure of the finite-dimensional problem allows us to develop very efficient algorithms. It turns out that cumbersome calculations can be tabulated in small-size lookup tables. In this case, the algorithms in question can be interpreted as decoding algorithms which, by using the initial data in the form of small-size tables, build the matrix of the discrete problem. If an eigenvalue problem is considered, it remains to calculate the eigenvalues of the matrix just constructed. If, however, we need to solve the Poisson equation, it turns out that efficient solution can be found in two-dimensional and some three-dimensional domains.

As an example, two subroutines containing 41 and 35 FORTRAN operators implementing the algorithm, as well as the small-size tables used by these subroutines as the initial data, are presented in Appendix 2.

3.2. Interpolation formula for a function of two variables on a disc domain and its properties

To derive the discretization with required properties (i.e., non-saturating), K.I.Babenko's interpolation formula for a function of two variables defined on a disc domain is applied. A property of this interpolation formula is that the stricter smoothness conditions the interpolated function satisfies, the higher is the rate of its error reduction with the increase in the number of interpolation nodes. In other words, the function in question does not suffer from saturation.

Introduce on a unit disc $|\zeta|\leq 1$ a grid containing the nodes $\zeta_{\nu l} = r_\nu exp(i\theta_l)$, $r_\nu = \cos((2\nu - 1)\pi/4/m)$, $\nu = 1,2,...,m$, $\theta_l = 2\pi\, l/N$, $N = 2n + 1$, $l = 0,1,...,2n$. I.e., on the disc we introduce m circles with radii r_ν, $\nu = 1,2,...,m$, and on each circle we chose N nodes at equal angles $2\pi/N$. Here, r_ν, $\nu = 1,2,\dots,m$ are the positive roots of the Chebyshev polynomial T_{2m} of the even order $2m$. All in all, $M = mN$ nodes are chosen on the disc.

Using these nodes, we construct the interpolating formula of the form:

$$(P_M f)(r,\theta) = \sum_{l=0}^{2n}\sum_{\nu=1}^{m} f_{\nu l} L_{\nu l}(r,\theta), \qquad (3.2.1)$$

$$L_{\nu l}(r,\theta) = \frac{2T_{2m}(r)}{NT'_{2m}(r_\nu)}\left(\frac{D_n(\theta-\theta_l)}{r-r_\nu} - \frac{D_n(\theta-\theta_l+\pi)}{r+r_\nu}\right),$$

$$D_n(\theta) = 0.5 + \sum_{k=1}^{n}\cos k\theta, \quad T_m(r) = \cos(m \arccos x).$$

Here, $D_n(\theta)$ is the Dirichlet kernel, $T_m(r)$ is the Chebyshev polynomial of the order m.

The essence of this interpolation is that on the diameter of the disc the function is interpolated by the Lagrange polynomial with the nodes at the root points of the Chebyshev polynomial of the order $2m$, whereas in the θ direction, the function is interpolated by the trigonometric polynomial of the order n. In what follows, a single index will be used instead of two indices to number the interpolation nodes. In this case, the interpolation nodes are numbered sequentially, starting from the first circle ($\nu = 1$) counterclockwise ($l = 0,1,...,2n$).

The interpolating formula (3.2.1) possesses the desired properties. Indeed, (3.2.1) is an exact formula for the polynomials of two variables of the order $\omega = min(n,m-1)$. Denote the set of these polynomials by P_ω, while E_ω will denote the best approximation of the function $f \in C[D]$ (D is the unit disc) by a polynomial belonging to P_ω. Then, defined is the projector

$P_M: C[D]\to L^M$, $L^M = L(L_1,\dots, L_M)$

and the classical inequality holds:

$$|f(r,\theta) - (P_M f)(r,\theta)| \leq (1 + |P_M|_\infty) E_\omega(f), \qquad (3.2.2)$$

in which $|P_M|_\infty$ is the norm of the projector P_M. Similar to the one-dimensional case, inequality (3.2.2) shows that the corresponding interpolating formula is non-saturating. The norm of the projector P_M satisfies the relation

$$|P_M|_\infty = O(ln^2 M), \qquad (3.2.3)$$

This estimate can be further improved in a straightforward way; the slow growth of the norm $|P_M|_\infty$ is especially important in the case of biharmonic equation.
By making some assumptions on the smoothness of the class of interpolated functions, we can estimate the rate at which the best approximation E_ω is diminished as $M\to\infty$, and to obtain the particular estimates for the error of interpolating formula (3.2.1). Let

$$f(r,\theta) = (P_M f)(r,\theta) + \rho_M(r,\theta;f), \qquad (3.2.4)$$

where $\rho_M(r,\theta;f)$ is the error of interpolating formula (3.2.1) (i.e., the residual). Then, the following K.I.Babenko's theorem holds.

Theorem 7

Consider the class of functions $H^M_\infty(K;D)\subset C(D)$ satisfying on a disc D the conditions

$$\left|\frac{\partial^{k+l} f}{\partial x^k \partial y^l}\right| \le K, \quad k+l\le\mu,$$

Then, provided that $f\in H^M_\infty(K;D)$, we have

$$|\rho_M(.\,;f)|_\infty \le c_\mu K M^{-\mu/2}\log^2 M, \qquad (3.2.5)$$

where c_μ is a constant depending on μ.
Thus, analysis of formula (3.2.5) shows that, for a fixed number of interpolating nodes M, the reduction rate of the interpolation error of formula (3.2.1) increases with μ, i. e. with the smoothness of the interpolated function f. This means that the interpolating formula obtained is non-saturating.
By using the interpolating formula (3.2.1), it is easy to derive a quadrature formula for the calculation of definite integrals when the integration domain is a disc. Indeed, substituting Eq.(3.2.1) for the integrand, we arrive at the quadrature formula:

$$\int_D f(r,\theta)d\sigma = \sum_{\nu,l} f(r_\nu,\theta_l)c_{\nu l} + \delta(f), \qquad (3.2.6)$$

where $d\sigma$ is the area element, $c_{\nu l}$ are the weight coefficients, and $\delta(f)$ is the error. For $c_{\nu l}$, we have

$$c_{\nu l} = \int_D L_{\nu l}(r,\theta)d\sigma, \qquad (3.2.7)$$

they are not dependent on l. Introduce a block-diagonal matrix

$$C = \text{diag}(c_1, c_2,\ldots, c_m), \qquad (3.2.8)$$

where c_ν, $\nu = 1,2,\ldots,m$ are diagonal matrices of dimension $N\times N$ with equal values on the diagonal. For the residual of the quadrature formula, we have the following estimate:
$|\delta(f)|\le 2\pi E_\omega(f)$.
Note that all $c_{\nu l}$ are positive for large enough number of interpolating nodes.

3.3. Discretization of the Laplace operator

On an arbitrary domain $\Gamma\in R^2$ with smooth enough boundary $\partial\Gamma$, consider the problems (3.3.1), (3.3.2); (3.3.1), (3.3.3); (3.3.1), (3.3.4):

$$\Delta u(z) + f(z) = 0,\ z\in\Gamma, \qquad (3.3.1)$$

$$u|_{\partial\Gamma} = 0\ , \qquad (3.3.2)$$

$$\left.\frac{\partial u}{\partial n}\right|_{\partial\Gamma} = 0, \qquad (3.3.3)$$

$$au + \left.\frac{\partial u}{\partial n}\right|_{\partial\Gamma} = 0. \qquad (3.3.4)$$

Here, the function *f(z)* is either given, or *f(z)* = [*q(z)* + λ*p(z)*]*u(z),* where *q(z)* and *p(z)* are given functions, and in the latter case we have the eigenvalue problem for the Laplace operator; *a* is a smooth function defined on the boundary *∂Γ*; *n* is the unity vector of the outer normal to *∂Γ*. In what follows, we consider *f*, *q*, and *p* smooth functions.

Let $z = \varphi(\zeta)$, $|\zeta|\le 1$ be the conformal mapping of the unity disc onto the domain *Γ*, then in the ζ plane we obtain the same relations (3.3.1) – (3.3.4) in which, however, *u(z)* and *f(z)* must be substituted by $u(\zeta) = u(z(\zeta))$ and $|\varphi'(\zeta)|^2 f(z(\zeta))$, while instead of *a* we have $\alpha(\theta) = a(z(e^{i\theta}))\,|\varphi'(e^{i\theta})|$.

Denote by

$$K(\varsigma,\xi) = -\frac{1}{2\pi}\ln|(1-\varsigma\bar{\xi})/(\varsigma-\xi)|$$

Green's functions of the Laplace operator on a disc with the Dirichlet boundary condition. From (3.3.1), we have

$$u(\varsigma) = -\int_{|\xi|\le 1} K(\varsigma,\xi)\,|\varphi'(\xi)|^2\,[q(\xi)+\lambda p(\xi)]u(\xi)d\xi + \int_0^{2\pi} K_0(\varsigma,\theta)\psi(\theta)d\theta,$$

$$K_0(\varsigma,\theta) = \frac{1-\rho^2}{2\pi(1+\rho^2-2\rho\cos(\theta-\varphi))}, \quad \varsigma = \rho e^{i\varphi}. \qquad (3.3.5)$$

Here, ψ(θ) is the value of *u* on the boundary. For the Dirichlet problem being considered in this section, ψ(θ) = 0, while for the remaining problems the formulation needs to be changed in view of the corresponding boundary condition.

Substitute relation (3.2.1) for the function $F(\zeta) = |\varphi'(\zeta)|2f(\zeta)$, $\zeta = r\exp(i\theta)$ into (3.3.5) and, after analytical integration, we obtain

$$u(\varsigma) = \sum_{l=0}^{2n}\sum_{\nu=1}^{m} H_{\nu l}(\varsigma) z_{\nu l} f_{\nu l} + R_M(\varsigma, F), \qquad (3.3.6)$$

$$R_M(\varsigma; F) = -\int_{|\xi|\le 1} K(\varsigma,\xi)\rho_M(\xi;F)\,d\xi, \qquad (3.3.7)$$

$$H_{\nu l}(\varsigma) = -\int_{|\xi|\le 1} K(\varsigma,\xi)L_{\nu l}(\xi)d\xi, \quad \xi = r\exp(i\theta). \qquad (3.3.8)$$

If ζ in (3.3.6) runs through the interpolation nodes, we obtain the finite-dimensional problem of the form

$$u = HZf + R. \qquad (3.3.9)$$

Here, *u* is the column vector with the components containing the values of the solution being sought (or the eigenfunction) at the nodes of the grid; *H* is the matrix of dimension *M*×*M*, obtained from Eq. (3.3.8) when ζ runs through the grid nodes; *Z* is the diagonal matrix with values $z_{\nu l}$, ν = 1,2,…,*m; l* = 0,1,…,2*n* on the diagonal (see Section 3.3); *f* is either the given column vector with the components equal to values of the corresponding function at the grid nodes, or *f* = *(Q* + λ*P)u*, where *Q* and *P* are the diagonal matrices containing on the diagonal the values of corresponding functions at the grid nodes; in the latter case we have the eigenvalue problem; *R* is the discretization error vector containing the values of

function $R_M(\varsigma;F)$ (see. 3.3.7) at the grid nodes. By discarding in (3.3.9) the discretization error R, we obtain an approximate finite-dimensional problem. The perturbation introduced in the eigenvalue by discarding the approximation error will be estimated below. The error estimate for the Poisson equation differs from (3.2.5) only by an absolute constant.

3.4. Theorems on h-matrix

Theorem 8

Matrix H has the following block structure:

$$H = \begin{Vmatrix} h_{11} & h_{12} & \dots & h_{1m} \\ h_{21} & h_{22} & \dots & h_{2m} \\ \dots & \dots & \dots & \dots \\ h_{m1} & h_{m2} & \dots & h_{mm} \end{Vmatrix}, \qquad (3.4.1)$$

where $h_{\mu\nu}$, $\mu,\nu = 1,2,\dots,m$ are symmetric circulants of dimension $N\times N$, $N = 2n + 1$, the first row takes the form $b_0,b_1,\dots,b_n,b_n,\dots,b_1$, while the remaining rows are obtained from the first one by the cyclic permutation. For brevity, we refer to such matrices as h-matrices.
Proof. Calculating the integrals in (3.3.8), we obtain

$$H_{\nu l}(\varsigma) = \frac{1}{N} a_{\nu 0}(\rho) + \frac{2}{N}\sum_{k=1}^{n} a_{\nu k}(\rho)\cos k(\varphi - \theta_l), \quad \varsigma = \rho\exp(i\varphi_l), \quad \theta_l = 2\pi l / N. \qquad (3.4.2)$$

If ζ in (3.4.2) runs through the grid nodes, we obtain

$$H = \frac{2}{N}\sum_{k=0}^{n}{}' \Lambda_k \otimes h_k, \qquad (3.4.3)$$

where the prime on the summation sign means that the term for $k = 0$ is taken with the coefficient ½; Λ_k , $k = 0,1,\dots,n$ are $m\times m$ matrices:

$$\Lambda_{k\mu\nu} = a_{\nu k}(\rho_\mu), \ \mu,\nu = 1,2,\dots,m,$$

where ρ_μ is the radius of the μ-th circular grid line in the unit circle; h_k, $k = 0,1,\dots,n$ are $N\times N$ matrices:

$$h_{kij} = \cos[k2\pi(i - j)/N)], \ i,j = 1,2,\dots,N,$$

where the $\otimes$ sign denotes the Kronecker matrix product. The form of the functions $a_{\nu k}(\rho)$ is irrelevant to the proof of the theorem and will therefore be omitted. (see [3]).
The theorem follows from (3.4.3). Thus, there are a total of $m^2(n + 1)$ different elements in the matrix H. For example, for a matrix of dimensions 104×104 (8 circles with 13 points) 448 elements must be stored, and for a matrix of dimensions 1230×1230 (30 circles with 41 points) 18900 elements must be stored.
Using this property, we can compute the eigenvalues of the matrix HZ (that is, the approximate eigenvalues of the Laplace operator in an arbitrary plane region) by simple iteration combined with elimination.

Theorem 9

Let H be a real h-matrix. Then this matrix is orthogonally similar to the partitioned diagonal matrix

$$\Lambda = \mathrm{diag}(\Lambda_0, \Lambda_1, \dots, \Lambda_{2n}),$$

where Λ_j is an $m\times m$ matrix, the element (k,l) of which is the j-th eigenvalue of the matrix h_{kl}:

$$\lambda_j = b_0 + 2\sum_{p=1}^{n} b_p \cos(p\varphi_j), \quad \varphi_j = 2\pi j / N, \quad j = 0,1,....,2n, \tag{3.4.4}$$

where $b_0,b_1,...,b_n$ are the first elements of the first row of the matrix h_{kl}, with $\Lambda_j = =\Lambda_{N-j}$, $j = 1,2,\ldots,n$, that is, all the cells Λ_j, apart from Λ_0, are paired. The eigenvectors of the matrix H can also be represented in the form

$$y_\nu^{(k)} = c_\nu^{(k)} \otimes x^{(k)}, \tag{3.4.5}$$

where $x^{(k)} = [1, \exp(ik\psi_1,..., \exp(ik\psi_{2n})], \quad \psi_j = 2\pi j / N, \quad k = 0,1,...,2n,$

while $c_\nu^{(k)}$, $\nu = 1,2,...,m_1$, $m_1 \le m$ is an eigenvector of the matrix Λ_k.

Proof. We will first consider the properties of symmetric circulants of dimensions $N\times N$, $N = 2n + 1$, i. e. matrices for which the first row takes the form $b_0,b_1,...,b_n,b_n,...,b_1$, while the remaining rows are obtained from the first one by the cyclic permutation. Thus, such a matrix contains $(n + 1)$ different elements.

All matrices of this class have the same eigenvectors

$$x_j = (1, \theta_j, ..., \theta_j^{N-1}), \quad \theta_j = \exp(i\varphi_j), \quad \varphi_j = 2\pi j / N, \quad j = 0,1,...,2n,$$

the corresponding eigenvalues are

$$\lambda_j = b_0 + 2\sum_{p=1}^{n} b_p \cos(p\varphi_j), \quad j = 0,1,....,2n.$$

Evidently, λ_0 is a simple eigenvalues, while $\lambda_1,\lambda_2,...,\lambda_n$ are double ones. It can be easily checked that the class S of symmetric circulants of dimension $N\times N$ ($N = 2n + 1$) is closed with respect to algebraic operations, i.e., if $A,B\in S$, then $A + B\in S$, $AB\in S$, $A^{-1}\in S$, provided that A^{-1} exists. Also, $AB = BA$. For the algebraic operations performed for the matrices of class S, similar operations are performed on their eigenvalues. Note that we consider here only real-valued matrices, and the complex-valued form is used for the eigenvector x_j just for convenience. It means that the eigenvectors corresponding to the eigenvalue λ_j are $Re\, x_j$ and $Im\, x_j$, $j = 1,2,\ldots,n$.

A symmetric circulant can be represented in the form:

$$B_{ij} = \frac{2}{N} \sum_{k=0}^{n}{}' \lambda_k \cos[k 2\pi (i - j) / N], \quad i, j = 1,2,..., N, \tag{3.4.6}$$

where λ_k, $k = 0,1,\ldots,n$ are the eigenvalues of this matrix (see 3.4.4), the prime on the summation sign means that the term for $k = 0$ is taken with the coefficient ½.

Denote by x_{ij} ($i = 1,2,\ldots,N$, $j = 0,1,\ldots,2n$) the i-th component of the orthonormal eigenvector x_j of the symmetric circulant, and consider an orthogonal matrix

$$X = \left\| \begin{matrix} x_{10}...0\ ...\ 0\ ...\ x_{12n}\ ...\ 0 \\ .... \\ x_{N0}..0\ ...\ 0\ ...\ x_{N2n}...\ 0 \\ .... \\ 0..........x_{10}........0..........x_{12n} \\ .... \\ 0..........x_{N0}.......0..........x_{N2n} \end{matrix} \right\|.$$

Then it is easy to check that

$$\Lambda = X'HX$$

Thus, the first statement of Theorem 9 has been proven. The eigenvector of matrix H is presented in the form

$$Y = XC, \tag{3.4.7}$$

where C is the eigenvector of block-diagonal matrix Λ. Therefore, C can be presented in the block form:

$$C = \left\| \begin{matrix} c^0 \\ ... \\ c^{2n} \end{matrix} \right\|, \tag{3.4.8}$$

where c^i, $i = 0,1,\ldots,2n$ are m-dimensional vectors. In relation (3.4.8) all $c^i = 0$ for $i \neq k$, while c^k is an eigenvector of matrix Λ_k, $k = 0,1,\ldots,2n$. Now, the second statement of Theorem 9 follows from relation (3.4.7).

Corollary 1. If the eigenvalues of matrices Λ_k are simple, the corresponding matrix H has m simple eigenvalues, and all other eigenvalues are double.

Corollary 2. Matrix H is then тoand only then an h-matrix, when it is represented in form (3.4.3). This follows from Theorem 8 and formula (3.4.6) for a symmetric circulant.

Corollary 3. Let L be the class of h-matrices, and $H_1, H_2 \in L$, then $c_1H_1 + c_2H_2 \in L$ (c_1, c_2 are constants), $H_1H_2 \in L$, $H_1^{-1} \in L$, provided that H_1^{-1} exists. The inverse matrix H_1^{-1} exists then and only then, when the matrices Λ_j, $j = 0,1,\ldots,n$ are non-degenerate, and in this case $H_1^{-1} = X'\Lambda^{-1}X$, $\Lambda^{-1} = \mathrm{diag}(\Lambda_0^{-1},\ldots,\Lambda_{2n}^{-1})$ or

$$H_1^{-1} = \frac{2}{N}\sum_{k=0}^{n}{}' \Lambda_k^{-1} \otimes h_k \tag{3.4.9}$$

(compare with 3.4.3). As an example, consider the calculation of eigenvalues for a matrix of dimension 1230×1230 (30 circles, each containing 41 node). In Table 3.1, the eigenvalues calculated for a Λ_{20} matrix of dimension 30×30 are presented in the left column. In the right column, the zeroes J_{20} taken from tables are showns. Thus, even the 20-th zero of function J_{20} is calculated with the accuracy of about 6,6 %.

Table 3.1

l	***Calculated values*** $1/\sqrt{\mu_{20,l}}$	***Tabular values for zeroes of*** J_{20}
1	25.4171408136	25.4171408141
5	41.41306548	41.4130655139
10	58.600	58.6020220738
15	75.18	75.0763080700
20	97.3	91.2635481625

3.5. Construction of cells of h-matrix by discretization of Bessel equations

Consider the spectral Dirichlet problem for the Laplace operator for $q = 0$ and $p = 1$. It is known that on a disc domain, the eigenfunctions $u_{kj}(r,\theta)$ and eigenvalues λ_{kj} are related by

$$u_{kj}(r,\theta) = J_k(\sqrt{\lambda_{kj}}\,r)\exp(ik\theta), \quad k = 0,1,..., \quad j = 1,2,... \quad . \tag{3.5.1}$$

It follows from the boundary condition that $\sqrt{\lambda_{kj}}$ is the j-th zero of the Bessel function J_k, and λ_{0j} are simple eigenvalues, while all other eigenvalues are double. The meaning of Theorem 9 is that the corresponding finite-dimensional problem inherits the properties described below.

1. Two-dimensional eigenvalue problem for the Laplace operator on a disc is reduced, by separation of variables, to one-dimensional problems (Bessel equations); the matrix H is orthogonally similar to the block-diagonal matrix Λ, and calculation of its eigenvalues is reduced to the calculation of eigenvalues of matrices Λ_j, $j = 0,1,\dots,n$ of dimension $m\times m$ (m – is the number of points in the radial direction).
2. Some of the eigenvalues of the Laplace operator with the Dirichlet boundary condition are simple, the others are double; this remains true for the corresponding matrix H: the eigenvalues of matrices Λ_0 are simple and, since $\Lambda_j = \Lambda_{N-j}$, $j = 1,2,\dots,n$, the remaining eigenvalues are double.
3. The form of eigenfunctions is inherited [compare (3.5.1) with (3.4.5)].
4. To the k-th Bessel equation, having the solution $J_k(\sqrt{\lambda_{kj}}\,r)$, corresponds a cell Λ_k in the block-diagonal matrix H, i. e. the eigenvalues μ_{kj} of this matrix are approximations to λ_{kj}^{-1}; the eigenvectors of matrix Λ_k: $y_j = (y_{j1} \dots\ y_{jm})'$ satisfy the approximate equality $y_{jp} \approx const\, J_k(\sqrt{\lambda_{kj}}\,r_p)$, r_p is the radius of p-th circular grid line on the disk.

Thus, by calculating the eigenvectors and eigenvalues of matrix H, we obtain the approximations for the Bessel functions and their zeroes. Vice versa, with an algorithm for the calculation of Bessel functions and their tabulated zeroes in hand, we can construct the corresponding matrices Λ_k, $k = 0,1,\dots,n$, and, afterwards, the matrix H (see. 3.4.3). The matrices Λ_k can also be calculated by discretizing the corresponding Bessel equations:

$$-[V''(r) + (1/r)V'(r)] + (k/r)^2V(r) = \lambda V(r), \;\; V(1) = 0,\ |V(0)| < \infty$$

on the grid r_ν, $\nu = 1,2,\dots,m$ (see. Section. 2).

As a result of numerical experiments, the following algorithm for construction of matrices Λ_k has been chosen:

1) matrices Λ_0 and Λ_1 are calculated using the approach described above, then their inverse matrices are calculated, Λ_0^{-1} and Λ_1^{-1}; these arrays are presented in tabular form for m = 3,5,7,9 in [4];

2) $\Lambda_{2k}^{-1} = \Lambda_0^{-1} + 4k^2R$, $\Lambda_{2k+1}^{-1} = \Lambda_1^{-1} + 4k(k+1)R$, $k = 1,2,\ldots,n$, $R = diag(r_1^{-2},\ldots,r_m^{-2})$ is a diagonal matrix.

After these matrices have been constructed, the approximate calculation of H^{-1} is performed by formula (3.4.9).

Thus, we have constructed the matrix of discrete operator $-\Delta$ on a disc with the Dirichlet boundary condition. An arbitrary domain can be reduced to the disc by appropriate conformal mapping:

$$Z^{-1}H^{-1}U = (Q + \lambda P)U$$

Here, $U = (u_i,\ldots,u_M)'$, $M = mN$ is a vector with components u_i equal to the approximate values of eigenfunction $u(\zeta)$ in i-th grid node (the nodes are numbered counterclockwise, starting from the first grid circle), i. e. $u_i \approx u(\zeta_i)$, while λ is the corresponding approximate eigenvalue; Z, Q, and P are diagonal matrices having on the diagonal the values of corresponding functions $z = |\varphi'(\zeta)|^2$, $q(\zeta)$, and $p(\zeta)$ at the grid nodes.

Finally, to construct the matrix of the discrete Dirichlet problem for the Laplace operator on a disc, two additional small arrays of numbers have to be stored, i.e., all cumbersome calculations have been put into lookup tables, and the matrix H^{-1} is calculated by simple formula (3.4.3). In [4], two small FORTRAN subroutines for the construction of h-matrix H^{-1} are presented: HMATR (41 operator) и RASPAK (35 operators). Note that the matrix H is used for the calculation of discrete matrix in the biharmonic problem.

In [3], test calculations following the approach described in this section were carried out. The domain was obtained from the disc $|\zeta|\le 1$ by the conformal mapping

$$z = \zeta(1 + (1/6)\zeta^4),\ \zeta = r\exp(i\theta),$$

and the first eigenvalues of the operator $-\Delta$ with the Dirichlet boundary condition were evaluated. The results were compared with those calculated on the grid with 30 × 41 = 1230 nodes [3]. On the grid with 3 × 49 = 147 nodes, the first eigenvalue was obtained with three correct digits after the decimal point, while the 6-th eigenvalue was obtained with one correct digit (below, the digits which coincided with those calculated on the fine grid 30×41 are presented). Note that in this calculation, two tables, each containing only 9 numbers were used to construct the matrix of the discrete problem. The results of calculations are presented in Table3.2.

Table 3.2

i	$\sqrt{\lambda_i}$				
	3×49 = 147 points	***5×29 = 145 points***	***7×21 = 147 points***	***9×15 = 135 points***	***30×41 = 1230 points***
I	2.382	2.38439	2.3844462	2.3844461	2.38444650947
2	3.7351	3.73463	3.7346119	3.73479	3.73461160260
3	3.7351	3.73483	3.7346119	3.73479	3,73461160262
4	4.64	4.6033	4.602969	4.6028	4.60299170652
5	5.24	5.214	5.21300	5.212	5.21305408450
6	5.6	5.4101	5.409670	5.409	5.40967176981

3.6. Numerical experiments

The first calculation was carried out for the epitrochoid with $n_p = 4$, $\varepsilon = 1/6$. On the disc, a grid with 135 nodes was introduced, the nodes were distributed over circles NL = 27,25,23,21,17,9,7,3,3 (starting from the first circle) [3]. In the calculations, many complex-valued pairs with the imaginary parts of the order of 10^{-4} were obtained. The second calculation was carried out on a uniform grid $9 \times 15 = 135$; all the eigenvalues obtained were real-valued. The results of calculations are presented in Table 3.3. The digits which coincide with those obtained on a fine grid $30 \times 41 = 1230$ (see. Table 3.2) are presented. The results in the third column of Table 3.2 agree quite well with those from Table 3.3. The accuracy on the non-uniform grid is much worse (the second column in Table 3.3). The reasons for this are analysed in detail in [3]. In short, one can say that in the second calculation the discrete problem inherits the properties of infinite-dimensional problem.

Table 3.3

$\sqrt{\lambda_i}$		
i	***135***	***9×15 = 135***
1	2.389	2.3844462
2	3.74	3.73479
3	3.74	3.73479
4	4.68	4.6028
5	5.22	5.2112
6	5.37	5.409

The second problem considered is the eigenvalue problem on the disc:

$$\Delta u + \lambda e^{-ar^2} u = 0,$$

$$u\big|_{r=1} = 0$$

The calculation were performed on the 15×31 grid, and the second eigenvalue was evaluated. The results are presented in Table 3.4, the second column contains the results obtained by S.V.Nesterov.

Table 3.4

a	λ_1	
	Author	***S.V.Nesterov***
0.2	6.0355037914	6.036051
0.3	6.1616424673	6.1617386
0.4	6.2878601882	6.2875
0.5	6.4139790729	6.413976
0.6	6.5400232874	6.540042
0.8	6.7917939883	6.791812

In the third calculation, the remote eigenvalues were evaluated for the domain considered in Example 1. The boundary-value problem was considered:

$$-\Delta u(x) = \lambda u(x),\ x \in G,$$

$$u\big|_{\partial G} = 0.$$

The eigenvalues are described by the asymptotic formula

$$\lambda_n = \frac{4\pi}{mesG} n + O(n^{1/2} \ln n),$$

where *mesG* is the area of domain *G*. For the epitrochoid, $mesG = \pi(1 + \varepsilon^2(n_p + 1))$. The asymptotic formula was sought for in the form $\lambda_n = a + bn + c\sqrt{n}\ln n.$ By knowing λ_n for two values of *n*, one can obtain *a* and *c*. In the calculation on grid 15×31 with $n = 100$ and $n = 200$ we obtained $a = -257.8878054$, $b = 3.51219512$, $c = 7.3121964$. Then, the results obtained from this formula were compared with those calculated directly for $100<n<200$. The difference was between 0.5 % – 4.7 %. However, a better agreement could not be reached.

3.7. Fast multiplication of h-matrix by vector with the use of Fast Fourier Transform

To estimate the number of operations necessary to multiply the *h*-matrix *H* by a vector *f*, we represent *f* in the block form:

$$f = (f_1 f_2 \dots f_m)',$$

where the vectors $f_\nu \in R^N$, $\nu = 1,2,\dots,m$, then

$$Hf = \begin{Vmatrix} h_{11} f_1 + \dots + h_{1m} f_m \\ h_{21} f_1 + \dots + h_{2m} f_m \\ \dots\dots\dots\dots\dots\dots\dots \\ h_{m1} f_1 + \dots + h_{mm} f_m \end{Vmatrix}.$$

Thus, the problem is reduced to the development of a fast algorithm for multiplication of a symmetric circulant $h_{\mu\nu}$ by vector $f_\nu \in R^N$, $\mu,\nu = 1,2,\dots,m$.
Represent the components of this vector in the form:

$$f_{\nu j} = a_{\nu 0} + \sum_{k=1}^{n} [a_{\nu k} \cos(k\varphi_j) + b_{\nu k} \sin(k\varphi_j)],\ \varphi_j = 2\pi j / N,\ N = 2n+1,\ j = 0,1,\dots,2n,$$

where

$$a_{\nu 0} = \frac{1}{N} \sum_{j=0}^{2n} f_{\nu j}, \qquad (3.7.1а)$$

$$a_{\nu p} = \frac{2}{N} \sum_{j=0}^{2n} f_{\nu j} \cos(p\varphi_j), \quad p = 1,2,\dots,n, \qquad (3.7.1б)$$

$$b_{\nu p} = \frac{2}{N} \sum_{j=0}^{2n} f_{\nu j} \sin(p\varphi_j), \quad p = 1,2,\dots,n, \quad \nu = 1,2,\dots,m. \qquad (3.7.1в)$$

Then

$$\sum_{j=0}^{2n} h_{\mu\nu ij} f_{\nu j} = a_{\nu 0}\lambda_{\mu\nu 0} + \sum_{p=1}^{n} [\lambda_{\mu\nu p} a_{\nu p} \cos(p\varphi_i) + \lambda_{\mu\nu p} b_{\nu p} \sin(p\varphi_i)],\ \ i = 0,1,\dots,2n. \quad (3.7.2)$$

Therefore, we must have an algorithm for fast calculation of the sums (3.7.1), as well as the sums involved in relation (3.7.2). These procedures are reduced to the calculation of the sums of the following form:

$$A_q = \sum_{j=0}^{N-1} f_j \exp(2\pi i \frac{qj}{N}), \quad q = 0,1,\dots,N-1, \qquad (3.7.3)$$

where $N = 2n + 1$ is an odd number. If $N = 3^\mu$, $\mu = 1,2,\dots$, the calculations will require $4N\mu$ operations; the proof is similar to the classic case.
We count now the number of operations necessary to multiply an *h*-matrix by a vector. First, we need to calculate the Fourier coefficients of vectors f_ν, $\nu = 1,2,\dots,m$ from relations (3.7.1), and then multiply m^2 circulants by the vector according to formula (3.7.2). Also, we have to perform $Nm(m-1)$ additions; all in all we obtain $O(m^2 N\log N)$ operations. For exam-

ple, with N = 27 and large m, the saving is 53 % of operations, as compared to the direct multiplication of matrix H by the vector.

To check the stability of the proposed method for the solution of the Poisson equation, we have to evaluate the norm of matrix H. Note that the exact solution of the Dirichlet problem for the Poisson equation on a disk is given by the formula

$$u(\varsigma) = \sum_i H_i(\varsigma) f_i.$$

Since for $f \equiv 1$ the solution of the corresponding Poisson equation is $u = 0.25(1\text{-}r^2)$, we have

$$\sum_i H_i(re^{i\theta}) = \frac{1}{4}(1-r^2),\ \varsigma = re^{i\theta}.$$

If $H_i(\zeta) \geq 0$, it is clear from the last equality that

$$|H|_\infty = \frac{1}{4}(1-r_m^2) < 0.25, \quad r_m = \cos\frac{(2m-1)\pi}{4m}, \tag{3.7.4}$$

where m is the number if grid circles on the disk. From the numerical experiments it was obtained that very few are negative, and their absolute values are of the order of 10^{-8}–10^{-12}. Therefore, formula (3.7.4) gives a practically exact estimate for the norm of matrix H. This estimate is supported by practical calculations.

3.8. Symmetrization of h-matrix

Theorem 10

Matrix $B = CH$, $C = diag(c_1,\dots,c_m)$ is asymptotically symmetric (see Section 3.4.1).

Proof. Denote by K the integral operator on $L_2(D)$:

$$(Kf)(x) = \int_D K(x,\varsigma) f(\varsigma) d\varsigma,$$

where $K(x,\zeta)$ is Green's function for the Dirichlet problem for the Laplace equation on a disc, and D is the unity disc. Then

$$(Kf, \mathrm{v}) = (f, K\mathrm{v}),\ \forall f, \mathrm{v} \in L_2.$$

Here, (,) denotes the scalar product on $L_2(D)$. We set

$$f(x) = L_k(x),\ v(x) = L_j(x),\ j \neq k$$

(see 2.1), then

$$(Kf, v) = \int_D H_k(\varsigma) L_j(\varsigma) d\varsigma. \tag{3.8.1}$$

Calculate now the integral involved in this relation by the quadrature formula (3.2.6):

$$\int_D H_k(\varsigma) L_j(\varsigma) d\varsigma = H_{jk} c_j + \delta_M(H_k L_j), \tag{3.8.2}$$

where δ_M is the error of the quadrature formula, while M is the number of interpolation nodes. In the same manner, we obtain that

$$(f, Kv) = H_{kj} c_k + \delta_M(H_j L_k). \tag{3.8.3}$$

Denote $B_{il} = H_{il} c_i$, then from (3.8.1) – (3.8.2) we have

$$B_{jk} - B_{kj} = \delta_M(H_k L_j) - \delta_M(H_j L_k). \tag{3.8.4}$$

The statement of the theorem follows from relation (3.8.4).

Corollary.

$$\left|B_{jk} - B_{kj}\right| \leq 2\pi E_\omega(H_k L_j) + 2\pi E_\omega(H_j L_k).$$

The data presented in Table 3.5 confirm the asymptotic symmetry of matrix $B = CH$.

Table 3.5

M	104 = 8×13	210 = 10×21	820 = 20×41
max$\lvert B_{jk}-B_{kj}\rvert$	7.8×10^{-7}	1.3×10^{-7}	3.1×10^{-9}

Let $q\neq0$, but we still consider the problem on a disc ($z\equiv1$) with $p\equiv1$. Note that in the above algorithm, the case $q\equiv0$ means that the operator Δ turns to zero, while in the case $q\neq0$ the same holds approximately for the operator $\Delta + q$. I.e., if the error to which this operator turns to zero is taken into account, all other reasoning remains valid and, therefore, the matrix $C(I-HQ)^{-1}H$ is asymptotically symmetric.

Consider now an arbitrary domain ($z\neq1$) for $p\neq1$, $p\geq p_0>0$, and assume that $q\equiv0$ (the case $q\neq0$ is treated in a similar way). Left-multiply (3.3.9) by matrix C and make substitution $u = (ZPC)^{-1/2}w$. Then, we obtain an eigenvalue problem for matrix $A = (ZPC)^{1/2}B(ZPC)^{1/2}$, where $B = CH$, while matrix $(ZPC)^{1/2}$ is diagonal, with elements $\sqrt{z_i p_i / c_i}$ on the diagonal. It is evident that matrix A, as well as B, is asymptotically symmetric.

3.9. Example of error estimate for the Dirichlet problem

As an example, consider the case $q(\varsigma) = 0$, i.e. the eigenvalue problem for the operator $-\Delta^{-1}pz$ on a unity disc D, where we denote by Pz the operator of multiplication by the function $p(\varsigma)\lvert\varphi'(\varsigma)\rvert^2$, while Δ^{-1} is the (integral) operator with kernel K. Let $\eta = 1/\Lambda_j$ be the eigenvalue being sought, then we obtain from (3.3.9) the exact equality

$$HPZu = \eta u + \eta R. \qquad (3.9.1)$$

Discarding in (3.9.1) the discretization error ηR, we obtain an approximate eigenvalue problem for the matrix HPZ.

To evaluate the error with which a simple eigenvalue is obtained, we apply the estimate (1.3.2):

$$\lvert\eta-\tilde{\eta}\rvert \leq C_M \lVert\eta R\rVert_2 .$$

Thus, the relative error $\delta\eta = \lvert\eta-\tilde{\eta}\rvert/\eta$ with which the eigenvalue was obtained does not exceed $C_M \lVert R\rVert_2$, where $\lVert R\rVert_2 = \left(\sum_{i=1}^{M} R_i^2\right)^{1/2}$, while the quantities

$$R_i = R_M(\varsigma_i; pzu), \quad z(\varsigma) = \lvert\varphi'(\varsigma)\rvert^2, \quad i = 1,2,...,M$$

are defined in (3.3.7), i. e. $R_M(\varsigma; pzu)$ is the solution of the Poisson equation with the right-hand side $\rho_M(\varsigma, pzu)$ and non-zero Dirichlet boundary condition. Due to continuous dependence of the Poisson equation solution on the right-hand side, we obtain that, for large enough M

$$\lvert R\rvert_\infty \leq C\lvert\rho_M\rvert_\infty ,$$

where by $\lvert.\rvert_\infty$ the norm in $C(D)$ is denoted. Taking into account the inequality between the vector norms $\lVert.\rVert_2$ and $\lvert.\rvert_\infty$, we obtain the inequality

$$\delta\eta \leq CC_M KM^{(1-\mu)/2}\log^2 M. \qquad (3.9.2)$$

Thus, the stricter smoothness conditions hold for the function $p(\varsigma)\left|\varphi'(\varsigma)\right|^2 u(\varsigma),\ \varsigma\in D,$ i. e. $\mu\to\infty$, the smaller is the relative error $\delta\eta$ of the calculated eigenvalue. The estimate (3.9.2) shows, therefore, that the numerical algorithm described is non-saturating.

3.10. Mixed problem

In this section, we consider the problem (3.3.1), (3.3.4). For the discretization, we apply relation (3.3.5), in which an unknown yet function $\psi(\theta)$ is involved. This functions has to be chosen in such a way, that the boundary condition (3.3.4) is satisfied.

Discretization of the first term in (3.3.5) is carried out in the same way as in Section 3, while for the function $\psi(\theta)$ we apply interpolation by a trigonometric polynomial of n-th order:

$$\psi(\theta)=\frac{2}{N}\sum_{j=0}^{2n}D_n(\theta-\theta_j)\psi_j+\rho_n(\theta;\psi),\quad \psi_j=\psi(\theta_j),$$

$$\theta_j=\frac{2\pi j}{N},\quad j=0,1,\dots,2n,$$

$$D_n(\theta-\theta_j)=\frac{1}{2}+\sum_{k=1}^{n}\cos k(\theta-\theta_j).$$

Here, ρ_n is the interpolation error, while $N = 2n + 1$ is the number of nodes on the boundary of the disc, which coincides with the number of nodes on the internal circular grid lines. Denote

$$H_j^0=\frac{2}{N}\int_0^{2\pi}K_0(\varsigma,\theta)D_n(\theta-\theta_j)d\theta=\frac{2}{N}\left\{\frac{1}{2}+\sum_{L=1}^{n}\rho^L\cos L(\varphi-\theta_j)\right\},\quad \varsigma=\rho e^{i\varphi}. \tag{3.10.1}$$

Then, we obtain from (3.3.5)

$$u(\varsigma)=\sum_{p=1}^{M}H_p(\varsigma)f_p+\sum_{j=0}^{2n}H_j^0(\varsigma)\psi_j+R_M(\varsigma;f)+\tilde{\rho}_n(\varsigma;\psi),$$
$$\tilde{\rho}_n(\varsigma;\psi)=\int_0^{2\pi}K_0(\varsigma,\theta)\rho_n(\theta;\psi)d\theta, \tag{3.10.2}$$

where $R_M(\varsigma;f)$ is the same as in Eq. (3.3.7). Eliminate now the unknowns ψ_j from relation (3.10.2). To this end, we differentiate (3.10.2) with respect to ρ and set $\rho = 1$ in the resulting relationship. Taking into account that

$$H_p(\rho e^{i\varphi})\,|_{\rho=1}=0,$$

$$H_j^0(\rho e^{i\varphi})\,|_{\rho=1}=\frac{2}{N}D_n(\varphi-\theta_j),$$

we arrive at a system of linear equations for the determination of vector $\psi = (\psi_0\psi_1\ldots\psi_{2n})$:

$$\sum_{j=0}^{2n}B_{ij}\psi_j+\sum_{p}H_p'(\theta_i)f_p+\delta_i,$$
$$B_{ij}=\alpha_i\delta_{ij}+H_j^{0'}(\theta_i),\quad \alpha_i=\alpha(\theta_i),$$
$$H_j^{0'}(\theta_i)=\tfrac{2}{N}\sum_{L=1}^{n}L\cos L(\theta_i-\theta_j), \tag{3.10.3}$$
$$H_{\nu l}{}'(\theta_i)=\frac{1}{N}a_{\nu 0}{}'(1)+\frac{2}{N}\sum_{k=1}^{n}a_{\nu k}{}'(1)\cos k(\theta_i-\theta_l).$$

Here, the prime denotes the derivative with respect to the argument in parentheses. It is straightforward now to obtain an explicit formula for the error δ_i.
Denote $C = B^{-1}$, i. e. the matrix inverse to B**,** then we obtain from (3.10.3)

$$\psi_j = -\sum_{i=0}^{2n} C_{ji} \left(\sum_p H'_p(\theta_i) f_p + \delta_i \right).$$

Substite this relation into (3.10.2) to obtain

$$u(\varsigma) = \sum_p H_p(\varsigma) f_p - \sum_{j=0}^{2n} H_j^0(\varsigma) \sum_{i=0}^{2n} C_{ji} \sum_p H'_p(\theta_i) f_p + \hat{\delta}. \tag{3.10.4}$$

Let in (3.10.4) $\varsigma = \varsigma_q$, and $q = 1,2,...,M$ runs through all interpolation nodes, then we have

$$u = (H - E) f + \hat{\delta}. \tag{3.10.5}$$

Here, $u = (u_1,u_2,...,u_M)'$ is a column vector, while $u_i = u(\varsigma_i)$, $i = 1,2,\ldots,M$ are the values of the function being sought at the grid nodes; f is either a given vector, or $f = Z(Q + + \lambda P)$, where Z, Q, and P are diagonal matrices. For the error $\hat{\delta}$, an explicit formula can be easily obtained. The elements of matrix E are determined by the relation

$$E_{pq} = \sum_{j=0}^{2n} H_j^0(\varsigma_q) \sum_{i=0}^{2n} C_{ji} H_p{}'(\theta_i), \quad p,q = 1,2,...,M. \tag{3.10.6}$$

Discarding the discretization error $\hat{\delta}$ in (3.10.5), we obtain an approximate finite-dimensional problem.

We analyze now the structure of matrix E. Denote by $H_0 = \begin{pmatrix} b_1 \\ b_2 \\ ... \\ b_m \end{pmatrix}$ the block matrix. Here, the matrices b_ν are symmetric circulants of dimension $N\times N$. For the elements of these matrices, we have the following expression

$$b_{\nu ij} = \frac{1}{N} + \frac{2}{N} \sum_{l=1}^{n} r_\nu^l \cos l(\theta_i - \theta_j), \quad i, j = 1,2,...,N, \tag{3.10.7}$$

where r_ν is the radius of ν-th circle on the disc. Introduce another block matrix

$$H_1 = (d_1\, d_2 \ldots d_m),$$

where d_ν, $\nu = 1,2,\ldots,m$ are symmetric circulants of dimension $N\times N$, and

$$d_{\nu ij} = \frac{1}{N} a_{\nu 0}{}'(1) + \frac{2}{N} \sum_{k=1}^{n} a_{\nu k}{}'(1) \cos k(\theta_i - \theta_j), \quad i, j = 1,2,...,N,$$
$$a_{\nu k}{}'(1) = \frac{d}{d\rho} a_{\nu k}(\rho) \Big|_{\rho=1} \tag{3.10.8}$$

(see Section 4.2). For the elements of matrix B it is straightforward to write explicit formulas (see 3.10.3):

$$B_{ij} = \frac{2}{N} \sum_{l=1}^{n} l \cos l(\theta_i - \theta_j), \quad \theta_i = \frac{2\pi i}{N}, \quad i, j = 1,2,... , \ N, \quad i \neq j;$$

$$B_{ii} = \alpha_i + \frac{n(n+1)}{2n+1}, \quad i = 1,2,... , \ N.$$

Thus, if $\alpha \equiv const$, the matrices B and $C = B^{-1}$ are symmetric circulants. In view of the introduced notation, we have the following expression for matrix E:

$$E = H_0 C H_1 = \begin{pmatrix} b_1 \\ b_2 \\ \dots \\ b_m \end{pmatrix} C \; d_1 \quad d_2 \quad \dots \quad d_m \; .$$

Therefore, when $\alpha \equiv const$, the matrix $D = H\text{-}E$ is an h-matrix. This follows from the rules of operations with the circulants and h-matrices formulated in Section 3.4. Thus, for a disc with $Q = 0$, $P = 1$ and boundary condition

$$const\, u + \left.\frac{\partial u}{\partial n}\right|_{r=1} = 0$$

the structure of the matrix of finite-dimensional problem is completely similar to the structure of matrix H of the Dirichlet problem. It follows that all properties of the finite-dimensional problem formulated in Sections 3.4–3.6 are relevant to this case. The statement that the matrix D is nearly symmetrizable.

The maximum number of nodes for which calculations for a disc were carried out is 820 (20 circles, each containing 41 nodes). In the left column of Table 3.6, the simple eigenvalues are presented which are obtained for a mixed problem with boundary condition

$$u + \left.\frac{\partial u}{\partial r}\right|_{r=1} = 0. \qquad (3.10.9)$$

Table 3.6

i	$\sqrt{\lambda_i}$	
	Two-dimensional approach, 820 nodes	***One-dimensional approach, 100 nodes***
1	1.2557837116	1.25578371186
5	13.398397486	13.3983974896
10	29.08114	29.0812215613

To obtain these results, the eigenvalues of 20×20 matrix Λ_0 were calculated. In the right column, the eigenvalues are presented obtained on 100 nodes for the following one-dimensional problem:

$$\left(\frac{d^2}{dr^2} + \frac{1}{r}\frac{d}{dr}\right)u + \lambda u = 0, \quad 0 < r < 1,$$

$$u + u'\,|_{r=1} = 0,$$

where u is regular at zero point.

The approach to the solution of this problem is similar to that described above in the two-dimensional case. Note that in the left column, only the digits which coincide (except for the last one) with those obtained in the one-dimensional case are shown.

In Table 3.7, the eigenvalues calculated for 20×20 matrix Λ_1 are presented. For the comparison, in the right column, the zeroes of Bessel function J_0 are given.

Table 3.7

i	$\sqrt{\lambda_i}$	
	Two-dimensional approach, 820 nodes	***Zeroes of Bessel function J_0, tabular data***
1	2.4048255574	2.404825557695773
5	14.9309177085	14.930917708487786
10	30.6347	30.634606468431957

For a disc domain, the eigenfunctions of the Laplace operator take the form (3.5.1). For the boundary condition (3.10.9), the eigenvalues λ_{kj} satisfy the equation

$$J_n'(\mu)\mu + J_n(\mu) = 0, \quad \mu = \sqrt{\lambda_{kj}}.$$

Here, J_n is the Bessel function. However, $(\mu J_1)' = \mu J_0$, and, therefore, $\sqrt{\lambda_{1j}}, \quad j = 1, 2, \ ...$ are zeroes of the function J_0. In the proposed approach, these eigenvalues are matched by the eigenvalues of the matrix $\Lambda_{1.}$

In Table 3.8, the calculated eigenvalues of the matrix Λ_{20} are presented. Since no theoretical test is available in this case, we retain the same number of digital places as in Table 3.5.

Table 3.8

i	$\sqrt{\lambda_i}$
	Two-dimensional approach, 820 nodes
1	22.4446432826
5	39.6184129615
10	56.5866

In Table 3.9, the eigenvalues are presented which were calculated on a domain obtained from the disc $|\varsigma|\leq 1$ by the conformal mapping z = $\varsigma(1 + + 0{,}0625\varsigma^{12})$. The boundary of this domain has the curvature equal to -2710, i. e. of the order of 10^3 at twelve points. In the left column, the results calculated on a grid with 99 = 9 × 11 nodes (9 circles, each with 11 nodes) are presented. The middle column in Table 3.9 gives the results obtained on 369 = 9 × 41 nodes, while the right column contains the data obtained on 615 = 15 × 41 nodes. In the right column, the results are given with 8 decimal places, while in the first and second columns only the coinciding digits are shown.

Table 3.9

i	$\sqrt{\lambda_i}$		
	99 = 9 × 11 nodes	***369 = 9 × 41 nodes***	***615 = 15 × 41 nodes***
1	1.27	1.306999	1.30699932
5	3.459	3.457197	3.45719393
10	5.44	5.39657	5.39656302
15	6.8	6.66864	6.66860961
20	8.5	7.84332	7.84327034
100		19.0	18.7633305

3.11. Neumann Problem

In this section, we consider the Neumann problem (3.3.1), (3.3.3). Discretization of this problem is carried out along the lines of Section 3.10, however, in relation (3.11.3) the matrix

$$B_{ij} = \frac{2}{N}\sum_{l=1}^{n} l\cos l(\varphi_i - \varphi_J), \quad i,j = 1,2,...,N \tag{3.11.1}$$

is degenerate (the sum of all elements in each row of matrix B is zero**).** Therefore, we have to solve the system of linear equations (3.11.1) with a degenerate matrix.
Represent the matrix B in the form $B = \Omega\Lambda\Omega^{-1}$ **,** where $\Lambda = diag(\Lambda_1 ... \Lambda_N)$ is a diagonal matrix with the diagonal elements equal to the eigenvalues of the matrix B $(\lambda_N = 0)$; Ω and Ω^{-1} are $N\times N$ matrices with the elements defined as:

$$\Omega_{pq} = \theta_q^{p-1},\ \Omega_{pq}^{-1} = \frac{1}{N}\theta_p^{1-q},\ \theta_q = \exp(i\varphi_q),\ \ p,q = 1,2,...,N.$$

Thus, we need to solve a degenerate system of linear equations of the form $\Omega\Lambda\Omega^{-1}$ = d, with the right-hand side d defined in (3.10.3). Let $\xi = \Omega^{-1}\psi$, $\eta = \Omega^{-1}d$, then

$$\xi_j = \frac{1}{\lambda_j}\eta_j, \quad j = 1,2,...,N-1,$$

$$\psi_p = \sum_{q=1}^{N}\Omega_{pq}\xi_q = \sum_{q=1}^{N-1}\Omega_{pq}\xi_q + \xi_N.$$

Taking into account the form of matrices Ω and Ω^{-1}, we obtain then

$$\psi_p = \xi_N + \frac{2}{N}\sum_{l=1}^{N}\left(\sum_{q=1}^{n}\mathrm{Re}\frac{\theta_q^{p-l}}{\lambda_q}\right)d_l .$$

Substitute this relation into (3.7.2) to obtain

$$u(\varsigma) = \sum_i H_i(\varsigma) f_i + \sum_{p=0}^{2n}\left\{H_p^0(\varsigma)(\xi_N - \sum_{q=1}^{N} C_{pq}\sum_i H_i^{'}(\theta_q) f_i\right\} + \delta_0(\varsigma),$$
$$\mathrm{C_{pq}} = \frac{2}{N}\sum_{j=1}^{n}\mathrm{Re}\frac{\theta_j^{p-q}}{\lambda_j}, \ \ p,q = 1,2,...,N, \tag{3.11.2}$$

where $\delta_0(\zeta)$ is the discretization error which can be obtained in a straightforward way.
Let ζ in relation (3.11.2) run through all interpolation nodes, then we obtain

$$u = (H-E)Zf + \xi_N e + \delta, \tag{3.11.3}$$

Here, $u = (u_1,u_2,...,u_M)'$ is the column vector containing the values of the eigenfunction being sought at the interpolation nodes; f is either a given vector, or $f = Z(Q + \lambda P)u$, where Z, Q, and P are the diagonal matrices; ξ_N is an unknown yet parameter; $e = (1,1,...,1)'$ is a column vector with all elements equal to unity; the matrix E is represented in the form similar to (3.10.6), with the matrix C being a symmetric circulant defined in (3.11.2). Also, the block form $E = H_0CH_1$ is valid, with the matrices H_0 and H_1 defined in Section 3.10. If the Poisson equation with the Neumann boundary condition is considered, the vector f is given, and relation (3.11.3) shows expectedly that the problem solution can be found only to an arbitrary constant. To reduce the spectral problem (3.11.3) to the standard form, it is neces-

sary to eliminate the unknown parameter ξ_N. To this end, left-multiply relation (3.11.3) by the matrix R of the form

$$R = \begin{pmatrix} 1 & 0 & ... & 0 \\ -1 & 1 & ... & 0 \\ .... \\ -1 & 0 & ... & 1 \end{pmatrix},$$

to obtain

$$R(I-(H-E)ZQ)u = \lambda R(H-E)ZPu + \xi_N e_1 + R\delta. \quad (3.11.4)$$

Here, $e = (1,0,\ldots,0)'$ unity vector, i.e., the unknown parameter ξ_N now enters only the first equation. Thus, an additional equation is required to determine the parameter ξ_N.
This equation can be obtained from the solvability condition for the Neumann problem

$$\int_{|\varsigma|\le 1} f(\varsigma)d\varsigma = 0. \quad (3.11.5)$$

To discretize relation (3.11.5), we apply the quadrature formula considered in Section 3.2. Then we have

$$\sum_i c_i f_i + \delta_1 = 0, \quad f_i = Z_i(Q_i + \lambda P_i), \quad (3.11.6)$$

with the coefficients of the quadrature formula described by (3.2.7) (δ_1 is the discretization error).
Substituting the first row in (3.11.4) by (3.11.6), we arrive at the equation:

$$A_1 u = \lambda A_2 u + \delta_2,$$

with the matrices A_1 and A_2 obtained from the matrices $R(I-(H-E)ZQ)$ and $R(H-E)ZP$ by substituting the first row by $c_1q_1z_1...c_Mq_Mz_M$ and $-c_1p_1z_1...-c_1p_1z_M$, respectively. Inverting the matrix A_1 and discarding the discretization error, we obtain an approximate finite-dimensional eigenvalue problem

$$u = \lambda Du, \; D = A_1^{-1}A_2. \quad (3.11.7)$$

Note. If the function $q = 0$, the matrix A_1 is degenerate. However, in this case we can set $q = 1$, which is equivalent to shifting all eigenvalues by unity.

Consider the Neumann problem on a disc with $q = 0$ and $p = 1$. In this case, $\sqrt{\lambda_{nj}}$ are zeroes of J_n', i. e. zeroes of the derivatives of the Bessel functions, with λ_{0j} being simple eigenvalues ($\lambda_{01} = 0$), and the others being double. We check now how this manifests itself in the approach described above. Left-multipy relation (3.11.3) by the block-diagonal matrix $\boldsymbol{B}$ of dimension $m\times m$: $\boldsymbol{B} = diag(B...B)$, where the $N\times N$ matrix B is defined in (3.11.1). Evidently, the vector e is an eigenvector of matrix $\boldsymbol{B}$, with the corresponding eigenvalue equal to zero. Therefore, we obtain

$$Bu = B(H-E)f + \hat{\delta}, \; \hat{\delta} = B\delta. \quad (3.11.8)$$

The matrices $\boldsymbol{B}$ and $\boldsymbol{B}(H\text{-}E)$ are h-matrices, they are reduced to the block-diagonal form in the same basis, with the corresponding blocks Λ_0 identically equal to zero. Therefore, one can approximately obtain from relation (3.11.8) only the multiple eigenvalues, while the simple eigenvalues have to be obtained from the general relation (3.11.7).

The maximum number of nodes used in the calculations for a disc was 820 (20 circles, each containing 41 node). In Table 3.10, the calculated eigenvalues are presented for the matrix $(1/20)\Lambda_{20}$ of dimension 20×20 (Λ_{20} is the corresponding block in the block-diagonal form of matrix ***B****(H-E)*, while *diag*(20…20) is the corresponding block of the block-diagonal matrix ***B***).

Table 3.10

i	$\sqrt{\lambda_{20,i}}$	***Zeroes of J_{20}', tabular data***
1	22.21914648	22.21914648
2	27.71212684	27.71212684
3	31.97371525	31.97371522
4	35.6739414	35.87394150
5	39.58453	39.58453089
6	43.1765	43.17653646
7	46.688	46.68716642
8	50.13	50.13856248
9	53.6	53.54502716
10	56.6	56.91634767

In the right column, the tabulated zeroes of J_{20}' are presented, while in the left column only the coinciding digits (the last one is rounded) are shown.

As an example of calculation on a non-circular domain, consider the domain G obtained from the disc $|\varsigma|\leq 1$ by the conformal mapping $z = \varsigma(1 + 0{,}0625\varsigma^{12})$. The boundary of this domain has the curvature equal to -2710, i. e. of the order of 10^3 at twelve points. In the left column, the results calculated on a grid with 99 = 9 × 11 nodes (9 circles, each with 11 nodes) are presented. The middle column in Table 3.11 gives the results obtained on 369 = 9 × 41 nodes, while the right column contains the data obtained on 615 = 15 × 41 nodes. In the right column, the results are given with 9 decimal places, while in the first and second columns only the coinciding digits are shown.

Table 3.11

i	$\sqrt{\lambda_i}$		
	99 точек	***369 точек***	***615 точек***
2	1.763	1.7762353	1.77623579
6	3.77	3.731809	3.73180707
11	5.2	5.17767	5.17765590
16	7.0	6.47896	6.47893376
21	8.5	8.00561	8.00557953
101		19.16	19.12050681

3.12. High-precision calculation of eigenvalues for Dirichlet problem

Discretization of the zeroth-order Bessel equation is considered in Section 2; it turns out that it is sufficient to discretize the two-dimensional Laplace problem (see Section 3.5). On a unit disc, the discrete Laplace operator takes the form:

$$H = \frac{2}{N}\sum_{k=0}^{n}{}' \Lambda_k \otimes h_k,$$

where the prime on the summation sign means that the term for $k = 0$ is taken with the coefficient ½, Λ_k, $k = 0,1,\dots,n$ is a $m \times m$ matrix; h_k, $k = 0,1,\dots,n$ is a matrix of dimension $N{\times}N$: $h_{kij} = cos[k2\pi(i\text{-}j)/N)]$, $i,j = 1,2,\dots,N$, the $\otimes$ sign denotes the Kronecker matrix product. Here, a uniform grid is introduced in θ direction: $\theta_l = 2\pi l/N$, $N = 2n + 1$, $l = 0,1,\dots,2n$. In r direction, the grid can be arbitrary; here we choose $r_\nu = (1 + \cos((2\nu\text{-}1)\pi/2m))/2$, $\nu = 1,2, \dots , m$, i. e. on the unity disc we choose m circles, and introduce a uniform in θ grid on each circle.
$\Lambda_0 = \boldsymbol{B}^{-1}$, where $\boldsymbol{B}$ is the matrix of discrepe operator (inverse to the Bessel operatoe), which was obtained in Chapter 2;
$\Lambda_k = \Lambda_0 + k^2 R$, , $k = 1,2,\dots,n$; R is a diagonal matrix with elements $(1/r_\nu)^2$, $\nu = 1, 2, \dots , m$ on the diagonal.
On an arbitrary domain, the matrix of the discrete Laplace operator takes the form: $Z^{-1}H$, where Z is the diagonal matrix with elements $z_{\nu l} = |\psi'(\zeta_{\nu l})|2$, $\zeta_{\nu l} = r_\nu \exp(i\theta_l)$, $\nu = 1, 2, \dots , m$; $l = 0,1,\dots,2n$ (see the beginning of Section 3.3).

3.12.1. Numerical examples

For an analytically defined conform mapping, calculations were carried out for the epitrochoid, i.e., the domain obtained from a disc by the conformal mapping $z = \varsigma(1+\varepsilon\varsigma^{n_p})$, $|\varsigma|\le 1$, $\varepsilon < 1/(n_p + 1)$. On the grid $m = 50$, $N = 61$, the first 73 eigenvalues were obtained for $\varepsilon = 1/6$ and $n_p = 4$. Some of the results are presented in Table 3.12, the digits coinciding with those obtained on the 30×41 grid are shown in bold typeface.

Table 3.12

No.	$\sqrt{\lambda_i}$	μ	*k*	***Zeroes of Bessel function***
1	**2.38444650949604970517317**500817529	0	1	2.40483
2	**3.734811602643362**70303800592942815	1	1	3.83171
3	**3.734811602643362**70303800592946108			
4	**4.602991706363 4**1650906486673149750	2	1	**5.13562**
5	**5.213054084476 36**59441516736155214 0			
6	**5.40987176983 3**40399646015402762260	0	2	5.52008
7	**5.952840202 54**9570742666676647269 53	3	1	6.38016
8	**5.952840202 54**9570742666676647350 62			
9	**6.850462456**758452520097148416659 51	1	2	7.01559
10	**6.850462456**758452520097148416713 00			
11	**7.137450650 5**9079443266158516815009	4	1	7.58834
12	**7.259642357**62084739781928108470845			
13	**7.43089698**2285224503808439992471 77	2	2	**8.41724**
14	**8.2064159**3737488872010002074487221			

3.12.2. Discussion of results obtained

The computations were performed on a 3.00 GHz Pentium IV with 1 GB RAM. The last computation on a 50×61 grid took about 12 h. A computation on a 30×41 grid took about 30 min. A comparison of the results of computations on these two grids shows that 30 eigenvalues are computed reliably, with 6–7 digits after the decimal point. In the first eigenvalue, 21 digits after the decimal point were determined correctly. Computations were performed

with quadrupled accuracy by using a translator from Fortran (Intel Visual Fortran 9.1). The table contains all digits computed with quadrupled accuracy. The digits given in boldface are definitely correct. The first six eigenvalues were computed on a 30×41 grid on a BESM-6 computer [Table 3.2]. All digits given in the table coincided with those thus obtained (except the last ones, because of rounding).

3.12.3. Application of regular perturbation theory

The table presented above contains the eigenvalues calculated for the domain obtained from a disc by the conformal mapping $\varsigma = z(1+\varepsilon z^{n_p})$, $|z| \le 1$. Consider now a more general conformal mapping $\zeta = z(1 + \varepsilon\varphi(z))$, where $\varphi(z)$ is regular on a disc $K = \{z\colon |z|\le 1\}$, and $\forall z_1, z_2 \in K$: $|z_1\varphi(z_1) - z_2\varphi(z_2)| \le M|z_1 - z_2|$. If $|\varepsilon|\le 1/M$, the function $\zeta(z)$ maps univalently the disc K into a domain B with the boundary $\partial B = \{\varsigma : \varsigma = e^{i\theta}(1+\varepsilon\varphi(e^{i\theta})), 0 \le \theta \le 2\pi\}$. For the domains of this kind, the first eigenfunctions and eigenvalues can be obtained with the aid of perturbation theory, considering the problem solved on a disc. To analyse the numerical results, we give here the well-known formulas of this theory. Transforming the domain B to the disc, we obtain the problem on a disc domain:

$$\Delta u + |\varsigma'|^2 \lambda u = 0, \ |z| < 1 \qquad (3.12.1)$$

$$u\big|_{|z|=1} = 0, \qquad (3.12.2)$$

where

$$|\varsigma'|^2 = 1 + \varepsilon q_1(z) + \varepsilon^2 q_2(z) \qquad (3.12.3)$$

$$q_1(z) = 2(\mathrm{Re}(\varphi(z)) + \mathrm{Re}(z\varphi'(z)))$$

$$q_2(z) = |\varphi(z)|^2 + |z\varphi'(z)|^2 + 2\,\mathrm{Re}(z\varphi'(z)\overline{\varphi}(z))$$

Let $u_k(z,\varepsilon)$ and $\lambda_k(\varepsilon)$ be the solution of the eigenvalu (3.12.1), (3.12.2). Then

$$u_k(z,\varepsilon) = u_{k0}(z) + \varepsilon u_{k1}(z) + \varepsilon^2 u_{k2}(z) + \dots \qquad (3.12.4)$$

$$\lambda_k(\varepsilon) = \lambda_{k0} + \varepsilon\lambda_{k1} + \varepsilon^2\lambda_{k2} + \dots \qquad (3.12.5)$$

Substituting (3.12.4) and (3.12.5) into (3.12.1) and equalizing the terms with the same powers of ε, we obtain:

$$\Delta u_{k0} + \lambda_{k0} u_{k0} = 0, \ u_{k0}\big|_{\partial K} = 0 \qquad (3.12.6)$$

$$\Delta u_{k1} + \lambda_{k0} u_{k1} = F_1, \ u_{k1}\big|_{\partial K} = 0 \qquad (3.12.7)$$

where $F_1 = -\lambda_{k1}u_{k0} - q_1\lambda_{k0}u_{k0}$ etc. The problem (3.12.7) is solvable provided that the right-hand side F_1 satisfies the condition

$$\int_K F_1 u_{k0}\, ds = 0. \qquad (3.12.8)$$

Let λ_{k0} be a double eigenvalue, with v_{k1}, v_{k2} orthonormal in the norm $L_2(K)$ eigenfunctions (the exact for of these functions is known but is now written down here); then $u_{k0} = c_1 v_{k1} + c_2 v_{k2}$ and we obtain from (3.12.8) than

$$(\lambda_{k1} + \lambda_{k0} p_{11})c_1 + \lambda_{k0} p_{21} c_2 = 0$$

$$\lambda_{k0} p_{12} c_1 + (\lambda_{k1} + \lambda_{k0} p_{22}) c_2 = 0$$

The solvability condition gives

$$\lambda_{k1} = \lambda_{k0}\left[-\frac{p_{11}+p_{22}}{2} \pm \sqrt{0.25(p_{11}+p_{22})^2 - p_{11}p_{22} + p_{21}p_{12}}\right] \qquad (3.12.9)$$

where $p_{11} = (q_1 v_{k1}, v_{k1})$, $p_{21} = (q_1 v_{k1}, v_{k1})$, $p_{12} = (q_1 v_{k1}, v_{k2})$, $p_{22} = (q_1 v_{k2}, v_{k2})$.

For simple eigenvalues, we obtain in a similar way

$$\lambda_{k1} = \lambda_{k0}(q_1 u_{k0}, u_{k0})$$

After λ_{k1} has been found, u_{k1} can be obtained by solving the Helmgoltz equation (3.12.7).
In the particular case $\varphi(z) = z^{n_p}$, the mapping $\zeta(z)$ is univalent on the disc when $|\varepsilon| \le 1/(n_p + 1)$. In this case

$$q_1(z) = 2(n_p+1)r^{n_p}\cos n_p\theta,\ q_2(z) = (n_p+1)^2 r^{2n_p},$$

while $v_{k1} = \cos\mu\theta J_\mu(\sqrt{\lambda_k}r),\ v_{k2} = \sin\mu\theta J_\mu(\sqrt{\lambda_k}r),$

where k is the number of eigenvalue (in the increasing order), $m = m(k)$ is some function. For a large enough number k, the form of this function is known from tables [5]. We have

$$p_{11} = I_{n,\mu}\int_0^{2\pi}\cos n\theta\cos^2\mu\theta d\theta,\ p_{22} = p_{12} = I_{n,\mu}\int_0^{2\pi}\cos n\theta\sin^2\mu\theta d\theta,$$

$$p_{21} = I_{n,\mu}\int_0^{2\pi}\cos n\theta\sin\mu\theta\cos\mu\theta d\theta,$$

$$I_{n,\mu} = 2(n+1)\int_0^1 r^n J_\mu^2(\sqrt{\lambda_k}r)dr / \pi\int_0^1 J_\mu^2(\sqrt{\lambda_k}r)dr.|$$

From these, we obtain

$$p_{11} + p_{22} = 0,$$

$$\lambda_{k1} = \pm\lambda_{k0}\sqrt{p_{22}(p_{21} - p_{11})}.$$

If $p_{21} = p_{11}$, then $\lambda_{k1} = 0$, i. e. the perturbations of the eigenvalues are of the order of ε^2. Evidently, $p_{21} \ne p_{11}$ in the single case when $\mu = n_p/2$. In this case, the multiple eigenvalues are shifted substantially, while in all other cases the shift is of the order of ε^2. This subtle fact can be clearly seen in the Table presented above.
We present here, in the increasing order, the zeroes of the Bessel functions from the tables [5]:

(0,1) 2.40483; (1,1) 3.83171; **(2,1) 5.13562**; (0,2) 5.52008; (3,1) 6.38016; (1,2) 7.01559; (4,1) 7.58834; **(2,2) 8.41724**; (0,3) 8.65373; (5,1) 8.77148; (6.1) 9.3611; (3.2) 9.76102; (1,3) 10.17347; (4.2) 11.064471; (7.1) 11.08637; (2,3) 11.61984; (0,4) 11.79153; (8,1) 12.22509; (5,2) 12.33860; (3,3) 13.01520; (1,4) 13.32369; (9,1) 13.35430; (6,2) 13.58929; (4,3) 14.37254

Here, the first number in parentheses is the order of the Bessel function, the second number in the number of its zero. In bold tipeface, the first and second zeroes of J_2 are shown. They are matched by the pairs with numbers 4,5 and 13,14 in the above Table. These eigenvalues have the shift of the order of ε, whereas for all other eigenvalues the shift is of the order of ε^2. Note also that the second and third eigenvalues seem to be multiple because their values coincide for all decimal digits available.

3.13. On the calculation of eigenvalues of the Laplace operator on doubly connected domain

We considered above the eigenvalue problems for the Laplace operator on an arbitrary simply connected smooth domain, and the coefficients were constant. However, eigenvalue

problems for the Laplace operator on doubly connected domains often arise in mathematical physics. As an example, consider the flow of viscous fluid past a circular cylinder [6].
The boundary conditions at infinity are mapped onto the outer boundary of an annulus of large radius. To discretize the Navier-Stokes equations, we need to discretize the Laplace operator on the annular domain in the first place. This problem is considered below. A more generic problem, also considered below, is the eigenvalue problem for the Laplace operator on a doubly connected domain.
To construct a non-saturating algorithm, it is necessary to map the annulus onto the given doubly connected domain. In the example considered below, the conformal mapping is defined by an analytical formula. Note that reliable non-saturating algorithms for the numerical construction of conformal mapping of an annulus onto a given doubly connected domain and back are available [7, 8]. Discretization of the Laplace operator on an annular domain is performed by the *h*-matrix theory (see Sections 3.4–3.5).

3.13.1. Statement of the problem and discretization

On an arbitrary domain $\Gamma \in R^2$ with smooth enough boundary $\partial\Gamma = \partial\Gamma_1 \cup \partial\Gamma_2$, consider the problem

$$\Delta u(z) + f(z) = 0,\ z \in \Gamma, \quad (3.13.1)$$

$$u|_{\partial\Gamma_i} = 0 \quad (3.13.2)$$

$$\left.\frac{\partial u}{\partial n}\right|_{\partial\Gamma_i} = 0 \quad (3.13.3)$$

$$Au + \left.\frac{\partial u}{\partial n}\right|_{\partial\Gamma_i} = 0\,. \quad (3.13.4)$$

Here, *f(z)* is either a given function, or $f(z) = [q(z) + \lambda p(z)]u(z)$, where *q(z)* and *p(z)* are given functions; in the latter case we have an eigenvalue problem for the Laplace operator. In what follows, we assume that *f,A*, *q*, and *p* are smooth functions.
Let $z = \varphi(w)$, $\rho \le |w| \le R$ be the conformal mapping of the annulus onto domain Γ; then in the plane *w* we formally obtain the same relations (3.13.1) – (3.13.4), in which, however, *u(z)* and *f(z)* must be substituted by $u(w) = u(z(w))$ and $|\varphi'(w)|^2 f(z(w))$, while A must be substituted by $\alpha(w) = A(z(w))|\varphi'(w)|$.
On the annular domain, the discrete Laplacian is represented by an *h*-matrix (see Sections 3.4–3.5).

$$H = \frac{2}{N}{\sum_{k=0}^{n}}' \Lambda_k \otimes h_k, \quad (3.13.\ 5)$$

where the prime on the summation sign means that the term for $k = 0$ is taken with the coefficient ½, Λ_k, $k = 0,1,\dots,n$ is a $m \times m$ matrix (*m* is the number if grid circular lines on the disk, $N = 2n + 1$ is the number of nodes on each circle). The matrices Λ_k can be obtained by the discretization of the Bessel equation (see Section 2.4).

$$\varpi = \frac{z-\alpha}{\alpha z - 1}; \quad z = \frac{\varpi - \alpha}{\alpha\varpi - 1};$$

$$\alpha = \frac{1 + x_1 x_2 + \sqrt{1 - x_1^2 \quad 1 - x_2^2}}{x_1 + x_2}$$

$$R = \frac{1 - x_1 x_2 + \sqrt{1 - x_1^2 \quad 1 - x_2^2}}{x_1 - x_2}, \; (x_2 < x_1)$$

Fig. 3.1

3.13.2. Results of numerical calculations

The proposed approach was tested in numerical calculations performed for a unity disc domain with a circular cutout of the radius of 0.1 centered at the point 0.2 on the real axis. On the outer boundary, the Dirichlet boundary condition was posed, while the Neumann boundary condition was used on the inner boundary. The conformal mapping onto an annulus was carried out by the fractional linear function [9, p. 203, Fig. 1]. The results obtained are presented in Table 3.13.

Table 3.13

№	*N = 101, M = 40*	*N = 151, M = 40*
1	5.76440210757410	5.76440211324461
2	14.5747911525768	14.5747911366198
3	14.6694560235128	14.6694560125607
4	26.5370120410139	26.5370120449611
5	26.5673295743309	26.5673295924867
6	30.1504923208563	30.1504923282571
7	41.1995752439943	41.1995752225500
8	41.3273782291153	41.3273782291731
9	46.5257064528378	46.5257064185371
10	50.7190239516203	50.7190239279168
100	435.845001932850	435.845002040277
200	856.178194896293	856.178194899004
300	1301.51827733956	1301.51827732829
400	1721.46674979217	1715.78405518922
500	2182.72634222189	2176.93758302320

In Fig. 3.2, the first eigenform of the problem is presented, while in Fig. 3.3 the contours of this eigenform are shown.

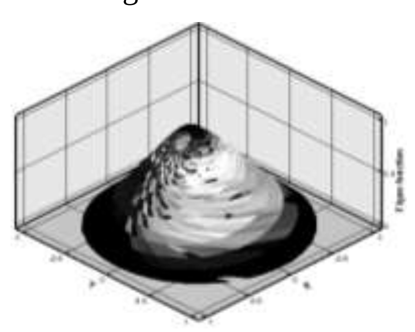


Fig. 3.2

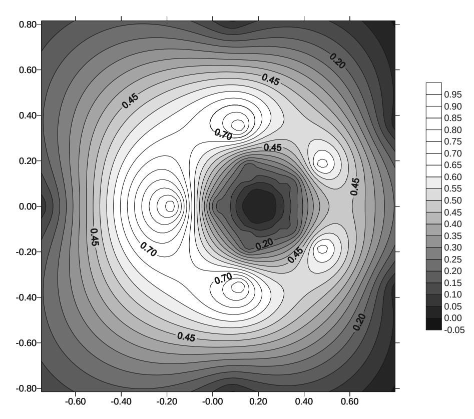


Fig. 3.3

References

1. Babenko K.I. Foundations of numerical analysis. Moscow, Nauka, 1986, 744 p.
2. Kazandzhan E.P. On a numerical method for conformal mapping of simply connected domains. Moscow, 1977. 60 p. (Preprint IPM; No. 82).
3. Algazin S. D., Kiyko I. A. Flutter of plates and shells. Moscow, Nauka, 2006, 247 p.
4. Algazin S. D., On the tabulation of eigenvalues of two-dimensional Laplace operator. M., 1982. 13 p. (Preprint, IPM; No. 34).
5. Tables of zeroes of Bessel functions. Library of mathematic tables, Issue 44. Moscow, Comput. Center USSR Acad. Sci., 1967. 95 p.
6. K. I. Babenko, N. D. Vvedenskaya, M. G. Orlova, "Steady-state viscous fluid flow around a circular cylinder," Preprint No. 41, Inst. Appl. Math. of the USSR Acad. of Sci. (1969), 36 p.
7. Volevich L. R., Kazandzhan E.P. Numerical method for conformal mapping of a doubly connected domain onto an annulus. Moscow, 1993. 25 p. (Preprint IPM No. 82)
8. Volevich L. R., Kazandzhan E.P. Numerical method for conformal mapping of an annulus onto a doubly connected domain. Moscow,1994. 19 p. (Preprint IPM No. 101).
9. Lavrik V. I., Savenkov V. N. Handbook of conformal mappings. Kiev, Naukova Dumka, 1970, 252 p.

Chapter 4.
Biharmonic problem

In Chapter 4, the results obtained in Chapter 3 are generalized to the case of biharmonic equation. We consider here the free vibrations problems for a plate, as well as the primary biharmonic problem, i.e., the boundary-value problem for the biharmonic equation for which the values of the solution and its normal derivative are posed on the boundary. For the free vibrations problem in a circular domain, the matrix of the discrete problem is an *h*-matrix and, therefore, the propositions formulated in Theorem 9 hold. In particular, this ma-

trix has a large number of repeating elements, which enables us to perform calculations on a grid with large number of nodes. This circumstance can also be used for the solution of a boundary-value problem, e.g., of the primary biharmonic problem. It is known that planar elasticity problems are reducible to the primary biharmonic problem, therefore, this problem is of high applied value.

Note that solution of the biharmonic equation is a more involved problem than solution of the Laplace equation, and larger number of grid points is required.

4.1. Statement of the problem and discretization

Algorithms are considered for the numerical solution of the boundary value problems (4.1.1) – (4.1.3) and (4.1.1), (4.1.2), (4.1.4):

$$\Delta^2 u(z) = F(z), \quad z \in G, \tag{4.1.1}$$

$$u\big|_{\partial G} = 0, \tag{4.1.2}$$

$$\left.\frac{\partial u}{\partial n}\right|_{\partial G} = 0, \tag{4.1.3}$$

$$\left.\frac{\partial^2 u}{\partial n^2} + \nu\left(\frac{\partial^2 u}{\partial s^2} + \frac{1}{\rho}\frac{\partial u}{\partial n}\right)\right|_{\partial G} = 0. \tag{4.1.4}$$

Here *G* is a domain in the complex *z* -plane with a sufficiently smooth boundary ∂G; *n* is the unit vector of the external normal to ∂G; $\partial/\partial s$ denotes differentiation with respect to the arclenqth (the length is measured counterclockwise), $1/\rho$ is the curvature of ∂G, and ν is constant (the Poisson's ratio). The function $F(z)$ is either given, or has the form $F(z) = (Q(z) + \lambda P(z))u(z)$, where *Q* and *P* are certain functions, and we have an eigenvalue problem for the biharmonic equation in this case. In particular, for $Q = 0$ and $P = 1$ we obtain the free vibrations problem for a plate, where the natural frequency ω is related to the spectral parameter λ by the relationship $\sqrt{\lambda} = \omega\sqrt{\rho_0 / D}$, where ρ_0 is the density, while *D* is the cylindrical stiffness. The boundary conditions (4.1.2) and (4.1.3) signify that the plate is clamped along the edge, while the boundary conditions (4.1.2) and (4.1.4) correspond to the case of edge support. Let $z = \varphi(\zeta)$, $|\zeta|\le 1$ be a function giving the conformal mapping of the unit radius circle onto the domain *G*. Then, in place of (4.1.1) – (4.1.4) we obtain the following relations in the plane ζ:

$$\Delta\ |\varphi'(\varsigma)|^{-2}\,\Delta u\ = |\varphi'(\varsigma)|^{2}\, f(\varsigma), \quad \varsigma = re^{i\varphi}, \ \ r < 1, \tag{4.1.5}$$

$$u\big|_{r=1} = 0, \tag{4.1.6}$$

$$\left.\frac{\partial u}{\partial r}\right|_{r=1} = 0, \tag{4.1.7}$$

$$\left.\frac{\partial^2 u}{\partial r^2} + \left\{\nu + (\nu - 1)\,\mathrm{Re}\left(\varsigma\frac{\varphi''(\varsigma)}{\varphi'(\varsigma)}\right)\right\}\frac{\partial u}{\partial r}\right|_{r=1} = 0. \tag{4.1.8}$$

Here, $f(\varsigma) = F(z(\varsigma))$; also, the condition (4.1.6) is taken into account in the boundary condition (4.1.8), i.e., we set $\partial^2 u/\partial s^2 = 0$.

A priori information about the solution, its analyticity, should be used for successful discretization of the boundary value problems (4.1.5) – (4.1.8). To this end, we invert the differential operator in the left side of relation (4.1.5) and we apply the interpolation formula

(3.2.1) for a function of two variables on a disc. Details of this procedure are to follow. We first invert the first Laplace operator in (4.1.5) to obtain

$$\Delta u(\varsigma)=|\varphi'(\varsigma)|^2\int\limits_{|\xi|\le 1}K(\varsigma,\xi)|\varphi'(\xi)|^2 f(\xi)d\xi+|\varphi'(\varsigma)|^2\int\limits_0^{2\pi}K_0(\varsigma,\theta)v\ e^{i\theta}\ d\theta\equiv S(\varsigma). \qquad (4.1.9)$$

Here, $K(\varsigma,\xi)$ is the Green's function of the Dirichlet problem for the Laplace equation, $K_0(\varsigma,\theta)$ is the Poisson kernel (see Section 3.3), and $v\ e^{i\theta}=|\varphi'\ e^{i\theta}|^2\Delta u(e^{i\theta})$ is an unknown function. We invert the Laplace operator in (4.1.9) and obtain, taking into account the boundary condition (4.1.6), that:

$$u(\varsigma)=\int\limits_{|\xi|\le 1}K(\varsigma,\xi)S(\xi)d\xi. \qquad (4.1.10)$$

We apply now the interpolation formula (3.2.1) to the functions of two variables $S(\xi)$ and $|\varphi'(\xi)|^2 f(\xi)$ on a disc, while for $v(e^{i\theta})$ we use the trigonometric interpolation

$$v(e^{i\theta})=\frac{2}{N}\sum_{j=0}^{2n}D_n(\theta-\theta_j)v_j+r_n(\theta;v),\quad \theta_j=\frac{2\pi j}{N}. \qquad (4.1.11)$$

Here, D_n is the Dirichlet kernel, $N = 2n + 1$ is the number of interpolation nodes on the boundary of the disc, while r_n is the interpolation error. We then obtain

$$u(\varsigma)=\sum_j H_j(\varsigma)z_j\sum_i H_{ji}z_i f_i-\sum_j H_j(\varsigma)z_j\sum_{p=0}^{2n}H_p^0(\varsigma_j)v_p+\delta(\varsigma), \qquad (4.1.12)$$

where $H_j(\varsigma),\ H_{ji},\ H_p^0(\varsigma),\ z_j$ were defined in Sections 3.3 and 3.10; δ is the discretization error; $v_0,v_1,\dots,v_{2n}$ are unknown quantities. We use the second boundary condition (4.1.7) or (4.1.8); for their determination tt is convenient to consider a more general problem. Let L denote the differential operator on the left-hand side of the second boundary condition, while the first boundary condition is assumed to have the same form of (4.1.6) as before. We apply the differential operator L to (4.1.12), and set in the relation obtained $\zeta = e^{i\theta}$, where θ runs through the interpolation nodes θ_j, $j = 0,1,\dots,2n$ on the boundary of the circle (see Eq. 4.1.11). Then, to determine the vector $v = (v_0,v_1,\dots,v_{2n})'$ we obtain a system of linear equations with the matrix A:

$$A_{pq}=\sum_{i=1}^{M}H_{i,p}^1 z_i H_q^0(\varsigma_i),\quad p,q=1,2,\dots,N;$$
$$H_{j,p}^1=L(H_j(\varsigma))|_{\varsigma=e^{i\theta_p}},\quad j=1,2,\dots,M,\ \ p=1,2,\dots,N \qquad (4.1.13)$$

and right-hand side $R = (R_0,R_1,\dots,R_{2n})'$, where $R_p=\sum_{i,j}^{M}H_{i,p}^1 z_i H_{ij}z_j+\delta_1$ and δ_1 is the error.

Let $C = A^{-1}$, then $v = CR$. We substitute this expression into (4.1.12), and let ζ run through the interpolation nodes within the disc in the relationship obtained. This leads to

$$u=(B^2-BEB)f+\hat{\delta}. \qquad (4.1.14)$$

Relation (4.1.14) is the end point of our considerations. Here, $u=(u(\varsigma_1),\dots,u(\varsigma_M))'$ is the vector of function $u(\zeta)$ values at the grid nodes; f is the corresponding vector of values of the right-hand side of the biharmonic equation; $B = HZ$ is the matrix of the discrete Dirichlet problem for the Laplace equation in the domain G; for the matrix E we have the following relation

$$E_{lj} = \sum_{p=0}^{2n} H_p^0(\varsigma_l) \sum_{q=0}^{2n} C_{qp} \sum_i H_{i,q}^1 z_i, \quad l, j = 1, 2, ..., M, \tag{4.1.15}$$

where $\hat{\delta}$ is the discretization error. Discarding the error $\hat{\delta}$ in (4.1.14), we obtain an approximate finite-dimensional problem. Therefore, the solution of the plate bending problem reduces to multiplying the matrix $D = B^2–BEB$ by a vector, whereas the eigenvalue (free vibrations) problem corresponds to the approximate finite-dimensional problem

$$u = (B^2 – BEB)Z(Q + \lambda P)u,$$

where $Q = diag(q(\zeta_1)...q(\zeta_M))$, $P = diag(p(\zeta_1)...p(\zeta_M))$, $Z = diag(z(\zeta_1)...z(\zeta_M))$ are the diagonal matrices having on the diagonals the values of the appropriate functions at the interpolation nodes. For the free vibrations problem $Q = 0$, $P = 1$, i.e., this problem is reduced to the calculation of eigenvalues of matrix D. Note that note that the form of the second boundary value problem is taken into account by the structure of array E.

4.2. Calculation of the matrix of finite-dimensional problem

In the algorithm described in Section 4.1, it was implied that the matrix (4.1.13) can be inverted with high enough accuracy. This issue requires detailed analysis. It turns out that the system of linear equations with this matrix is a discretized form of some on-dimensional integral equation of the first kind. Therefore, the question of finding an inverse matrix is reduced to whether the corresponding integral equation can be solved numerically. The difficulty of the numerical solution of an integral equation of the first kind depends on the rate at which its eigenvalues tend to zero.

As an example, consider the boundary condition краевое условие (4.1.3). If $\zeta = re^{i\varphi}$, then, by the differentiation of relation (4.1.10) with respect to r and setting then $r = 1$, we obtain an integral equation of the first kind from which v can be found:

$$\int_{-\pi}^{+\pi} L(\varphi,\theta) v(e^{i\theta}) d\theta = \Phi(\varphi),$$

$$\Phi(\varphi) = -\int_{|y|\le 1} K_0(y,\varphi)\left(|\varphi'(y)|^2 \int_{|\varsigma|\le 1} K(y,\varsigma)\,|\varphi'(\varsigma)|^2 f(\varsigma) d\varsigma \right) dy,$$

where we have the following relation for the kernel $L(\varphi,\theta)$:

$$L(\varphi,\theta) = \int_{|y|\le 1} K_0(y,\varphi) K_0(y,\theta)\,|\varphi'(y)|^2\, dy.$$

In particular, for the disc domain ($|\varphi'(y)|^2 = 1$)

$$L(\varphi,\theta) = L(\theta,\varphi) = \frac{1}{2\pi}\left(\frac{1}{2} + \sum_{l=1}^{\infty} \frac{\cos l(\varphi-\theta)}{l+1} \right)$$

and, evidently, the eigenfunctions of the operator L are $u_k = exp(ik\theta)$, $k = 0,1,2,\ldots$, while the corresponding eigenvalues are $\lambda_k = 1/2(k + 1)$, $k = 0,1,2,\ldots$. If a condition holds

$$0 < p_0 \le |\varphi'(\varsigma)|^2 \le p_1,\ |\varsigma| \le 1,$$

then, in a general case,

$$\frac{p_0}{2(k+1)} \le \lambda_k \le \frac{p_1}{2(k+1)}, \quad k = 0,1,2,... \ ,$$

i. e. $\lambda_k \sim 1/k$. This reasoning is confirmed by the numerical calculations. In practice, the conditioning number of the matrix A never exceeded 10^2 (the maximum n in the calculations was equal to 20).

4.3. Structure of finite-dimensional problem

We show now that, for a disc domain, the matrix $D = B^2 – BEB$ has a structure similar to that of the matrix H in the Dirichket problem, i. e. it is an h-matrix. First, consider the boundary condition (4.1.3). Then the matrix A (see 4.1.13) can be presented in the following form

$$A = (d_1 z_1 \ldots \; d_m z_m)\begin{pmatrix} b_1 \\ \ldots \\ b_m \end{pmatrix} = H_1 Z H_0 = d_1 z_1 b_1 + \ldots + d_m z_m b_m, \qquad (4.3.1)$$

where b_ν and d_ν are symmetric circulants of dimension $N\times N$ (see. 3.10.7, 3.10.8); z_ν, $\nu = 1,2,\ldots,m$ are diagonal matrices which contain on the diagonal the values of function $|\varphi'(\zeta)|^2$ at the interpolation nodes belonging to the ν-th circle, while $Z = diag(z_1 \ldots z_m)$. On a disc domain, z_ν are unity matrices and, therefore, the matrices A and $C = A^{-1}$ are symmetric circulants in this case. We then have

$$E = \begin{pmatrix} b_1 \\ \ldots \\ b_m \end{pmatrix} C(d_1 z_1 \ldots \; d_m z_m) = H_0 C H_1 Z, \qquad (4.3.2)$$

therefore, the matrix E is an h-matrix on the disc domain. It follows that the matrix D is also of the same kind. Consider now the boundary condition (4.1.4). In this case, the matrix H_1 must be substituted in (4.3.1) and (4.3.2) by the matrix

$$H_2 = (d_1^0 + \psi d_1 \;\ldots\; d_m^0 + \psi d_m)\,.$$

Here, $\psi = diag(\psi_0 \ldots \psi_{2n})$ is a diagonal matrix with

$$\psi_j = \nu + (\nu - 1)\,\mathrm{Re}\left(\varsigma \frac{\varphi''(\varsigma)}{\varphi'(\varsigma)} \right)\Bigg|_{\varsigma = e^{i\theta_j}}, \quad \theta_j = \frac{2\pi j}{N}, \quad j = 0,\ldots,2n,$$

where d_ν are symmetric circulants of dimension $N\times N$, while

$$d_{\nu ij}^0 = \frac{1}{N} a_{\nu 0}'' + \frac{2}{N}\sum_{k=1}^{n} a_{\nu k}''(1)\cos k(\theta_i - \theta_j)$$

(compare with relation 3.10.8). On a disc domain, $\psi_j = \nu$, therefore the structure of matrix H_2 is similar to that of matrix H_1, i. e. the corresponding matrix D is an h-matrix.

Thus, all properties of the finite-dimensional problem formulated above in the case of Laplace equation (see Theorem 9 in Chapter. 3) remain valid. The reasoning on the asymptotic symmetry of the matrices of finite-dimensional problem can also be extended to the present case.

4.4. Numerical solution of the fundamental biharmonic problem

The approach described above is also applicable to the solution of boundary-value problems for the biharmonic equation. As an example, consider the fundamental biharmonic problem, i.e., the boundary-value problem (4.4.1) – (4.4.3)

$$\Delta^2 u(z) = F(z), \quad z \in G, \tag{4.4.1}$$

$$u\big|_{\partial G} = \mathrm{X}(z), \tag{4.4.2}$$

$$\left.\frac{\partial u}{\partial n}\right|_{\partial G} = \Psi(z). \tag{4.4.3}$$

Suppose that F, X, and Ψ are smooth enough functions on the domain G with smooth boundary ∂G; n is a unity vector of the outer normal to ∂G. Similar to Section 4.1, we apply the conformal mapping $z = \varphi(\varsigma),\ |\varsigma| \le 1$ and reduce the problem to that for a disc domain:

$$\Delta\left(\left|\varphi'(\varsigma)\right|^{-2} \Delta u\right) = \left|\varphi'(\varsigma)\right|^{2} f(\varsigma), \quad \varsigma = re^{i\varphi},\ r < 1, \tag{4.4.4}$$

$$u\big|_{r=1} = \chi(\theta), \tag{4.4.5}$$

$$\left.\frac{\partial u}{\partial r}\right|_{r=1} = \psi(\theta), \tag{4.4.6}$$

Here, $f(\varsigma) = F(\varphi(\varsigma)),\ \chi(\theta) = \mathrm{X}(\varphi(e^{i\theta})),\ \psi(\theta) = |\varphi'(\varsigma)|\,\Psi(\varphi(\varsigma))\big|_{\varsigma=e^{i\theta}}$. The reduction of the problem (4.4.4) – (4.4.6) to its finite-dimensional form is performed along the lines of Section 4.1. Denote by

$$z(\varsigma) = |\varphi'(\varsigma)|^2, \quad u = (u_1 \ldots u_M)', \quad f = (f_1 \cdots f_M)', \quad \psi = (\psi_1 \ldots \psi_{2n})', \quad \chi = (\chi_1 \ldots \chi_{2n})'$$

the vectors of values of corresponding functions at the interpolation nodes in the interior of the disc and on its boundary. We then have

$$u = Df + BH_0C\psi + (H_0 - BH_0C\boldsymbol{B})\chi + \delta, \tag{4.4.7}$$

where δ is the interpolation error for which an explicit expression is easily obtainable. The matrices D, B, H_0, and C are defined in Section 4.1, while the elements of $N\times N$ matrix $\boldsymbol{B}$ are described by relations (3.10.3).

Thus, to obtain the approximate solution to the boundary-value problem (4.4.4) – (4.4.6) at the interpolation nodes, it is necessary to multiply the matrices D, BH_0C and H_0–$BH_0C\boldsymbol{B}$ by на вthe vectors f, ψ, and χ, correspondingly. In relation (4.4.7), the particular type of the domain is taken into account in the diagonal matrix $diag(z_1 \ldots z_M)$, while the form of the right-hand side of Eq. (4.4.1) and of the boundary conditions (4.4.2), (4.4.3) are accounted for by defining the appropriate vectors. The remaining arrays H, H_0, H_1 and $\boldsymbol{B}$ are calculated only once (they are reused in other problems). Also, there arrays contain large number ot repeating elements and can be stored in a packed form, i.e., only the non-coinciding elements have to be stored. This enables one to carry out calculations with large number of points, i.e., use fine grids and obtain solutions for complex domains.

4.4.1. Boundary-value of the second kind in plane elasticity

Let $\vec{N} = \{l, m\}$ be the vector of outer normal to the boundary of a planar domain G. In the boundary-value problem of the second kind in elasticity theory, the quantities $\bar{X} = l\sigma_x + m\tau_{xy}, \bar{Y} = m\sigma_y + l\tau_{xy}$ are given as functions of the arc length s.

$$\sigma_x = \frac{\partial^2\varphi}{\partial y^2}, \sigma_y = \frac{\partial^2\varphi}{\partial x^2},\ \tau_{xy} = -\frac{\partial^2\varphi}{\partial x \partial y} \Rightarrow \bar{X} = \frac{d}{ds}\left(\frac{\partial\varphi}{\partial y}\right),\ \bar{Y} = -\frac{d}{ds}\left(\frac{\partial\varphi}{\partial x}\right), \tag{4.4.8}$$

because $l = \frac{dy}{ds},\ m = -\frac{dx}{ds},\ \frac{d\varphi}{dn} = l\frac{\partial\varphi}{\partial x} + m\frac{\partial\varphi}{\partial y}$. We integrate the relations (4.4.8) along some arc s in positive direction (i.e., the domain remains on the left) between some point A to an arbitrary point B. As a result, we obtain the derivaives of the Airy functions at an arbitrary point B:

$$\left(\frac{\partial\varphi}{\partial x}\right)_B = K - \int_A^B \bar{Y}ds,\ \left(\frac{\partial\varphi}{\partial y}\right)_B = N - \int_A^B \bar{X}ds, \qquad (4.4.9)$$

where K and N are constants, equal to the derivatives of the Airy function at the initial point A of the arc s.

$$\frac{d\varphi}{ds} = \frac{\partial\varphi}{\partial x}\cdot\frac{dx}{ds} + \frac{\partial\varphi}{\partial y}\cdot\frac{dy}{ds}, \quad \frac{d\varphi}{dn} = \frac{\partial\varphi}{\partial x}\cdot l + \frac{\partial\varphi}{\partial y}\cdot m \Rightarrow \qquad (4.4.10)$$

$$\frac{\partial\varphi}{\partial n} = \left(K - \int_A^B \bar{Y}ds\right)l + \left(N + \int_A^B \bar{X}ds)\right)m \qquad (4.4.11)$$

Integrating relation (4.4.3) along the arc AB, we obtain

$$\varphi = M + \int_A^B \left(\frac{\partial\varphi}{\partial x}\cdot\frac{dx}{ds} + \frac{\partial\varphi}{\partial y}\cdot\frac{dy}{ds}\right)ds, \qquad (4.4.12)$$

where M is a constant, equal to the value of the Airy function at the initial point A of the arc s. For a simply connected domain, we can take $M = K = N = 0$. Relations (4.4.11) – (4.4.12) give the required boundary conditions for the Airy stress function.

Example. A disc of unity radius subjected to uniform pressure P.

$$\begin{aligned} &l = \cos\theta,\ m = \sin\theta;\ \int_0^{\theta_B} \bar{Y}ds = \int_0^{\theta_B} (-P\sin\theta)d\theta = P(\cos\theta_B - 1) \\ &\int_0^{\theta_B} \bar{X}ds = \int_0^{\theta_B} (-P\cos\theta)d\theta = -P\sin\theta_B \Rightarrow \frac{\partial\varphi}{\partial n} = P(\cos\theta - 1). \end{aligned} \qquad (4.4.13)$$

$$\begin{aligned} &\frac{dx}{ds} = -\sin\theta,\ \frac{dy}{ds} = \cos\theta;\ \frac{\partial\phi}{\partial x} = \int_0^{\theta_B} P\sin\theta d\theta = -P(\cos\theta_B - 1); \\ &\frac{\partial\phi}{\partial y} = -\int_0^{\theta_B} P\cos\theta d\theta = -P\sin\theta_B \Rightarrow \varphi = P(\cos\theta - 1). \end{aligned} \qquad (4.4.14)$$

One can see that the solution to the biharmonic equation for the stress function φ is $\varphi(r,\theta) = \Pr\cos\theta - P\frac{r^2+1}{2}$, $\Delta\varphi = -P$, $\Delta^2\varphi = 0$, $\sigma_r = -P$, $\sigma_\theta = -P$, $\sigma_{r\theta} = 0$. Below, these relations are verified numerically.

4.4.2. Numerical results

M = 3

LAMDA0

411.941825936000	-45.1418752798000	35.1897397936000
-61.1418752812000	29.3333333334000	-24.1914580529000
7.47692687292000	-8.19145805268000	14.7248407322000

LAMDA1

457.798232344000	-58.2837505577000	26.6666666663000
-80.1401570151000	37.3333333328000	-21.4734903555000
26.6666666637000	-15.6170838946000	32.8684342717000

H
3.072703287102967E-003 4.897108054159670E-005 7.912661629519048E-003
9.225931542088425E-004 1.851480750724176E-003 9.834251950685169E-004
5.091108187864103E-003 7.422023971035210E-006 5.864197530894739E-002
1.003086419751928E-002 2.637849805529612E-002 7.405923002689522E-003
8.491365332530898E-004 -1.891902224943439E-005 5.271915806639309E-002
2.663186736894871E-002 7.022976584898476E-002 2.811460916650774E-002
H0
0.977283884192709 1.135805790356844E-002 0.804737854124341
9.763107293777336E-002 0.505879363401625 0.247060318299167
H1
-0.108587098243639 -1.262006433727989E-003 -0.223538292812323
-2.711974248272058E-002 -5.620881815570976E-002 -2.745114647766744E-002
Calculated values
-5.805246567609952E-004 -1.44946926409002 -1.44946926409134
-4.289321881254655E-002 -1.10355339059199 -1.10355339059296
-0.274674603947669 -0.662903171601183 -0.662903171601538
Exact solution of biharmonic equation
-5.805246570408373E-004 -1.44946926409023 -1.44946926409155
-4.289321881341146E-002 -1.10355339059312 -1.10355339059409
-0.274674603951133 -0.662903171605274 -0.662903171605630
Calculated values of SR
-0.999999999995613 -0.999999999996407 -0.999999999996634
-1.00000000000812 -1.00000000000960 -1.00000000001144
-1.00000000002038 -1.00000000002165 -1.00000000002718
Calculated values of ST
-0.999999999943313 -0.999999999939767 -0.999999999930829
-0.999999999976463 -0.999999999979729 -0.999999999979501
-1.00000000001654 -1.00000000001965 -1.00000000002134
Calculated values of SRT
9.653502482184841E-013 5.162537064506978E-013 -1.480371381035184E-012
-9.150363476285156E-013 1.972200180944128E-012 -1.057376408652999E-012
-9.286324583257371E-013 3.566924533515703E-012 -2.639222174138922E-012

4.4.3. Conclusions

To solve the test problem, two tables were requred: H contained 18 numbers, H0 contained 6 numbers, and H1 contained 6 чисел. Thus, we can state that the tabulation problem has been solved.

4.5. Numerical examples

Consider first the problem of free vibrations of a disc. The maximum number of points with which the computations were performed is 820 (20 circles of 41 points). As was mentioned above, evaluation of the eigenvalues of the corresponding matrix of dimension 820×820 is reduced to the evaluation of eigenvalues of 2l matrices of dimension 20×20. Therefore, all eigenvalues of the original matrix can be obtained. In Table 4.1, the single eigenvalues of the corresponding discrete problem matrix are presented (columns 1 and 3); for comparison, the values obtained by a one-dimensional method on a grid with 100 nodes are (in a circular domain, by separation of variables the eigenvalue problem for the biharmonic equation can be reduced to one-dimensional problems which can be solved by the method similar to that developed for the two-dimensional problems). For the second-type boundary condition problem Poisson's ratio ν was taken equal to 0.25. The results obtained by one-dimensional method are given in Table 4.1 with twelve significant digits; while for the data obtained by the two-dimensional method only the correct (coinciding) digits are retained.

Table 4.1

i	λ_i			
	first-type boundary value problem 820 nodes	***One-dimensional method, 100 nodes***	***second-type boundary value problem 820 nodes***	***One-dimensional method, 100 nodes***
1	104.3631056	104.363105916	23.62085804	23.6208580299
2	1581.744	1581.74636379	879.8434	879.843510932
3	7939.549	7939.54527889	5491.016	5491.02409476
4	25022.26	25022.1915197	19117.1548	19117.1544172
5	61012.	61014.1567852	49356.	49357.5252428

It is of interest to compare these results with those obtained on a coarse grid. For example, on a grid with $9 = 3 \times 3$ nodes on the disc domain, we obtain the first eigenvalue for the boundary-value problems of the first and second kinds the values 103.1 and 23.66 respectively. Note that, when constructing the matrix D of the discrete problem, the array H is obtained according to the approach described in Section 3.5. Note also that seven lowest eigenvalues for both boundary-value problems were obtained in [1]. These results are given in Table 4.2. Here, the 1st and 4th eigenvalues are simple, they correspond to the 1st and 2nd eigenvalues in Table 4.1. Thus, the calculations presented in [1] are inaccurate (especially for the boundary condition of simple support). As an example, we also present the 1st eigenvalue of the matrix block Λ_4 for the boundary-value problem of the second kind: 3224.568989. This eigenvalue is matched by the seventh eigenvalue from Table 4.2.

Table 4.2

i	***Results*** [*1*]	
	Boundary-value problem of the 1st kind	***Boundary-value problem of the 2nd kind***
I^x	104.344	24.774
2	452.044	194.192
3	1216.673	658.139
4^x	1561.306	885.481
5	2604.748	1594.386
6	3699.608	2353.339
7	4854.245	3259.626

Consider now the results obtained for a non-circular domain, namely, for the domain on which the Dirichlet problem was solved for the Laplace equation (see results in Table 3.2). The method of simple iteration was applied here as well, however, a larger number of calculations was performed. The following grid sizes were used: 104 (8 circles with 13 nodes), 205 (5 circles with 41 nodes), 410 (10 circles with 41 nodes) и 1230 (30 circles with 41 nodes).

The results obtained for the boundary-value problem of the first kind are presented in Table 4.3. In the last column, the results are given with 12 decimal places, while in the other columns only the digits coinciding with this result are retained. We remind that the boundary of the domain has the curvature of the order of 10^2 at four points. Nevertheless, the first eigenvalue is calculated with the error of the order of 10^{-9}.

Table 4.3

i	λ_i				
	104 nodes	***205 nodes***	***410 nodes***	***820 nodes***	***1230 nodes***
1	119.	122.58	122.60360	122.603650158	122.603650157
2	452.	461.80	461.8863	461.886402882	461.886402889
3	459.	461.84	461.9195	461.9195728	461.919572661
4	827.	827.0	827.2752	827.275347	827.275346369
5	1329.	1326.	1329.6928	1329.69367744	1329.69367746
6	1657.	1698.	1701.433	1701.4343766	1701.43437638
7	1991.	2041.	2036.1185	2036.11887	2036.11887644
8	2018.	2042.	2036.3867	2036.3871404	2036.38714010
9	3263.	3654.	3639.464	3639.46578	3639.46577182
10	3428.	3653.	3639.159	3639.16092	3639.16089134

The results obtained for the boundary-value problem of the second kind on the same domain are presented in Table 4.4.

Table 4.4

i	λ_i			
	205 nodes	***410 nodes***	***820 nodes***	***1230 nodes***
I	66.7	68.283	68.28134302	68.2813430387
2	247.	245.203	245.197378	245.197370928
3	244.	242.702	242.6973158	242.697315693
4	388.	389.321	389.3203381	389.320337997
5	–	726.904	726.9001235	726.900124761

In Table 4.5, the eigenvalues calculated for the boundary-value problem of the second kind on the domain obtained from a disc by conformal mapping $z = \zeta(1 + 0{,}0625\zeta^{12})$ are presented. The boundary of this domain (epitrochoid) has the curvature -2710 (i. e. of the order of 10^3) at 12 points.

Table 4.5

i	λ_i		
	410 nodes	***820 nodes***	***1230 nodes***
1	10.57	10.64343900	10.6434390886
2	95.6	95.7918066	95.7918067703
3	272.6	272.32445319	272.324453259
4	470.6	471.2710702	471.271070279
5	587.6	587.1410688	587.141069472

The last example to be considered in the calculation of the main vibration frequency of a clamped elliptic plate. Conformal mapping of a circle onto an ellipse was carried out numerically [2] (on 141 nodes). In Table 4.6, comparison of the results obtained with those of papers [6–7] is presented (*a* and *b* denote the semi-axes of the ellipse). The author's result is given in the last row of Table 4.6, for the first column the calculations were performed on 104 nodes (8 circles with 13 nodes), while for the second column 410 nodes were used (10 circles with 41 nodes).

Table 4.6

Author	$\sqrt{\lambda_i}$	
	a = 1, b = 0.5	***a = 1, b = 1/3***
[6]	28.5148	60.3179
[7]	27.5	56.9
x	27.2	56.4

4.5.1. Further numerical studies

The first calculation was carried out or the epitrochoid (n = 4, ε = 1/6*)*. The boundary-value problem of the first kind was solved. On the disc, a grid with 9 circular lines was introduced, with the number of nodes on the circles equal to NL = 27,25,23,21,17,9,7,3,3, the total number of nodes was NT = 135; the number of nodes on the outer boundary of the disc was NG = 31. The results obtained are presented in Table 4.7 (first column), in the second column the results obtained on the 15×31 grid are shown, while in the third column the results obtained on the 30×41 grid from Table 4.3 are presented.

Table 4.7

i	λ_i		
1	117.	122.3	122.6037
2	391.	461.2	461.8864
3	391.	461.2	461.9196
4	845.	827.1	827.2753
5	1304.	1329.1	1329.6937
6	1305.	1698.	1701.4344

From this Table it is evident that the accuracy of the calculations is rather low, which is explained by the challenging nature of this problem. The second calculation was carried out for the same domain; the boundary-value problem of the second kind was solved with Poisson's ratio taken to be 0.25. In Table 4.8, the first column contains the results obtained on the 15×31 grid, while in the second column the results obtained on 30×41 grid are given (see Table 4.4).

Table 4.8

i	λ_i	
1	60.	68.2813
2	227.	242.6973
3	235.	245.1974
4	389.2	389.3203
5	717.	726.9001

One can see that the accuracy is even worse, which is explained by the more computationally challenging nature of the boundary-value problems of the second kind.

Remark. During the calculation of eigenvalues of matrix D, the subroutine *HQR*2 from the package *EISPACK* returned an error due to reaching the maximum number of iterations equal to 31. This subroutine was modified, and the maximum number of iterations was taken equal 100. The modified subroutine is named *HQR*2*M*. The final calculation to be considered in the boundary-value problem of the first kind on a disc:

$$\Delta^2 u - \lambda e^{-ar^2} u = 0,\ u\big|_{r=1} = \frac{\partial u}{\partial r}\bigg|_{r=1} = 0.$$

The first eigenvalue was calculated on the 13×25 grid. The results obtained are presented in Table 4.9, in the second column. In the third column, results obtained by S.V.Nesterov are presented. Calculations were performed by program *BIG12P* [16].

Table 4.9

a	λ_i	
0.1	105.99635034	105.996279
0.2	107.63336375	107.6332949
0.3	109.27398562	109.2739274
0.4	110.91806178	110.91801
0.5	112.56544328	112.56540
0.6	114.21598673	114.222951
0.7	115.86955396	115.869517
0.8	117.52601185	117.5259747
0.9	119.18523224	119.1851870
1.0	120.84709172	120.8686813
1.2	124.17825731	124.178184
1.4	127.51861130	127.518526
1.6	130.86732337	130.866855
1.8	134.22362586	134.223645
2.0	137.58680951	137.58700

4.5.2. More numerical calculations

Calculations were carried out for a clamped elliptic plate with different eccentricities, they were compared with the results from [3] and, in particular, with the experiment. For e = 0.866, we obtained $\sqrt{\lambda_1} = 27.3714$, while the experimental value is 27.281 (the error is 0,3 %). The calculations carried out in [3] gave a higher value 27.737. For the same value of eccentricity, we obtained $\sqrt{\lambda_2} = 39.4700$, while the experimental value is 38.86 (the error is 1.5 %). In [3], an overestimated value 40.477 was obtained in the calculations. For other eccentricities, the calculated results coincided with those from [3], except for e = 0.95. The results of these calculations are presented in Table 4.10.

Table 4.10

i	$\sqrt{\lambda_i}$		
	Author 15×31	***Author 13×25***	[2]
1	62.6414	61.7282	66.505
2	69.5722	68.0335	-
3	86.4613	88.4150	85.940

Thus, in is the third eigenfrequency, rather than the second one, that was obtained in [3].

Remarks.

Calculations for an elongated ellipse according to this approach are quite complicated. By introducing a uniform in θ grid on the disc, we obtain that the grid nodes on the ellipse are clustered towards the imaginary axis. This explains the noticeable differences in the results obtained on the 15×31 and 13×25 grids.

4.6. Vibrations of a variable-thickness plate of an arbitrary planform with free edges

In the above discussion, we did not consider the free edge boundary conditions. In this section, we study the vibrations of a variable-thickness plate of an arbitrary planform. Only the free-edge boundary condition is considered. In a resent paper [4], vibrations of superelliptic plates of varable thickness with clamped or simply supported edges were considered. Superelliptic plates are defined as the plates with the outer egde defined by the equation $\frac{x^{2n}}{a^{2n}}+\frac{y^{2n}}{b^{2n}}=1$, where n is the order of the superellipse.

Unfortunately, the free edge boundary condition was not considered in the quoted work, although the comprehensive references cited (relevant to the two applications) allow us to judge on the state-of-the-art of the question being studied. The classical book on the vibration theory is the work by Lord Rayleigh [5]. Vibrations of plates are considered in Chaper 10 of Volume 1. A work which is cited extensively is the book by Leissa [7], which is currently available on Internet. The results most close to the present work are available in [8]. Experimental determination of natural vibration frequencies of round plates with free edges are considered in [9–11]. Unfortunately, proper comparison of the results was not possible because the experimental results are presented in dimensional form, while the material constants were not reported. Review of the comprehensive list of papers leads to the conclusion that variable-thickness plates of arbitrary planform have not been considered before. Such studies are limited only to superelliptic (or, as a particular case, elliptic and round), as well as rectangular plates. This deficiency is eliminated in the following sections.

4.6.1. Derivation of equations and boundary conditions for transverse vibrations of an elastic isotropic plate of variable thickness

Consider an elastic isotropic plate of variable thickness *h(x,y),* with the boundary of arbitrary shape which is undergoing small transverse vibrations caused by initial deflection of external force. We assume that all assumptions used in the theory of small elastic vibrations of thin plates are satisfied [12, 13]. The neutral surface separates the stretched and compressed zones of the bended plate. The displacements *w(x,y)* of the points of the neutral surface in *z* direction are referred to as the plate deflections $w_{\max} << h_{\min}$. Under these assumptions, the displacement of a point of plate *(x,y,z*) located at a distance *z* from the neutral surface is [12, 13]:

$$u=-z\frac{\partial w}{\partial x},\qquad v=-z\frac{\partial w}{\partial y},\qquad w=w(x,y).$$

For small strains, the components of the strain tensor are determined by the relations

$$\varepsilon_{xx}=-z\frac{\partial^2 w}{\partial x^2},\ \varepsilon_{yy}=-z\frac{\partial^2 w}{\partial y^2},\ \varepsilon_{xy}=\varepsilon_{yx}=-z\frac{\partial^2 w}{\partial x\partial y},$$

$$\varepsilon_{xz}=\varepsilon_{yz}=0,\ \varepsilon_{zz}=0.$$

According to Kirchhoff' s hypothesis of a plane stress state, the stress tensor components are defined in accordance with Hooke's law [12, 13]

$$\sigma_{xx}=\frac{E}{1-\sigma^2}\left(\varepsilon_{xx}+\sigma\varepsilon_{yy}\right)=-\frac{Ez}{1-\sigma^2}\left(\frac{\partial^2 w}{\partial x^2}+\sigma\frac{\partial^2 w}{\partial y^2}\right),$$

$$\sigma_{yy}=\frac{E}{1-\sigma^2}\left(\varepsilon_{yy}+\sigma\varepsilon_{xx}\right)=-\frac{Ez}{1-\sigma^2}\left(\frac{\partial^2 w}{\partial y^2}+\sigma\frac{\partial^2 w}{\partial x^2}\right),$$

$$\sigma_{xy}=\sigma_{yx}=\frac{E}{1+\sigma}\varepsilon_{xy}=-\frac{Ez}{1+\sigma}\frac{\partial^2 w}{\partial x\partial y},\ \sigma_{xz}=\sigma_{yz}=\sigma_{zz}=0$$

where E is the elastic modulus and σ is Poisson's ratio of the plate material.
The potential energy of an elementary volume for elastic deformation of the plate is given by [12, 13]:

$$dF_n=\frac{1}{2}\left(\sigma_{xx}\varepsilon_{xx}+\sigma_{yy}\varepsilon_{yy}+2\sigma_{xy}\varepsilon_{xy}\right)dxdydz.$$

or

$$dF_n=\frac{Ez^2}{2(1-\sigma^2)}\left\{\left(\Delta w\right)^2+2(1-\sigma)\left[\left(\frac{\partial^2 w}{\partial x\partial y}\right)^2-\frac{\partial^2 w}{\partial x^2}\frac{\partial^2 w}{\partial y^2}\right]\right\}dxdydz.$$

The total potential energy of the plate is equal to the integral of this quantity over the entire volume of the plate V. Going from the triple integral to the repeated one and integrating with respect to z from the lower surface of the plate $z=z_1(x,y)$ to the upper surface $z=-z_2(x,y)$, we find the total potential energy of the deformed plate

$$F_n=\frac{1}{2}\iint_S D\left\{\left(\Delta w\right)^2+2\left(1-\sigma\right)\left[\left(\frac{\partial^2 w}{\partial x\partial y}\right)^2-\frac{\partial^2 w}{\partial x^2}\frac{\partial^2 w}{\partial y^2}\right]\right\}dxdy,$$

where $D=\frac{E\left(z_1^3(x,y)+z_2^3(x,y)\right)}{3\left(1-\sigma^2\right)}$, S is the projection of the domain V onto the neutral surface.

The total kinetic energy of the plate is $K=\frac{1}{2}\iint_S \rho h\left(\frac{\partial w}{\partial t}\right)^2 dxdy$. For the problem of free vibrations, we have $U+K=const\to\delta(U+K)=0$, $w=\hat{w}(x,y)e^{i\omega t}$, $\left(\frac{\partial w}{\partial t}\right)^2=-\omega^2\hat{w}(x,y)e^{i2\omega t}$. The equation finally takes the form:

$$\delta\iint_S\left[D\left\{\left(\Delta\hat{w}\right)^2+2\left(1-\sigma\right)\left[\left(\frac{\partial^2 w}{\partial x\partial y}\right)^2-\frac{\partial^2\hat{w}}{\partial x^2}\frac{\partial^2\hat{w}}{\partial y^2}\right]\right\}-\omega^2\rho h\hat{w}^2\right]dS=0. \qquad (4.6.1)$$

In what follows, the hat above w is omitted. To make relations (4.6.1) non-dimensional, we introduce the scales:
Ω, s^{-1} – characteristic frequency, the end of the frequency range used in calculations;
L, m – characteristic linear size (diameter of the domain);
P_0, N/m^2 – characteristic pressure (1 physical atmosphere);

Introduce the non-dimensional quantities (denoted by prime):

$$x=x'L, y=' yL, w=w'L, z_1=z_1' L, z_2=z_2' L, h=h'L, D=D'p_0L^3,$$
$$\omega=\omega'\Omega, \rho=\rho' p_0/L^2\Omega^2$$

Substituting these into (4.6.1), we obtain that this relation retains its form. In what follows, we omit the primes of the dimensionless quantities.

4.6.2. Discretization

Instead of varying relation (4.6.1) and obtaining a complex equation of the fourth order in partial derivatives with boundary conditions of the second and third orders, we perform discretization of the quadratic functional (4.6.1) and obtain the problem of a stationary value of the quadratic form. The free-edge boundary conditions need not be satisfied because these boundary conditions are natural and are obtained automatically if the variation of the functional is equated to zero. To discretize the functional (4.6.1), we transform from an arbitrary region to a disc. Let $z = \psi(\varsigma)$, $\varsigma = re^{i\theta}$ be a conformal map of the disc $\varsigma| \le 1$ onto the region S, $z = x + iy$, $x = u(r,\theta)$, and $y = v(r,\theta)$, that satisfies the Cauchy-Riemann conditions:

$$\frac{\partial u}{\partial r} = \frac{1}{r}\frac{\partial v}{\partial \theta}, \quad \frac{\partial v}{\partial r} = -\frac{1}{r}\frac{\partial u}{\partial \theta}$$

Let $\Phi(x,y) = \Phi(u(r,\theta),v(r,\theta))$, then

$$\begin{pmatrix} \dfrac{\partial^2\Phi}{\partial x^2} \\ \dfrac{\partial^2\Phi}{\partial x\partial y} \\ \dfrac{\partial^2\Phi}{\partial y^2} \end{pmatrix} = A^{-1}\begin{pmatrix} \dfrac{\partial^2\Phi}{\partial r^2} \\ \dfrac{\partial^2\Phi}{\partial r\partial \theta} \\ \dfrac{\partial^2\Phi}{\partial \theta^2} \end{pmatrix} - \frac{1}{r^3\,|\,\psi'(\varsigma)\,|^6}\begin{pmatrix} c_1 \\ c_2 \\ c_3 \end{pmatrix}, \tag{4.6.2}$$

where

$$A^{-1} = \frac{1}{r^2\,|\,\psi'(\varsigma)\,|^4}\begin{pmatrix} v_\theta'^2 & \dfrac{2u'_\theta v'_\theta}{r} & \dfrac{u_\theta'^2}{r^2} \\ -u'_\theta v'_\theta & \dfrac{v_\theta'^2 - u_\theta'^2}{r} & \dfrac{v'_\theta u'_\theta}{r^2} \\ u_\theta'^2 & -\dfrac{2u'_\theta v'_\theta}{r} & \dfrac{v_\theta'^2}{r^2} \end{pmatrix}, \tag{4.6.3}$$

$$\begin{cases} c_1 = \dfrac{\partial\Phi}{\partial r} d_{11} + \dfrac{\partial\Phi}{\partial\theta} d_{12} \\ c_2 = \dfrac{\partial\Phi}{\partial r} d_{21} + \dfrac{\partial\Phi}{\partial\theta} d_{212} \\ c_3 = \dfrac{\partial\Phi}{\partial r} d_{31} + \dfrac{\partial\Phi}{\partial\theta} d_{312} \end{cases} \tag{4.6.4}$$

$$\begin{cases} e_1^{(r)} = v'_\theta u''_{r^2} - u'_\theta v''_{r^2} \\ e_2^{(r)} = v'_\theta u''_{\theta r} - u'_\theta v''_{\theta r} \\ e_3^{(r)} = v'_\theta u''_{\theta^2} - u'_\theta v''_{\theta^2} \end{cases} \tag{4.6.5}$$

$$\begin{cases} e_1^{(\theta)} = \dfrac{1}{r}(u'_\theta u''_{r^2} - v'_\theta v''_{r^2}) \\ e_2^{(\theta)} = \dfrac{1}{r}(u'_\theta u''_{\theta r} - v'_\theta v''_{\theta r}) \\ e_3^{(\theta)} = \dfrac{1}{r}(u'_\theta u''_{\theta^2} - v'_\theta v''_{\theta^2}) \end{cases} \tag{4.6.6}$$

$$\begin{cases} d_{11} = v'^2_\theta e_1^{(r)} + \dfrac{2u'_\theta v'_\theta}{r} e_2^{(r)} + \dfrac{u'^2_\theta}{r^2} e_3^{(r)} \\ d_{12} = v'^2_\theta e_1^{(\theta)} + \dfrac{2u'_\theta v'_\theta}{r} e_2^{(\theta)} + \dfrac{u'^2_\theta}{r^2} e_3^{(\theta)} \\ d_{21} = \dfrac{u'^2_\theta - v'^2_\theta}{r} e_1^{(r)} + \dfrac{v'^2_\theta - u'^2_\theta}{r} e_2^{(r)} + \dfrac{v'_\theta u'_\theta}{r^2} e_3^{(r)} \\ d_{22} = \dfrac{u'^2_\theta - v'^2_\theta}{r} e_1^{(\theta)} + \dfrac{v'^2_\theta - u'^2_\theta}{r} e_2^{(\theta)} + \dfrac{v'_\theta u'_\theta}{r^2} e_3^{(\theta)} \\ d_{31} = u'^2_\theta e_1^{(r)} - \dfrac{2u'_\theta v'_\theta}{r} e_2^{(r)} + \dfrac{v'^2_\theta}{r^2} e_3^{(r)} \\ d_{32} = u'^2_\theta e_1^{(\theta)} - \dfrac{2u'_\theta v'_\theta}{r} e_2^{(\theta)} + \dfrac{v'^2_\theta}{r^2} e_3^{(\theta)} \end{cases} \tag{4.6.7}$$

To discretize the functional (4.6.1), we apply the quadrature formula (see Section 3.2):

$$\int\limits_{|\varsigma|\le 1} f(\varsigma)d\sigma = \sum_{\nu,l} c_{\nu l} f_{\nu l}, \;\; f_{\nu l} = f(r_\nu e^{i\theta_l}),$$

$$r_\nu = \cos\frac{(2\nu-1)\pi}{4m}, \; \nu = 1,2,...,m; \; \theta_l = \frac{2\pi l}{N}, \; l = 0,1,...,2n; \; N = 2n+1. \tag{4.6.8}$$

$$c_\nu = \frac{4\pi r_\nu}{m(2n_\nu+1)}\left\{\frac{\cos\psi_\nu}{2} + \sum_{s=3(2)}^{m-1} t_s \cos s\psi_\nu\right\},$$

$$t_s = 1/(1+(-1)^{\frac{s-1}{2}} s), \; \psi_\nu = \frac{(2\nu-1)\pi}{4m}, \; s \ge 1 - \text{is odd}.$$

As a result, we obtain the steady state problem for the quadratic form:

$$J(w) = \sum_{\nu,l}\Big(\frac{c_{\nu l}}{|\psi'(\varsigma_{\nu l})|^2} D_{\nu l}\left\{(Hw)^2_{\nu l} + \frac{2(1-\sigma)}{r_\nu^4 |\psi'(\varsigma_{\nu l})|^4}\Big[(D^{(xy)}w)^2_{\nu l} - (D^{(xx)}w)_{\nu l}(D^{(yy)}w)_{\nu l}\Big]\right\}$$
$$- c_{\nu l}\omega^2\rho |\psi'(\varsigma_{\nu l})|^2 h_{\nu l} w^2_{\nu l}\Big),$$

where $(Hw)^2_{\nu l} = (\sum_{\mu,k} H_{\nu l,\mu k} w_{\mu k})^2$, H is the matric of the discrete Laplace operator obtained by the substitution of the interpolating formula (3.2.1) into the expression for the planar Laplace operator: $\Delta w = \frac{1}{r}\frac{\partial}{\partial r}(r\frac{\partial w}{\partial r}) + \frac{1}{r^2}\frac{\partial^2 w}{\partial\theta^2}$; $D^{(xy)}, D^{(xx)}, \text{and}\, D^{(yy)}$ are the matrices of numerical differentiation with respect to *x,y; x,x* and *y,y,* correspondingly. The formulas for these matrices are derived from (4.6.3) (without the factor $\frac{1}{r^2|\psi'(\varsigma)|^4}$). The matrices of numerical differentiation with respect to r and θ are determined by the numerical differentiation of the interpolating formula (3.2.1), see Chapter 3.

Introduce the (diagonal) matrices A and B:

$$A_{\nu l,\mu k} = \sum_{\nu,l} \Big(\frac{c_{\nu l}}{|\psi'(\varsigma_{\nu l})|^2} D_{\nu l} \{ H_{\nu l,\mu k} H_{\nu l,\tilde{\nu}\tilde{l}} + \frac{2(1-\sigma)}{r_\nu^4 |\psi'(\varsigma_{\nu l})|^4} [2D^{(xy)}_{\nu l,\mu k} D^{(xy)}_{\nu l,\tilde{\nu}\tilde{l}} -$$

$$- D^{(yy)}_{\nu l,\mu k} D^{(xx)}_{\nu l,\tilde{\nu}\tilde{l}} - D^{(xx)}_{\nu l,\mu k} D^{(yy)}_{\nu l,\tilde{\nu}\tilde{l}}]\},$$

$$B_{\tilde{\nu}\tilde{l}} = diag(c_{\tilde{\nu}} h_{\tilde{\nu}\tilde{l}} \rho |\psi'(\varsigma_{\tilde{\nu}\tilde{l}})|^2) .$$

As a result, we obtain the eigenvalue problem:

$$Aw - \omega^2 Bw = 0, \qquad (4.6.9)$$

where A is a symmetric matrix, B is a positively defined diagonal matrix.

Let $w = B^{-1/2} w' \Rightarrow B^{-\frac{1}{2}} A B^{-\frac{1}{2}} w' = \omega^2 w'$, then the problem is reduced to the standard algebraic eigenvalue problem.

4.6.3. Test calculations

To verify the proposed approach, calculations of eigenfrequencies were carried out for a round plate of the diameter 6.3 cm and thickness 1.00 cm. [8, Table 1, first row]. The following material constants were taken: σ = 0.25 – 0.33, E = $0.7 \cdot 10^6$ kg/см^2, ρ = 2.7 g/cm^3; the typical pressure 1 atm (physical) = $1.0133 \cdot 10^5$ N/m^2 = 1.0333 kg/cm^2. Consider first a disc of a constant-thickness:

Round plate of constant thickness, h = 0.318, σ = 0.25, M = 3, N = 7.

Below, we present three frequencies, in Hz, (starting with the fourth eigenfrequency). The bold typeface denotes the digits which coincide with the calculation on the 30×41 grid:

269.23250 **269.23**250 **439**.09552

The first three frequencies are close to zero. These arise due to the fact that the plate has free edges and can move as a rigid body. Therefore, we analyze here the fourth and higher frequencies (the results are presented in Hz).

Consider now the results for two epitrochoids. The domain is obtained by rolling a small disk of radius ε around a large disc of radius a. The trajectory of a point on a small disc is called epitrochoid. The conformal mapping of a unity disc onto this domain is defined by $\psi(\zeta) = \zeta(a + \varepsilon\varsigma^n)$, n is the number of lobes of the epitrochoid. The calculations were carried out for $2a$ = 6.3, n = 4, ε = 1/6 и n = 12, ε = 0.0625 (see above):

Epitrochoid of constant thickness h = 0.318, σ = 0.25, n = 4, ε = 1/6, M = 20, N = 41

The twelve calculated frequencies are presented below. The bold typeface shown the digits which coincide with those obtained on the 30×41 grid:

249.98432	**286.584**32	**432.21804**750
610.3171267	**610.31712**84	**983.389**49
983.38949	**1054.60509**46	**1093.6142**65
1573.1528	**1654.3861**55	**1654.3861**56

Epitrochoid of constant thickness h = 0.318, σ = 0.25, n = 12, ε = 0.0625, M = 20, N = 41.

274.76467	**282.466**50	**442.4477**8
628.72562	**628.9682**5	**999.334**10
999.50130	**1089.7138**4	**1094.1578**3
1664.890300	**1665.1821**39	**1714.69**855

Evidently, the multiple frequencies were separated into close pairs. However, in this case we obtained reliable results on a grid with 820 = 20 × 41 nodes. The bold typeface shown the digits which coincide with those obtained on the 30×41 grid.

Consider now the results obtained for a round and epitrochoid plates with variable thickness: $h = h_0(1 + \alpha_1 X + \beta_1 X^2)$, $X = x/a$, $0 \le x \le 1$ и $h = h_0(1 + \alpha_2 R + \beta_2 R^2)$, $R = r/a$, where a is the disc radius.

Results for a round plate of variable thickness

We consider first a round plate of variable thickness having the diameter of 6.3 см, thickness $h_0 = 0.318$, $\sigma = 0.25$; $\alpha_2 = 0.1$, $\beta_2 = 0.1$; M = 20, N = 41. The bold typeface shown the digits which coincide with those obtained on the 30×41 grid.

290.02341	**290.02**341	**461.9398**1
693.530831	**693.53083**2	**1076.1051**5
1076.10515	**1233.48835**64	**1233.48835**72
1884.49196	**1884.49**19585	**1906.31675**62

Then, consider a round plate of variable thickness with the diameter of 6.3 см, thickness $h_0 = 0.318$, $\sigma = 0.25$; $\alpha_1 = 0.1$, $\beta_1 = 0.1$; M = 20, N = 41. The bold typeface shown the digits which coincide with those obtained on the 30×41 grid

272.55564	**272.740**75	**439.00757**30
636.0964767	**636.10063**14	**1008.212**643
1011.598798	**1118.48739**67	**1118.48740**47
1717.0494301	**1717.04948**04	**1751.70**49

Results for an epitrochoid-shaped plate of variable thickness

Epitrochoid ($n = 4$, $\varepsilon = 1/6$) of variable thickness with the diameter of 6.3 cm, thickness $h_0 = 0.318$, $\sigma = 0.25$; $\alpha_2 = 0.1$, $\beta_2 = 0.1$; $M = 20$, $N = 41$. The bold typeface shown the digits which coincide with those obtained on the 30×41 grid.

269.09249	**309.366**392	**462.145**94
679.58259227	**679.58259**44	**1065.4926**31
1065.4926323	**1193.63349**140	**1236.90111**27
1725.5219004	**1888.4593**5906	**1888.4593**596

Epitrochoid ($n = 12$, $\varepsilon = 0.0625$) of variable thickness with the diameter of 6.3 cm, thickness $h_0 = 0.318$, $\sigma = 0.25$; $\alpha_2 = 0.1$, $\beta_2 = 0.1$; $M = 20$, $N = 41$. The bold typeface shown the digits which coincide with those obtained on the 30×41 grid.

297.51424	**307.737**14	**473.6257**63
701.9747975	**702.29257**77	**1080.758**67
1080.968931	**1234.0254**67	**1240.0909**62
1875.969	**1885.32**6695	**1903.5087**56

Epitrochoid ($n = 4$, $\varepsilon = 1/6$) of variable thickness with the diameter of 6.3 cm, thickness $h_0 = 0.318$, $\sigma = 0.25$; $\alpha_1 = 0.1$, $\beta_1 = 0.1$; $M = 20$, $N = 41$. The bold typeface shown the digits which coincide with those obtained on the 30×41 grid.

253.05042	**290.612**14	**437.50271**17
623.1580054	**624.07418**76	**996.092**92
997.4405256	**1083.85153**997	**1122.00569**54
1600.7515	**1699.243**49	**1703.850**95

Epitrochoid (n = 12, ε = 0.0625) of variable thickness with the diameter of 6.3 cm, thickness h_0 = 0.318, σ = 0.25; α_1 = 0.1, β_1 = 0.1; M = 20, N = 41. The bold typeface shown the digits which coincide with those obtained on the 30×41 grid.

278.76546	**287.074**94	**448.157**96
642.114048	**643.92996**7	**1012.164**54
1014.09035	**1118.88021**49	**1123.19799**90
1711.460192	**1715.8002**855	**1743.55**63

The vibration eigenmode is presented in Fig. 4.1.

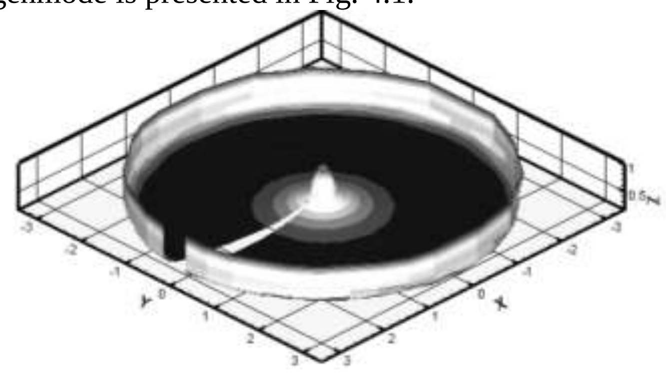


Fig. 4.1

The other vibration eigenmodes are qualitatively similar to the one just considered. Comparison with the results obtained in [14] shows that these vibration modes are also similar those corresponding to other clamping conditions at the plate edges.

4.6.4. Comparison with the results of paper " Circles in the sand: methods for reproducing Chladni's figures "✓

Table. Results for round plates, according to Kirchhoff ✓✓

v	*n = 0*	*n = 1*	*n = 2*	*n = 3*	*n = 4*	*n = 5*
0			1.0000	2.3124	4.0485	6.1982
1	1.6131	3.7032	6.4033	9.6445	13.3927	17.6304
2	6.9559	10.8383	15.3052	20.3249		
3	15.9031	21.25?				

Here, n is the number of grid diameters, v is the number of grid circles.
Comparison of author's results with tabular data:

1.00000000000000	1.00000000690236	1.59276733305282
2.39129260188748	2.39129260455010	3.71040792642247
3.71040792906338	4.25306482247617	4.25306482516895
6.49772364184144	6.49772364323961	6.57297549215343
6.57297549356766	6.94959020796884	9.34245234804938
9.34245234873495	9.88264574577113	9.88264574635396
10.8770153912733	10.8770153932567	12.5554639284132

✓ Circles in the sand: methods for reproducing Chladni's figures.
✓✓ Pitch of round plates according to Kirchhoff.

12.5554639289988	13.8214197757863	13.8214197760883
15.4415905776266	15.4415905780936	15.9300497273309
16.2075492763326	16.2075492772548	18.2917264165998
18.2917264168141	20.2952657849996	20.2952657854297
20.6224696357118	20.6224696360315	21.6484169060863

Evidently, the frequency ratios coincide with 1–2 decimal digits.

4.6.5. Comparison with results [7]

In Tables 2.5[7] and 2.6[7], the non-dimensional values of $\lambda^2 = \omega a^2(\rho/D)^{1/2}$ are presented, where ω is the vibration frequency, a is the disc radius, ρ is the mass per unit area of the plate, $D = Eh^3/12/(1-\nu^2)$ is the cylindrical rigidity (E is Young's modulus, ν is Poisson's ratio). The calculated results must coincide with the tabulated data up to a non-dimensional factor. By taking the values 5.253 (Table 2.5[7]) and 5.513 (Table 2.6[7]) for exact ones, we obtain the following results in the calculations on a grid with 20 × 41 = 820 nodes.

Table 2.5 [7].Values of $\lambda^2 = \omega a^2\sqrt{p/D}$ for a disc plate with free edge, Poisson's ratio ν = 0,***33***

s	*λ^2 as a function of n*						
	0	**1**	**2**	**3**	**4**	**5**	**6**
0	–	–	5.253	12.23	*21.6	33.1	46.2
1	9.084	20.52	35.25	52.91	*73.1	*95.8	*121.0
2	38.55	59.86	83.9	111.3	142.8	175.0	210.3
3	87.80	119.0	154.0	192.1	232.3	274.6	319.7
4	157.0	198.2	242.7	290.7	340.4	392.4	447.3
5	245.9	296.9	350.8	408.4	467.9	529.5	593.9
6	354.6	415.3	479.2	546.2	615.0	686.4	760.1
7	483.1	651.8	627.0	703.3	781.8	864.4	952.3
8	631.0	711.3	794.7	880.3	968.5	1061	1158.7
9	798.6	888.6	981.6	1076	1175	1277	1384
10	986.0	1086	1188	1292	1401	1513	1631

**Values correct within 2 % (see. 2.20 in the List of References of the quoted report)*

5.25300000000000	5.25300002193884	9.05375231514319
12.2234457145118	12.2234457315495	20.4787855881113
20.4787856007138	21.4912658398257	21.4912658464321
33.0066285792139	33.0066285911297	35.1819579171347
35.1819579211334	38.4425185282400	46.7305422735518
46.7305422775387	52.8326046977284	52.8326047003752
59.7583443348978	59.7583443413796	62.6346154276106
62.6346154295291	73.2557632678084	73.2557632689215
80.6975152336160	80.6975152363994	84.2283965643563
84.2283965657074		

Table. 2.6[7]. Values of $\lambda^2 = \omega a^2 \sqrt{p/D}$ for a disc with free edge, Poisson's ratio **ν** ***= 0,25***

s	λ^2 ***as a function of n***			
	0	**1**	**2**	**3**
0	–	–	5.513	12.75
1	8.892	20.41	35.28	53.16
2	38.34	59.74	84.38	112. 36
3	87.65	118.88	153.29	191.02
4	156.73	196.67	241.99	289.51
5	245.52	296.46	350.48	408.16
6	354.08	414.86	478.73	545.83
7	482.37	553.00	626.75	703.63
8	630.41	710.92	794.51	881.20
9	798.23	888.58	982.01	1078.5

5.51300000000000 5.51300004671415 8.89330760984207
12.7492269242642 12.7492269293874 20.4169965125856
20.4169965201104 22.3205298280694 22.3205298392738
34.1727794983379 34.1727795054332 35.3011631704333
35.3011631728132 38.3499809104209 48.2639909290734
48.2639909328545 53.1729139899471 53.1729139914736
59.7538502261771 59.7538502350771 64.5636837621202
64.5636837662562 73.8433812569470 73.8433812586368
83.0489818605929 83.0489818652054 84.3739854682652
84.3739854705684

4.6.6. Comparison with results of [8]

The results obtained in this work are presented in Tables 1[8]–7[8]. In what follows, we compare these with the results obtained by the current approach for a disc of constant and variable thickness.

Table 1**[8]**. Results for a constant-thickness disc (ν = 0.3) with free edge ✓

F	Present	5.3583	9.0031	12.439	20.475
F	Exact	5.3583	9.0031	12.439	20.475
F	[27]*	5.513	8.892	12.75	20.41
F	[5]**	5.253	9.084	12.23	20.52

* ν = 0.25
** 0.33.

M = 30 N = 41, Poisson's ratio ν = 0.3
5.35821033099024 5.35821050604358 9.00313639025165
12.4389878097456 12.4389879091879 20.4745414427208
20.4745415969835 21.8351625266926 21.8351626051079
33.4949314843156 33.4949315460849 35.2593124700112

✓ Results for uniform thickness (ν = 0.3).

Poisson's ratio ν = 0.33

5.26191979848889	5.26192010586215	9.06889749411773
12.2438907848989	12.2438908941195	20.5130769693259
20.5130771676494	21.5272151458138	21.5272152697727
33.0618418265923	33.0618418668024	35.2417793317563

Poisson's ratio ν = 0.25

5.51105186396318	5.51105210695181	8.88989471034279
12.7443333086226	12.7443334381724	20.4091891336574
20.4091891964617	22.3119598126259	22.3119598372450
34.1596580629660	34.1596582116240	35.2887640958267

***Table 2*[*8*]. *Five lowest eigenfrequencies* ✓ $\alpha_1 = 0.1$, $\beta_1 = 0$**

F	5.375	9.021	12.49	20.52	21.94

Poisson's ratio ν = 0.3; $\alpha_1 = 0.1$, $\beta_1 = 0.0$

5.35904498410518	5.35904953375535	9.00407486376741
12.4200221798616	12.4200228749320	20.4449698441097
20.4598354597854	21.7875004345318	21.7875004816792
33.4102572455602	33.4102575309901	35.2007110280961

***Table 3*[*8*]. *Five lowest eigenfrequencies* $\alpha_1 = 0$, $\beta_1 = 0.1$**

F	5.429	9.096	12.73	20.75	22.47

Poisson's ratio ν = 0.3; $\alpha_1 = 0.0$, $\beta_1 = 0.1$

5.42889963209096	5.43138351210372	9.09492086539602
12.7359490973689	12.7360356800276	20.7388651685036
20.7752960097401	22.4658528132978	22.4658535550569
34.5648851555082	34.5648854137330	35.8796636077262

***Table 4*[*8*]. *Five lowest eigenfrequencies* $\alpha_1 = 0$, $\beta_1 = 0.1$**

F	5.444	9.114	12.78	20.82	22.57

Poisson's ratio ν = 0.3; $\alpha_1 = 0.1$ $\beta_1 = 0.1$

5.42858490111721	5.43176446369384	9.09572511640332
12.7175646503886	12.7176461829392	20.7110433338299
20.7606675467376	22.4212440155523	22.4212441904947
34.4865575699206	34.4865581190285	35.8258410445658

***Table 5*[*8*]. *Five lowest eigenfrequencies* $\alpha_2 = 0.1$, $\beta_2 = 0$**

F	5.621	5.620	9.376	13.27	21.54

Poisson's ratio ν = 0.3; $\alpha_2 = 0.1$, $\beta_2 = 0.0$

5.62019561725068	5.62019577541118	9.37283216686625
13.2687898761595	13.2687899999075	21.5128829399769
21.5128830097989	23.4638938486293	23.4638939675125
36.1447158082075	36.1447158602994	37.2616578755316

✓ First five frequencies for.

Table 6*[*8*]. *Five lowest eigenfrequencies $\alpha_2 = 0$, $\beta_2 = 0.1$

F	5.510	9.179	13.04	21. 06	23.57

Poisson's ratio ν = 0.3; $\alpha_2 = 0.0$, $\beta_2 = 0.1$

5.51009739899146 5.51009769494616 9.17675716244429
13.0389589685491 13.0389591778323 21.0384780393279
21.0384781287549 23.1104037017769 23.1104038919022
35.6619850737445 35.6619851664199 36.5241569978989

Table 7*[*8*]. *Five lowest eigenfrequencies $\alpha_2 = 0.1$, $\beta_2 = 0.1$

F	5.783	9.564	13.88	22.13	25.31

Poisson's ratio ν = 0.3; $\alpha_2 = 0.1$, $\beta_2 = 0.1$

5.78237094152123 5.78237155338917 9.55701485174215
13.8811739486531 13.8811739914088 22.0780817754477
22.0780818535063 24.7518409042676 24.7518409915627
38.3238851484576 38.3238851750690 38.5227913752173

The results obtained generally coincide with those presented in Table 1[8]–7[8] of the above-cited work. However, the tabulated data cannot be considered accurate. The thing is that some of the eigenfrequencies for a constant-thickness disc with free edge are multiple (see Table 1[8]–7[8]). Perturbation of plate thickness results in the splitting of these multiple frequences into two close frequences. In Table 1[8]–7[8], only one frequency of a pair is given (except the first pair, see the last row of Table 5[8]), which is wrong. These frequencies are different, albeit close to each other.

4.6.7. Comparison with results of [4]

The results obtained were compared with those from Table 6 of [4] ($n = 1$, $a/b = 1$). The calculations were carried out according to the method presented in Section 4.1.

Table 6*[*4*]. *Frequency parameters, $\lambda^2 = \omega b^2\sqrt{\rho h/D}$, for simply supported super-elliptic plates of constant thickness ✓

n	***a/b***	λ_1^2			λ_2^2			λ_3^2		
		ν = 0.1	ν = 0.2	ν = 0.3	ν = 0.1	ν = 0.2	ν = 0.3	ν = 0.1	ν = 0.2	ν = 0.3
1	1.0	4.6192	4.7826	4.9351	13.7208	13.8564	13.8985	25.3757	25.4988	25.6188

POISSON'S RATIO 0.1
GRID:M = 13 N = 27
Square roots of the 8 lowest eigenvalues
THE FIRST 8 EIGENVALUES
0.46192341344E + 01 0.13638351202E + 02 0.13638351202E + 02
0.29484982369E + 02 0.25370665304E + 02 0.25370665304E + 02
0.39723589528E + 02 0.39723589528E + 02

POISSON'S RATIO 0.2
GRID:M = 13 N = 27

✓ Frequency parameters, $\lambda^2 = \omega b^2\sqrt{\rho h/D}$, for simply supported super elliptical plates of constant thickness.

Square roots of the 8 lowest eigenvalues
THE FIRST 8 EIGENVALUES
0.47825798840E + 01   0.13770540281E + 02   0.13770540281E + 02
0.29603706066E + 02   0.25493516817E + 02   0.25493516817E + 02
0.39841631798E + 02   0.39841631798E + 02

POISSON'S RATIO 0.3
GRID:M = 13 N = 27
Square roots of the 8 lowest eigenvalues
THE FIRST 8 EIGENVALUES
0.49351490454E + 01   0.13898165073E + 02   0.13898165073E + 02
0.29720004735E + 02   0.25613296726E + 02   0.25613296726E + 02
0.39957314118E + 02   0.39957314118E + 02

The results coincide, but the remark formulated at the end of the previous section must be taken into account.

4.6.8. Comparison with the results [15]

In book [15, p. 46] two tables are given which contain the calculated natural vibration frequencies for a disc of constant thickness with the free edge ($k^4 = \rho h a^4 \omega^2/D$), below we present the simple values of k calculated for ν = 0.333 (Table 2.7, second column): n = 0: 3,014; 6,209; 9,370; 12,53; 15,68; 18,83; 21,98; 25,12; 28,26; 31,40. By the above approach, the following results were obtained on the 20×41 grid:

3.01291163694831;   6.20666673566053;   9.37226290820142;
12.5267040301146;   15.6762237399511;   18.8229688902190;
21.9653378325853;   25.0951180023060;   28.2123896192012;
31.3151943454288.

4.6.9. Conclusions

The numerical results obtained have demonstrated the high efficiency of the proposed algorithm. For example, the lowest two natural vibration frequencies for a constant-thickness disc can be obtained with two decimal digits on a grid with as low as 21 nodes. Comparisons with the results of other authors are carried out, and some deficiencies in the published data have been highlighted. On particular, only one of a pair of two close frequencies is determined. Probably, these frequencies were considered as the double ones by those authors.

References

1. Glikman B. T., Free vibrations of a circular plate with mixed boundary conditions. Izv. Akad. Nauk SSSR, Mekhan, Tverd. Tela, No. l, 1972, p. 135-140.
2. E. P. Kazandzhan, “A numerical method for conformal mapping of simply connected domains,” Preprint No. 82, Applied mathematics institute, USSR Academy of Sciences, Moscow (1977).
3. Akulenko L. D., Nesterov S. V. Natural vibrations of an elliptic plate with the clamped edge. Izv. Ross. Akad. Nauk, Mekhan, Tverd. Tela, No. l, 2001, p. 174-180.

4. Seyit Ceribasi, Gulay Altay. Free vibration of super elliptical plates with constant and variable thickness by Ritz method // Journal of Sound and Vibration 319 (2009) P. 668–680.
5. J. W. S. Rayleigh, *The Theory of Sound*, Vol. 1, Dover New York (1945).
6. Sundararajan C. An approximate solution for the fundamental frequency of Plates // Trans. of the ASME. Journal of applied mechanics, 1978, 45, 12.
7. Leissa A. W. Vibration of Plates-NASA SP-160, US Government Printing Office, Washington, DC, 1969.
8. Singh B., Chakraverty S. Use of characteristic orthogonal polynomials in two dimensions for transverse vibration of elliptic and circular plates with variable thickness // Journal of Sound and Vibration (1994) 173 (3). C. 289–299.
9. By A. B. Wood, D.Sc., F. Inst. P. An experimental determination of the frequencies of free circular plates // Proc. Phys. Soc. 47, 794 (1935).
10. Waller, Mary D., Inst P. Vibration of free circular Plates. Part I: Normal Modes // Proc. Phys. Soc. 50, (1937), pp. 70–76; Part II: Compounded Normal Modes, pp. 77 82; Part 3: A Study of Chladni's original figures. P. 83–86.
11. Waller, Mary D. Vibration of free Elliptical Plates // Proc. Phys. Soc. 63, (1950). P. 451–456.
12. P. M. Ogibalov, *Bending, Stability, and Vibration of Plates* [in Russian], Izd. Mosk. Univ., Moscow (1958), 398 p.
13. I. M. Babakov, *Theory of Vibrations* [in Russian], Nauka, Moscow (1968). 559 p.
14. Analytical investigation of the acoustic radiation from linearly-varying thin circular plates by walter wanyama, b.s.a.e., m.s.m.e. a dissertation in mechanical engineering.Submitted to the Graduate Faculty of Texas Tech University in Partial Fulfillment of the Requirements for the Degree of doctor of philosophy Approved. August, 2000.
15. W. S. Gotkevich, *Natural Vibrations of Plates and Shells: Handbook* [in Russian], Naukova Dumka, Kiev (1964), 288 p.
16. S. D. Algazin, "Numerical algorithms of classical mathematical physics. II. Spectral problems for biharmonic equation," Preprint No. 678, Institute of Problems of Mechanics, Russian Academy of Sciences, Moscow (2001).

Chapter 5.
Flutter of plates and shallow shells

In this chapter, the state-of-the-art of the panel flutter problem is reviewed. The analysis starts with the fundamental work by A. A. Ilyushin [1] which provided the basis for a simpler formulation of flutter problems for plates and shallow shells [2]. The main point of the approach developed by A. A. Ilyushin and I. A. Kiyko, on which the current consideration is based, is that the complex problem of interaction of supersonic gas flow and elastic shell can be reduced to a non-self-adjoint eigenvalue problem with smooth solutions. A non-saturating numerical algorithm is described, which takes the advantage of this smoothness (unlike the classical algorithms, e.g., the finite-different and finite-element methods). This enables one to solve the panel flutter problems on PCs of modest computational power, e.g., Pentium – 100.

5.1. On the statement of panel flutter problem using A.A.Ilyushin's theory of planar sections

Panel flutter is an interesting and important phenomenon in high-speed applications. It consists in the excitation, at some critical velocities, of vibrations with increasing amplitude of skin panels and other thin-walled structural elements, like plates or shells, in the supersonic gas flow. This can result in the damage to the structure.

Theoretical study of the panel flutter in a correct, from the physical and mathematical points of view, statement of the problem became possible after the law of planar sections was established in high-speed supersonic aerodynamics in 1947 [1].

Analyzing the motion of thin solids at high supersonic velocities, A. A. Ilyushin discovered the following common property which he termed the law of planar sections: "If the velocity vector of some point of some body of aerodynamically regular form is *V*, and if the transversal velocities of its other points do not exceed εV, then, upon its steady or unsteady motion, the body causes in the ambient flow only transverse perturbations; the pressure at any point of the body surface calculated under this assumption, can differ from the true pressure only by the value of the order of

$$\frac{1+e^2}{2M^2} = \frac{1}{2}(\varepsilon^2 + \frac{1}{M^2})$$

in comparison with unity". Here, $M^2 = \frac{V^2}{c_0^2} >> 1$, where *M* is the Mach number, $e = \frac{\varepsilon\, V}{c_0}$ is Ilyushin's parameter expressed in terms of the body velocity *V*, inclination of the normal to elemental area ε and speed of sound in the unperturbed flow c_0, i. e. speed of sound at infinity; the latter parameter is of fundamental value because in the linearized and non-linearized theories, in the presence of vortices and shock waves, the pressure at the body surface is determined solely by this parameter and by body shape.

Therefore, if we cut by two parallel planes perpendicular to the body velocity vector *V* a layer of physical particles in front of the body, we can calculate the pressure field with the accuracy stated above by assuming that the flow particles are moving parallel to the planes, or that the planes will play the role of rigin impenetrable walls for them.

The law of planar sections led to a new formulation of supersonic aerodynamics problems (and to a method of aerodynamic modeling). Also, it enabled the steady and unsteady problems to be reduced to a simple problem on piston motion in a pipe of constant cross section, with the piston moving according to some prescribed law $v = v(t)$, the latter being the velocity with which the gas in an elementary column is compressed by the cutting surface. For any point of the surface, this velocity is equal to the projection of the absolute velocity vector of the surface element onto the normal to this element.

Thus, it became possible to formulate in correct and practically convenient form and to study theoretically many important problems relevant to the motion of thin-walled structures in gas, to determine the pressure and, therefore, all aerodynamic forces acting on the bearing surface at high supersonic velocities in the presence of shock waves and variable gas entropy. The calculations are especially straightforward in the linearized theory in which case, for example, the overpressure $\Delta p = p\text{-}p_0$ on any surface element is equal to the ambient gas pressure p_0 multiplied by the polytropic index *k* and the ratio of the normal component of the velocity vector of this surface element and the freestream speed of sound c_0

$$\Delta p = kp_0 \frac{v(t)}{c_0}$$

The above relation is the linear approximation for the pressure on the piston, obtained from the simple and shock wave theory

$$p = p_0 \left(1 + \frac{k-1}{2}\frac{\nu}{c_0}\right)^k, \quad k = \frac{2k}{k-1}$$

$$p = p_0 \left[1 + \frac{k(k+1)}{4}\frac{\nu^2}{c_0^2} + \frac{k\nu}{c_0}\left(1 + \frac{(k+1)^2}{16}\frac{\nu^2}{c_0^2}\right)^{1/2}\right]$$

The first formula is valid when the piston accelerates gradually to velocity v, the second one corresponds to the case where the piston instantaneously acquires a constant velocity v and then moves at this velocity; for the velocities $v/c_0 \le 2$ both formulas give close results. The flutter theory is based on the equality

$$v = \frac{\partial w}{\partial x}V + \frac{\partial w}{\partial t},$$

which follows from the condition of impenetrability; here, w is the normal deflection of the shell, V is the flow velocity (the axis Ox is parallel to the velocity vector).

The formula for overpressure takes the form

$$\Delta p = \frac{\kappa p_0}{c_0}\left(V\frac{\partial w}{\partial x} + \frac{\partial w}{\partial t}\right)$$

5.2. Flutter of a plate

In this chapter, the approach to the discretization and solution of eigenvalue problems is applied to study the flutter of plates of arbitrary shape in plan. From the mathematical point of view, the problem is reduced to non-self-adjoint eigenvalue problem for biharmonic equation with lower-order terms. To solve such a problem, a non-saturating algorithm has been developed which enables the problem to be solved in times from several minutes to several dozens of minutes on a PC with modest performance, like Pentium-100. For reliability, the calculations are performed on two grids: the coarse one 9×15 (with 9 circular grid lines, each containing 15 nodes), and the fine one 15×31 (15 circles with 31 nodes). Agreement of the critical flutter velocities obtained on these grids was the criterion of the accuracy of the results obtained. Also, the flutter problem for a rectangular grid is considered separately due to the specific discretization required in comparison with the generic case (i.e., with a plate having a smooth boundary).

Two types of the boundary conditions were considered: clamping and simple support. The dependence of the critical flutter velocity on the thickness was studied for different boundary conditions and directions of the velocity vector. It was found that this dependence takes the form $v_{кр.} = a + bh^3$, where a and b are constants depending on the problem parameters. This property is of high practical value. It is enough to obtain $v_{кр.}$ for two thicknesses, determine a and b, after which the above simple formula can be used for a range of plate thicknesses.

Note also that discretization of the equation for a plate having an arbitrary shape in plan requires the solution of an ill-posed problem (if the boundary conditions of the second kind are satisfied), therefore, great caution and accuracy are required.

5.2.1. Flutter of a plate of arbitrary shape in plan

We use the new formulation of the problem by A. A. Ilyushin and I. A. Kiyko [2]:

$$D\Delta^2\phi - \beta(\vec{v}, grad\phi) = \lambda\phi,\ \phi = \phi(z),\ z \in K, \tag{5.2.1}$$

$$\phi|_{\partial K} = 0, \tag{5.2.2}$$

$$\left.\frac{\partial\phi}{\partial n}\right|_{\partial K} = 0, \tag{5.2.3}$$

$$\left.\frac{\partial^2\phi}{\partial n^2} + \nu(\frac{\partial^2\phi}{\partial s^2} + \kappa\frac{\partial\phi}{\partial n})\right|_{\partial K} = 0. \tag{5.2.4}$$

Here, K is a domain of the complex z – plane with smooth enough boundary ∂K, n is the unity vector of outer normal to ∂K, $\partial/\partial s$ denoted differentiation with respect to the arc length (the length is reckoned counterclockwise); κ is the curvature of ∂K; ν is Poisson's ratio; $D = Eh^3/12(1-\nu^2)$ is the cylindrical rigidity of the plate (h is the plate thickness, E is Young's modulus); $\beta = kp_0/c_0$ (k is the polytropic index, p_0 and c_0 are the freestream pressure and speed of sound); $\lambda = -\rho h\omega^2 - \beta\omega$ (ω is the complex-valued frequency, ρ is the plate material density, h and β have been defined above); $\vec{v}$ is the air flow velocity vector. The equation of state is taken in the form:

$$p = p_0\left(\frac{\rho}{\rho_0}\right)^k,\ k \geq 1,$$

then the speed of sound in the air is determined by $c^2 = dp/d\rho$.

The boundary conditions (5.2.2) and (5.2.3) mean that the plate is clamped at its edge, while the boundary conditions (5.2.2) and (5.2.4) correspond to a simply supported plate. In what follows, the form of the second boundary condition is irrelevant, we write it in the form

$$L\phi|_{\partial K} = 0, \tag{5.2.5}$$

i. e. the method is developed for arbitrary L [the boundary condition of the firsk kind is taken in the form (5.2.2)].

For convenience, we turn to non-dimensional formulation of the problem. Introduce the scales: d is the characteristic linear size, p_0 is the freestream air pressure, c_0 is the freestream speed of sound. The non-dimensional parameters denoted by the primes are defined in the following way: $E = E'p_0$, $h = h'd$, $\rho = \rho' p_0/c_0^2$, $\omega = \omega' c_0/d$, $v = v'c_0$, $\varphi = \varphi' d$, $x = x'd$, $y = y'd$, $\kappa = \kappa'/d$. Substitute these into relations (5.2.1) – (5.2.4) to verify that, in the non-dimensional form, the system of equations maintains its form, provided that the parameter β is replaced by the non-dimensional parameter k. In what follows, we omit the primes. Whether the plate vibrations will be stable or not depends on whether $Re\omega > 0$ or $Re\omega < 0$; if $\lambda_1 = \alpha_1 + \beta_1 i$ is an eigenvalue, the above inequalities correspond to $F(\alpha_1,\beta_1) > 0$ or $F(\alpha_1,\beta_1) < 0$, where $F(\alpha_1,\beta_1) = \alpha_1 k^2 - \rho h\beta_1^2$. Let λ_1 be the first of the eigenvalues which satisfy the condition $F = 0$; therefore, the problem is reduced to finding out the zeroes of function $F(\alpha_1(v),\beta_1(v))$ for the given direction of flow velocity vector.

Thus, the plate vibrations will be stable or unstable depending on whether the eigenvalues λ of the spectral problem being considered belong to the interior of the parabola

$$y^2 = \frac{k^2}{\rho h} x \qquad (5.2.6)$$

Calculations were performed for the following parameters: p_0 = 1.0333 kg/cm^2, ρ_0 = 1.2928 kg/m^3, ν = 0.33, k = 1.4, $E = 0.7 \cdot 10^6$ kg/cm^2, $\rho = 2.7 \cdot 10^3$ kg/m^3. The non-dimensional density is $\rho' = k\rho/\rho_0$, therefore, the coefficient of the parabola is $k\rho_0/\rho h$. For the plate thickness of 0.003, we obtain 0.2234. The stability parabola takes the form $y^2 = 0.2234x$, i. e. the parabola touches the real axis. With the increase in h, the coefficient of x in the stability parabola is decreased.

Flutter of a simply supported rectangular plate was first considered by A.A.Movchan in 1955 [3]. At that time, it was impossible to solve problem exactly, i.e., to solve numerically the equation $F(\alpha_1(v),\beta_1(v)) = 0$ and find out the critical flutter velocity. A.A.Movchan searched for the conditions for the appearance, with the increase in the velocity v, of a complex-valued eigenvalue of the spectral problem. However, he did not consider what velocity increment is necessary for the eigenvalue to reach the stability parabola. Comparison with A.A.Movchan's results is presented below in section 5.2. Here we just note that the agreement is surprisingly good. Of course, this is attributed to the form of the stability parabola (5.2.6). Practical calculations show that, as the velocity v is increased, a single complex pair of eigenvalues appears in the spectral problem being considered (this pair has the minimum absolute value), and it is this pair that reaches the stability parabola. Thus, calculations confirm that for a round (and nearly-round) plates the stability study can be carried out by analyzing the first (i.e., having the minimum absolute value) eigenvalue.

Substitute the Cartesian coordinates (x,y) by the curvilinear ones (r,θ) according to the relations $x = U(r,\theta)$, $y = V(r,\theta)$. If the Cauchy-Riemann conditions are satisfied, i.e.,

$$\frac{\partial U}{\partial r} = \frac{1}{r}\frac{\partial V}{\partial \theta}, \quad \frac{\partial V}{\partial r} = -\frac{1}{r}\frac{\partial U}{\partial \theta},$$

the coordinate system (r,θ) is orthogonal. We choose now the functions $U(r,\theta)$ and $V(r,\theta)$ in such a way, that the function

$$\psi(\varsigma) = U(r,\theta) + iV(r,\theta), \quad \varsigma = r \cdot \exp(i\theta)$$

determined a conformal mapping of the disc $|\varsigma| = r \le 1$ onto the domain K. Then, in the coordinates (r,θ), equation (5.2.1) takes the form:

$$D\Delta(|\psi'(\varsigma)|^{-2}\Delta\phi) - k((v_x U_r + v_y V_r)\frac{\partial\phi}{\partial r} + \frac{1}{r}(v_y U_r - V_r v_x)\frac{\partial\phi}{\partial\theta}) = \lambda|\psi'(\varsigma)|^2\phi,$$
$$\left(U_r = \mathrm{Re}\left(\frac{\psi'(\varsigma)\varsigma}{r}\right), \quad V_r = \mathrm{Im}\left(\frac{\psi'(\varsigma)\varsigma}{r}\right)\right). \qquad (5.2.7)$$

The boundary conditions (5.2.2) – (5.2.4) take the form:

$$\phi|_{r=1} = 0, \qquad (5.2.8)$$

$$\left.\frac{\partial\phi}{\partial r}\right|_{r=1} = 0, \qquad (5.2.9)$$

$$\left.\frac{\partial^2\phi}{\partial r^2} + \nu\frac{\partial\phi}{\partial r} + (\nu-1)\mathrm{Re}\left(\varsigma\frac{\psi''(\varsigma)}{\psi'(\varsigma)}\right)\frac{\partial\phi}{\partial r}\right|_{r=1} = 0. \qquad (5.2.10)$$

Note that in relation (5.2.10) the boundary condition (5.2.8) has been taken into account, i. e. it was assumed that $\partial^2\varphi/\partial s^{2} = 0$.

Relations (5.2.7) – (5.2.10) give the statement of the eigenvalue problem in question.

5.2.2. Discretization

Denote

$$f(r,\theta)=k((v_xU_r+v_yV_r)\frac{\partial\varphi}{\partial r}+\frac{1}{r}(v_yU_r-V_rv_x)\frac{\partial\varphi}{\partial\theta})+\lambda\,|\,\psi'(\varsigma)\,|^2\,\varphi$$

and turn from the differential equation (5.2.7) to the integral one:

$$D\Delta\varphi=|\,\psi'(\xi)\,|^2\int\limits_{|\varsigma|\le 1}K(\xi,\varsigma)f(\varsigma)d\varsigma+|\,\psi'(\xi)\,|^2\int\limits_0^{2\pi}K_0(\xi,\theta)w(e^{i\theta})d\theta.$$

Here, $K(\xi,\zeta)$ is Green's function for the Laplace operator on a disc with the boundary condition (5.2.8), $K_0(\xi,\theta)=\frac{1}{2\pi}\frac{1-r^2}{1+r^2-2r\cos(\theta-\varepsilon)}$, $\xi=re^{i\varepsilon}$ is Poisson's kernel,

$$w(e^{i\theta})=|\,\psi'(\varsigma)\,|^{-2}\,\Delta\varphi(\varsigma)\,|_{\varsigma=e^{i\theta}}\,.$$

Let

$$R(\xi)=|\,\psi'(\xi)\,|^2\int\limits_{|\varsigma|\le 1}K(\xi,\varsigma)f(\varsigma)\,d\varsigma\,, \qquad (5.2.11)$$

$$S(\xi)=|\,\psi'(\xi)\,|^2\int\limits_0^{2\pi}K_0(\xi,\theta)w(e^{i\theta})d\theta\,. \qquad (5.2.12)$$

Then we obtain

$$D\Delta\varphi = R(\xi) + S(\xi).$$

Inverting the Laplace operator one more time, we obtain

$$\phi(\xi)=\frac{1}{D}\int\limits_{|q|\le 1}K(\xi,q)[R(q)+S(q)]dq+\frac{1}{D}\int\limits_0^{2\pi}K_0(\xi,\theta)\phi(e^{i\theta})d\theta. \qquad (5.2.13)$$

The latter integral turns to zero due to the boundary condition (5.2.8). Now, we have to determine the unknown yet function $w(e^{i\theta})$ in relation (5.2.13) from the boundary condition (5.2.9) or (5.2.10). We apply the trigonometric interpolation for the function $w(e^{i\theta})$:

$$w(e^{i\theta})=\frac{2}{N}\sum_{j=0}^{2n}D_n(\theta-\theta_j)w_j+\rho_n(\theta;w),\;\; D_n(\theta)=0.5+\sum_{k=1}^{n}\cos k\theta,$$

where $\rho_n(\theta;w)$ is the interpolation error. The functions $S(q)$ and $R(q)$ are interpolated by (3.2.1) to obtain

$$\int\limits_{|q|\le 1}K(\xi,q)S(q)dq=-\sum_{\nu,l}H_{\nu l}(\xi)S_{\nu l}+R_M(\xi;S),$$

where the quantities $H_{\nu l}(\xi)$ are defined in (3.3.8),

$$R_M(\xi;S)=\int\limits_{|q|\le 1}K(\xi,q)\rho_M(q,S)dq,$$

$\rho_M(q,S)$ is the error of the interpolation formula (3.2.1),

$$S_{\nu l}=z_{\nu l}\int\limits_0^{2\pi}K_0(\varsigma_{\nu l},\theta)w(e^{i\theta})d\theta=\frac{2z_{\nu l}}{N}\sum_{j=0}^{2n}\left(\int\limits_0^{2\pi}K_0(\varsigma_{\nu l},\theta)D_n(\theta-\theta_j)d\theta\right)w_j+$$

$$+R_n(\varsigma_{\nu l};w),\;\; R_n(\varsigma_{\nu l};w)=\int\limits_0^{2\pi}K_0(\varsigma_{\nu l},\theta)\rho_n(\theta;w)d\theta,\; z_{\nu l}=|\,\psi'(\varsigma_{\nu l})\,|^2\,.$$

Denote $H_j^0(\varsigma_{\nu l}) = \dfrac{2}{N}\int\limits_0^{2\pi} K_0(\varsigma_{\nu l},\theta)D_n(\theta-\theta_j)d\theta.$

This integral can be easily expressed in the explicit form. Thus,

$$\begin{gathered}\int\limits_{|q|\le 1} K(\xi,q)S(q)dq = -\sum_{\nu,l} H_{\nu l}(\xi)z_{\nu l}\sum_{j_1=0}^{2n} H_{j_1}^0(\varsigma_{\nu l})w_{j_1} - \\ -\sum_{\nu,l} H_{\nu l}(\xi)R_n(\varsigma_{\nu l};w) + R_M(\xi,S),\end{gathered} \tag{5.2.14}$$

$$\begin{gathered}\int\limits_{|q|\le 1} K(\xi,q)R(q)dq = -\sum_{\nu,l} H_{\nu l}(\xi)R_{\nu l} + \int\limits_{|q|\le 1} K(\xi,q)R_M(q;R)dq, \\ R_{\nu l} = z_{\nu l}\int\limits_{|\varsigma|\le 1} K(\xi_{\nu l},\varsigma)f(\varsigma)d\varsigma.\end{gathered} \tag{5.2.15}$$

We apply now the same interpolating formula to the function $f(\varsigma)$ and substitute it into relation (5.2.15)

$$\int\limits_{|q|\le 1} K(\xi,\varsigma)f(\varsigma)d\varsigma = -\sum_j H_j(\varsigma)f_j + \int\limits_{|q|\le 1} K(\xi,\varsigma)R_M(\varsigma;f)d\varsigma.$$

Therefore,

$$R_i = -z_i\sum_j H_j(\varsigma_i)f_j + z_i\int\limits_{|\varsigma|\le 1} K(\xi_i,\varsigma)R_M(\varsigma;f)d\varsigma. \tag{5.2.16}$$

Here, a single index i is used instead of two indices ν,l, i. e. the nodes of the grid on the disc are numbered counterclockwise, starting with the first circle; $H_{ij} = H_j(\varsigma_i)$ is the matrix of the Dirichlet problem for the Laplace operator on a disc domain.
Substitute now relation (5.2.16) into (5.2.15) to obtain

$$\begin{gathered}\int\limits_{|q|\le 1} K(\xi,q)R(q)dq = \sum_i H_i(\xi)z_i\sum_j H_{ij}f_j - \\ -\sum_i H_i(\xi)z_i\int\limits_{|\varsigma|\le 1} K(\xi_i,\varsigma)R_M(\varsigma;f)d\varsigma + \int\limits_{|q|\le 1} K(\xi,q)R_M(q;R)dq.\end{gathered} \tag{5.2.17}$$

Also, substitute (5.2.17) and (5.2.14) into (5.2.13) to obtain

$$\begin{gathered}\phi(\xi) = \frac{1}{D}\sum_i H_i(\xi)z_i\sum_j H_{ij}f_j - \frac{1}{D}\sum_i H_i(\xi)z_i\sum_{j_1=0}^{2n} H_{j_1}^0(\varsigma_i)w_{j_1} + \\ +R_{n,M}(\xi;f,R,S), \quad R_{n,M}(\xi;f,R,S) = \\ = \frac{1}{D}\left\{-\sum_j H_i(\xi)z_i\int\limits_{|\varsigma|\le 1} K(\xi_i,\varsigma)R_M(\varsigma;f)d\varsigma + \int\limits_{|q|\le 1} K(\xi,q)R_M(q,R)dq\right\} - \\ -\frac{1}{D}\left\{\sum_i H_i(\xi)R_n(\xi_i;w) + R_M(\xi;S)\right\}.\end{gathered} \tag{5.2.18}$$

In relation (5.2.18), the values of $w = (w_0, w_1,\ldots, w_{2n})$ have to be defined in such a way that the boundary condition (5.2.3) or (5.2.4) is satisfied. Denote by L the differential operator on the left-hand side of the boundary condition. Then, applying this operator to (5.2.18), we obtain:

$$\begin{gathered}\sum_{i,j} L(H_i(\xi))z_iH_{ij}f_j - \sum_i L(H_i(\xi))z_i\sum_{j_1=0}^{2n} H_{j_1}^0(\varsigma_i)w_{j_1} + \\ +LR_{n,M}(\xi;f,R,S) = L\phi(\xi).\end{gathered}$$

Introduce the notation:

$$L(H_i(\xi))\big|_{\xi=e^{i\vartheta_{j2}}} = \bar{H}_{i,j_2},\ \ j_2 = 0,1,....,2n,$$
$$\sum_{i,j} \bar{H}_{i,j_2} z_i H_{ij} f_j = R_{j_2},$$
$$\sum_{i} \bar{H}_{i,j_2}\ z_i H^0_{j_1}(\varsigma_i) = \bar{B}_{j_2,j_1},$$
$$\delta_{j_2} = LR_{n,M}(\xi; f, R, S)\big|_{\xi=e^{i\vartheta_{j2}}}.$$

Thus, the vector $w = (w_0, w_1, \ldots, w_{2n})'$ is determined from a system of linear equations:

$$\sum_{j_1=0}^{2n} \bar{B}_{j_2,j_1} w_{j_1} = R_{j_2} + \delta_{j_2}.$$

from which we obtain $w_{j_1} = \sum_{j_2=0}^{2n} C_{j_1,j_2}(R_{j_2} + \delta_{j_2}),\ C = \bar{B}^{-1}.$

Substituting it into relation (5.2.18), we obtain

$$\begin{aligned}\phi(\xi) &= \frac{1}{D}\sum_{i,j} H_i(\xi) z_i H_{ij} f_j - \\ &-\frac{1}{D}\sum_i H_i(\xi) z_i \sum_{j_1=0}^{2n} H^0_{j_1}(\varsigma_i) \sum_{j_2=0}^{2n} C_{j_1,j_2}(R_{j_2} + \delta_{j_2}) + R_{n,M}(\xi; f, R, S).\end{aligned} \quad (5.2.19)$$

Here, $f_j = \lambda z_j \phi_j + \Phi_j,\ \Phi_j = k\left((v_x U_r + v_y V_r)\frac{\partial\phi}{\partial r} + \frac{1}{r}(v_y U_r - V_r v_x)\frac{\partial\phi}{\partial\theta}\right)\Bigg|_{\varsigma=\varsigma_j},$

$$j = 1, \ldots, M.$$

Let ξ runs over the interpolation nodes ξ_i, $i = 1,2,\ldots,M$, then we have

$$\begin{aligned}\phi_i &= \frac{\lambda}{D}\sum_j (B^2_{ij} - \sum_l B_{il} E_{lj})\phi_j + \\ &+\frac{1}{D}\sum_j (\sum_l B_{il} H_{lj} - \sum_l B_{il} E^*_{lj})\Phi_j + \bar{R}_i\end{aligned} \quad (5.2.20)$$

$$E_{lj} = \sum_{j_1=0}^{2n} H^0_{j_1}(\varsigma_l) \sum_{j_2=0}^{2n} C_{j_1,j_2} \sum_i \bar{H}_{i,j_2} z_i B_{ij},$$
$$E^*_{lj} = \sum_{j_1=0}^{2n} H^0_{j_1}(\varsigma_l) \sum_{j_2=0}^{2n} C_{j_1,j_2} \sum_i \bar{H}_{i,j_2} z_i H_{ij},$$
$$\bar{R}_i = R_{n,M}(\xi_i; f, R, S) + \left(\frac{1}{D} - \frac{\lambda}{D}\right)\sum_l B_{il} \sum_{j_1=0}^{2n} H^0_{j_1}(\xi_l) \sum_{j_2=0}^{2n} C_{j_1,j_2}\delta_{j_2}.$$

Denote $G = B^2\text{-}BE$, then Eq. (5.2.20) takes the form

$$\phi_i - \frac{1}{D}\sum_j G_{ij} z_j^{-1}\Phi_j = \frac{\lambda}{D}\sum_j G_{ij}\phi_j + \bar{R}_i,\ i = 1,2,\ldots,M. \quad (5.2.21)$$

Denote by $D^{(r)}$ and $D^{(\theta)}$ the matrices of differentiation with respect to r and θ, obtained by the differentiation of the interpolating formula (3.2.1), then

$$\Phi_j = a_j\left(\sum_l D^{(r)}_{jl}\varphi_l + \delta^{(r)}_j\right) + b_j\left(\sum_l D^{(\theta)}_{jl}\varphi_l + \delta^{(\theta)}_j\right),\ j = 1,2,\ldots,M,$$
$$a_j = k(v_x U_r + v_y V_r)\,|_{\varsigma=\varsigma_j},\ b_j = \frac{k}{r}(v_y U_r - v_x V_r)\,|_{\varsigma=\varsigma_j},$$

where a and b denote the corresponding diagonal matrices.

Then we obtain from (5.2.21) in the matrix form

$$\phi - \frac{1}{D} G Z^{-1} (a D^{(r)} + b D^{(\theta)}) \phi = \frac{\lambda}{D} G \phi + \bar{R} + \delta,$$
$$\delta = \frac{1}{D} G Z^{-1} (a \delta^{(r)} + b \delta^{(\theta)}). \qquad (5.2.22)$$

Denote $A = I - \frac{1}{D} G Z^{-1} (a D^{(r)} + b D^{(\theta)})$

Then, inverting the matrix A in (5.2.2), we obtain

$$\phi = \frac{\lambda}{D} A^{-1} G \phi + R^*, \;\; R^* = A^{-1}(\bar{R} + \delta). \qquad (5.2.23)$$

Discarding the discretization error R^* in (5.2.23), we arrive at an approximate eigenvalue problem which is studied in the following subsection.

5.2.3. Numerical study of spectral problem

In this subsection, we study the spectral problem (5.2.1) – (5.2.4) for a round plate of unity radius. The parameters used in the calculations are the same as in Section 5.2. The relative thickness of the plate is taken to be 0.003. Twenty four cases were calculated for the velocity from v = 0 to v = 0.4 and five eigenvalues. These cases are given below:

V = 0.00		V = 0.01	
0.178514E + 00	0.0000000E + 00	0.1795529E + 00	0.0000000E + 00
0.773161E + 00	0.0000000E + 00	0.7731649E + 00	0.0000000E + 00
0.773161E + 00	0.0000000E + 00	0.7737315E + 00	0.0000000E + 00
0.208068E + 01	0.0000000E + 00	0.2080810E + 01	0.0000000E + 00
0.208068E + 01	0.0000000E + 00	0.2080810E + 01	0.0000000E + 00
V = 0.05		V = 0.1	
0.204827E + 00	0.0000000E + 00	0.2893258E + 00	0.0000000E + 00
0.772916E + 00	0.0000000E + 00	0.7671301E + 00	0.0000000E + 00
0.787438E + 00	0.0000000E + 00	0.8307226E + 00	0.0000000E + 00
0.208370E + 01	0.0000000E + 00	0.2091960E + 01	0.0000000E + 00
0.208374E + 01	0.0000000E + 00	0.2092567E + 01	0.0000000E + 00
V = 0.15		V = 0.16	
0.467860E + 00	0.0000000E + 00	0.5367171E + 00	0.0000000E + 00
0.721530E + 00	0.0000000E + 00	0.6859869E + 00	0.0000000E + 00
0.904503E + 00	0.0000000E + 00	0.9231474E + 00	0.0000000E + 00
0.210292E + 01	0.0000000E + 00	0.2105080E + 01	0.0000000E + 00
0.210600E + 01	0.0000000E + 00	0.2109058E + 01	0.0000000E + 00
V = 0.161		V = 0.162	
0.546201E + 00	0.0000000E + 00	0.5567974E + 00	0.0000000E + 00
0.679959E + 00	0.0000000E + 00	0.6728446E + 00	0.0000000E + 00
0.925086E + 00	0.0000000E + 00	0.9270390E + 00	0.0000000E + 00
0.210529E + 01	0.0000000E + 00	0.2105500E + 01	0.0000000E + 00
0.210936E + 01	0.0000000E + 00	0.2109678E + 01	0.0000000E + 00
V = 0.163		V = 0.164	
0.569116E + 00	0.0000000E + 00	0.5847359E + 00	0.0000000E + 00
0.664029E + 00	0.0000000E + 00	0.6519364E + 00	0.0000000E + 00
0.929005E + 00	0.0000000E + 00	0.9309856E + 00	0.0000000E + 00
0.210570E + 01	0.0000000E + 00	0.2105914E + 01	0.0000000E + 00
0.210998E + 01	0.0000000E + 00	0.2110301E + 01	0.0000000E + 00
V = 0.1645		V = 0.1648	
0.595469E + 00	0.0000000E + 00	0.6047802E + 00	0.0000000E + 00
0.642974E + 00	0.0000000E + 00	0.6347301E + 00	0.0000000E + 00
0.931980E + 00	0.0000000E + 00	0.9325796E + 00	0.0000000E + 00
0.210601E + 01	0.0000000E + 00	0.2106079E + 01	0.0000000E + 00
0.211045E + 01	0.0000000E + 00	0.2110550E + 01	0.0000000E + 00

```
    V = 0.1649          V = 0.16495
0.609408E + 00 0.0000000E + 00 0.6126738E + 00 0.0000000E + 00
0.630457E + 00 0.0000000E + 00 0.6273703E + 00 0.0000000E + 00
0.932779E + 00 0.0000000E + 00 0.9328794E + 00 0.0000000E + 00
0.210609E + 01 0.0000000E + 00 0.2106110E + 01 0.0000000E + 00
0.211058E + 01 0.0000000E + 00 0.2110597E + 01 0.0000000E + 00
    V = 0.16497         V = 0.16499
0.614464E + 00 0.0000000E + 00 0.6171668E + 00 0.0000000E + 00
0.625650E + 00 0.0000000E + 00 0.6230197E + 00 0.0000000E + 00
0.932919E + 00 0.0000000E + 00 0.9329595E + 00 0.0000000E + 00
0.210611E + 01 0.0000000E + 00 0.2106118E + 01 0.0000000E + 00
0.211060E + 01 0.0000000E + 00 0.2110610E + 01 0.0000000E + 00
    V = 0.164995        V = 0.164997
0.618404E + 00 0.0000000E + 00 0.6193236E + 00 0.0000000E + 00
0.621800E + 00 0.0000000E + 00 0.6208878E + 00 0.0000000E + 00
0.932969E + 00 0.0000000E + 00 0.9329735E + 00 0.0000000E + 00
0.210611E + 01 0.0000000E + 00 0.2106119E + 01 0.0000000E + 00
0.211061E + 01 0.0000000E + 00 0.2110612E + 01 0.0000000E + 00
    V = 0.164998        V = 0.164999
0.615611E + 00 0.0000000E + 00 0.6201093E + 00-0.1288604E-02
0.624539E + 00 0.0000000E + 00 0.9329775E + 00 0.0000000E + 00
0.932939E + 00 0.0000000E + 00 0.2106120E + 01 0.0000000E + 00
0.210611E + 01 0.0000000E + 00 0.2110613E + 01 0.0000000E + 00
0.211060E + 01 0.0000000E + 00 0.2743295E + 01 0.0000000E + 00
    V = 0.165           V = 0.17
0.620111E + 00-0.1672301E-02 0.6291597E + 00-0.7610678E-01
0.932979E + 00 0.0000000E + 00 0.9431576E + 00 0.0000000E + 00
0.210612E + 01 0.0000000E + 00 0.2107125E + 01 0.0000000E + 00
0.211061E + 01 0.0000000E + 00 0.2112181E + 01 0.0000000E + 00
0.274329E + 01 0.0000000E + 00 0.2745945E + 01 0.0000000E + 00
    V = 0.20            V = 0.2798
0.689641E + 00-0.2130506E + 00 0.9049170E + 00-0.4511531E + 00
0.101179E + 01 0.0000000E + 00 0.1269552E + 01 0.0000000E + 00
0.211207E + 01 0.0000000E + 00 0.2106709E + 01 0.0000000E + 00
0.212159E + 01 0.0000000E + 00 0.2136002E + 01 0.0000000E + 00
0.276452E + 01 0.0000000E + 00 0.2842563E + 01 0.0000000E + 00
    V = 0.3             V = 0.4
0.972456E + 00-0.5110125E + 00 0.1364564E + 01-0.8722558E + 00
0.135808E + 01 0.0000000E + 00 0.2001214E + 01-0.3055128E + 00
0.209906E + 01 0.0000000E + 00 0.2059245E + 01 0.0000000E + 00
0.213166E + 01 0.0000000E + 00 0.3072732E + 01 0.0000000E + 00
0.287062E + 01 0.0000000E + 00 0.4516915E + 01 0.0000000E + 00
```

The first calculation was carried out for the velocity value $v = 0$. Expectedly, the first eigenvalue is simple, while the other two are multiple (this was proven in Section 5.2.2). As the velocity is increased, the multiple eigenvalues are split but remain real-valued. Then, the first and second eigenvalues are approaching each other (probably, at some instant they will merge completely to form a double eigenvalue, but such studies have not been performed). For $v = 0.164999$, a complex-valued pair with small imaginary part appeares (in the Table, only the eigenvalue with negative imaginary part is presented). The real part of this complex-valued pair is close to the real eigenvalues obtained for the previous velocity $v = 0.164998$. As the velocity increases further, the absolute value of the complex pair increases as well (note that this complex pair remains the only one available) and at $v = 0.2798$ it reaches the stability parabola. This corresponds to the critical flutter velocity. For $v = 0.4$, a second complex-valued pair appears, but it lies in the interior of the stability parabola.

Thus, the mechanism of flutter instability is revealed. For a round plate, the study of flutter instability conditions was performed by the first eigenvalue. The condition of flutter onset detected by the appearance of a complex-valued pair for the spectral problem in question gives an underestimated value. Also, the functional form of the spectrum perturbation with the increase in the velocity is clarified for the spectral problem being considered.

5.2.4. Numerical results

In this section, we consider the results of numerical computation of the critical flutter velocity for a round plate and a plate obtained from a disc by the conformal mapping $z = \zeta(1 + \varepsilon\zeta^n)$, $|\zeta| \leq 1$. The curve obtained by this mapping is called epitrochoid. For $\varepsilon = 1/n$, this curve has n angular points, therefore all calculations were carried out for $\varepsilon < 1/n$. In particular, two domains were considered: $n = 4$, $\varepsilon = 0.1, 0.2, 0.24$; $n = 12$, $\varepsilon = 0.0625$, as well as two boundary-value problems: rigid clamping and simple support of the edge. The first of the above-mentioned domains is shown in Fig. 5.1.

The second domain has twelve petals; its shape is not shown here. First, we consider a round plate with clamped edge. The calculations were carried out on the 9×15 and 15×31 grids (the first number corresponds to the number of circular grid lines, the second one denotes the number of grid nodes on each circle). On both grids, the same critical velocity $v = 0.2798$ was obtained. The second calculation was carried out for a four-petal epitrochoid with $\varepsilon = 0.1$. For $\theta = 0$ (where θ is the angle between the flow velocity vector and axis *ox*) the same value of the critical velocity was obtained. The first eigenvalue to reach the stability parabola is the one with the minimum absolute value, $\lambda = (0.935906, 0.457245)$. In Fig. 5.2, the functions $Re\varphi(x,0)$ and $Re\varphi(0,y)$ are plotted.

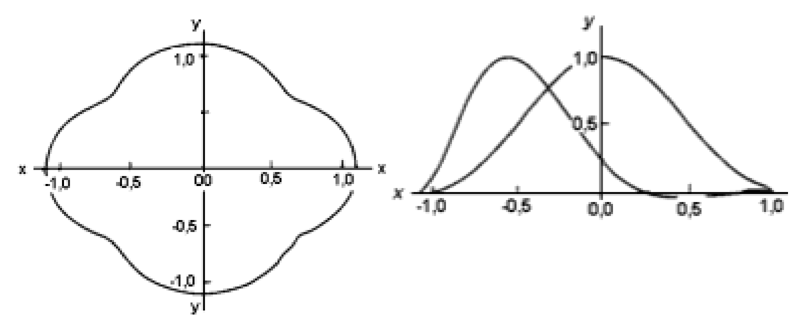


Fig. 5.1. *Planform of the plate: epitrochoid with n = 4, ε = 0.1*

Fig. 5.2. *Functions Re φ(x,0) and Re φ(0,y), v = 0.2798 for epitrochoid with n = 4, ε = 0.1*

The curve which has no intersections with the axis *ox* corresponds to the function $Re\varphi(0,y)$. The other curve is $Re\varphi(x,0)$. Thus, after intersecting the axis *ox*, the function $Re\varphi(x,0)$ gradually tends to zero. For $\theta = \pi/4$, the critical flutter velocity is $v = 0.2789$. Thus, for the domain being considered, the critical flutter velocity varies weakly with the direction of flow velocity. The second calculation was carried out for the same domain, but with $\varepsilon = 0.2$. The critical flutter velocity obtained on the 9×15 grid is $v = 0.2771$. A close value $v = 0.2796$ was obtained on the fine grid. The graphs *Re* of the eigenfunction are presented in Fig. 5.3. The first eigenvalue to reach the stability parabola is the one which has the minimum absolute value, $\lambda = (0.996053, 0.471697)$. Thus, the first eigenvalue and the critical flutter velocity changed by a small fraction in comparison with the previous calculation. The form of the eigenfunction (compare Fig. 5.2 and Fig. 5.3) has changed, but the oscillations of $Re\varphi(x,0)$

near the right boundary are most probably attributed to the computational error (note that the boundary of this domain has very large curvature at four points).
For $\theta = \pi/4$, on both grids we obtained the same value of the critical flutter velocity $v = 0.2826$. The eigenvalue with the smallest absolute value $\lambda = (0.940322, 0.458382)$ is the first to reach the stability parabola. The last calculation carried out on this domain with the clamping boundary condition was for $\varepsilon = 0.24$. The critical velocities obtained for $\theta = 0$ are $v = 0.2724$ on the 9×15 grid, and $v = 0.2751$ on the 15×31 grid. Stability was determined by the first eigenvalue $\lambda = (0.987082, 0.469646)$. For $\theta = \pi/4$, we obtained $v = 0.2821$ on the 9×15 grid, while a close value $v = 0.2809$ was obtained on the 15×31 grid. Stability was determined by the first eigenvalue $\lambda = (0.940836, 0.458527)$.

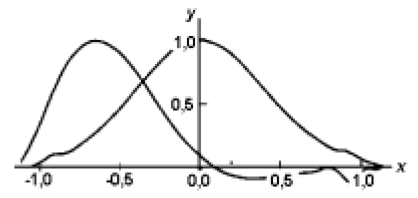


Fig. 5.3. *Plot of Re of the eigenfunction for $\theta = \pi/4$, $v = 0,2796$, $n = 4$, $\varepsilon = 0,.2$*

Then, the boundary value problem of the second kind was considered with $\varepsilon = 0.2$, $n = 4$. This problem is more computationally challenging than the first one, therefore, it was solved on 13×25 and 15×31 grids. For $\theta = 0$, we obtained $v = 0.2653$ on the first grid, and $v = 0.2581$ on the second one. It is interesting to note that in this problem the first eigenvalue in real-valued $\lambda_1 = 0.63323$, while stability is determined by the second eigenvalue $\lambda_2 = (0.680571, 0.390052)$. The plot of *Re* of the eigenvalue is presented in Fig. 5.4.

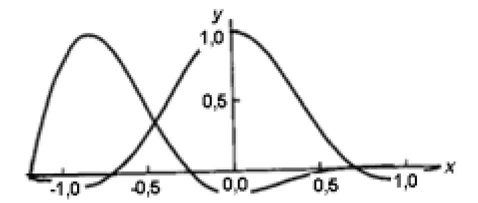


Fig. 5.4. *Plot of Re φ (boundary value problem of the second kind),*
$v = 0,2581$, $n = 4$, $\varepsilon = 0.2$

Thus, for a non-round plate, stability is not necessarily determined by the first eigenvalue. However, for $\theta = \pi/4$ stability is determined by the first eigenvalue. It was obtained on the 13×25 grid that $v = 0.2611$, while on the 15×31 grid we obtained $v = 0.2613$, with $\lambda_1 = (0.610680, 0.369400)$ being the eigenvalue which determined the stability. It is interesting to note that the plot of *Re* of the eigenfunction (see Fig. 5.4) is qualitatively different: $Re\varphi(0,y)$ has zeroes, because in this case stability is determined by the second eigenvalue.
We then considered a domain bounded by the 12-petal epitrochoid ($n = 12$, $\varepsilon = 0.0625$) and two boundary condition types: clamping and simple support. The air flow velocity vector is directed at an angle of $\theta = 0$, $\pi/12$, and $\pi/4$ with respect to the axis *ox*. Due to symmetry, the critical velocities for the latter two angles must coincide, and checking this was one of the purposes of our calculations. The boundary value problem of the first kind was considered first. For $\theta = 0$, we obtained on the 9×15 grid the critical flutter velocity $v = 0.2805$, while on the 15×31 grid it was obtained that $v = 0.2848$. Stability is determined by the first eigenvalue $\lambda = (0.940611, 0.458456)$. The plots of *Re* of the eigenfunction are shown in Fig. 5.5.

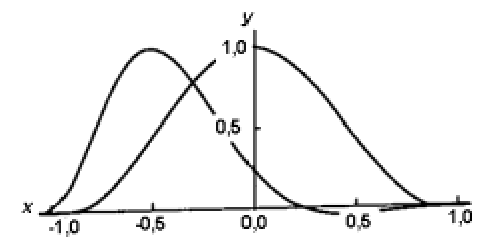


Fig. 5.5. *Plot of Re φ (boundary value problem of the first kind),*
v = 0,2848, n = 12, ε = 0,0625

The second calculation was carried out for θ = π/12. On the 9×15 we obtained the critical flutter velocity *v* = 0.2803, while on the 15×31 it was obtained that *v* = 0.2849. Stability is determined by the first eigenvalue λ = (0.940768, 0.458494). For θ = π/4, we obtained on the 9×15 grid that *v* = 0.2796, whereas on the 15×31 grid it was obtained that *v* = 0.2851. Thus, two last calculations gave practically coinciding results which confirms the reliability of the proposed approach.

Then, the boundary value problem of the second kind was considered on the same domain. For θ = 0, we obtained on the 9×15 grid that *v* = 0.2152, while on the 15×31 grid it was found that *v* = 0.2291.

Stability is determined by the first eigenvalue λ = (0.618777, 0.371835). The plot of *Re* of the eigenfunction is presented in Fig. 5.6.

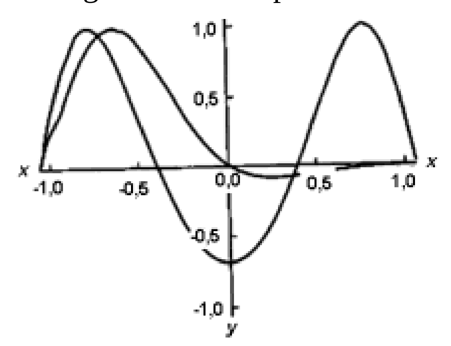


Fig. 5.6. *Plot of Re φ (boundary value problem of the second kind),*
v = 0.2291, n = 12, ε = 0.0625

The next calculation on this domain was carried out for the simply supported edge with θ = π/12. On the 13×25, it was obtained that *v* = 0.2351, while on the 15×31 grid we obtained *v* = 0.2305. Stability is determined by the first eigenvalue λ = (0.634463, 0.373240). For θ = π/4, the value obtained on the 15×31 grid is *v* = 0.2385. Evidently, results of the latter two calculations agree with high accuracy.

The problems described in this section were of test nature, they were aimed at the demonstration of predictive capabilities of the proposed approach. In the following section, we resort to a real research problem.

5.2.5. Dependence of the critical flutter velocity on the plate thickness

In this section, we consider the computational experiments in which the dependence of the critical flutter velocity on the plate thickness is studied. The following approach is taken: for a round plate, and a plate bounded by an epitrochoid (ε = 0.1, *n* = 4) we perform calcu-

lations in which the plate thickness is varied between $h = 0.001$ and $h = 0.01$ with the step of 0.001, then the critical velocities obtained are fitted by an analytical formula $v = v(h)$. The calculations were carried out for the same parameters of the plate as were used in the previous section.

For a round plate clamped at its edge, the following critical flutter velocities are obtained: 0.1404 (3), 0.1544 (2), 0.2791 (1), 0.4801 (1), 0.8361 (1), 1.3806 (1), 2.1482 (1), 3.1745 (1), 4.4955 (1), 6.1476 (1). Here, the number in parentheses denotes the number of the eigenvalue by which stability was determined. Interestingly, for a thin plate the stability is determined by the eigenvalue other than the first one (compare with calculations from the previous section). It turned out that the dependence of the critical flutter velocity on the plate thickness takes the form $v = a + bh^3$. The values of constants a and b are given in Fig. 5.7. It is evident from this graph that the above analytical formula approximates the data of numerical experiments with high accuracy.

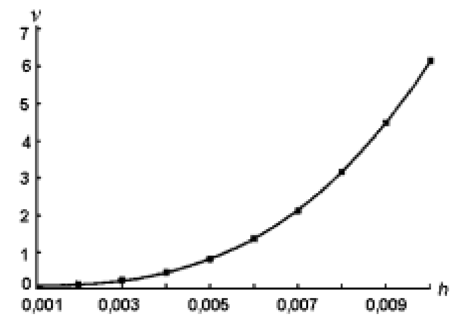


Fig. 5.7. *Dependence of the critical flutter velocity on the plate thickness (round plate clamped at its edge);* $v = a + bh^3$, $a = 0.091048718$; $b = 6124609.2$

The second calculation was carried out for a round plate simply supported at its edge. The following critical flutter velocities were obtained: 0.1283 (3), 0.1306 (3), 0.2241 (1), 0.3236 (1), 0.5237 (1), 0.8386 (1), 1.2862 (1), 1.8870 (1), 2.6618 (1), 3.6317 (1). The dependence $v = v(h)$ has the same form as in the first calculation, albeit with different constants a and b (Fig. 5.8).

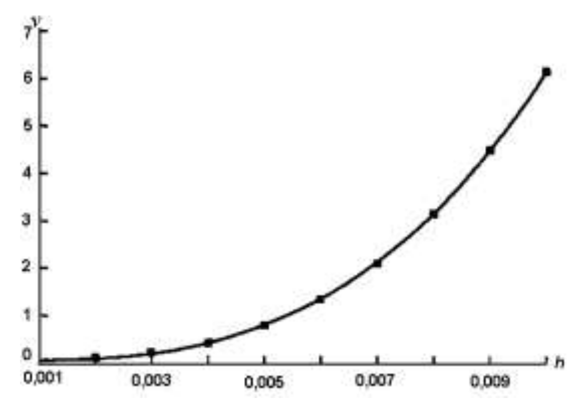


Fig. 5.8. *Dependence of the critical flutter velocity on the plate thickness (round plate simply supported at its edge);* $v = a + bh^3$, $a = 0.10004173$; $b = 6028457$

The last calculation was carried out for a plate with the outer contour formed by an epitrochoid ($\varepsilon = 0.1$, $n = 4$) and clamped edge (the air velocity vector was directed along the axis *ox*). The following critical flutter velocities were obtained: 0.08913 (3), 0.1531 (2), 0.2797

(1), 0.4878 (1), 0.8487 (1), 1.4001 (1), 2.1776 (1), 3.2171 (1), 4.5553 (1), 6.2289 (1). The dependence $v = v(h)$ has the same form as in the first calculation, albeit with different constants a and b (Fig. 5.9).

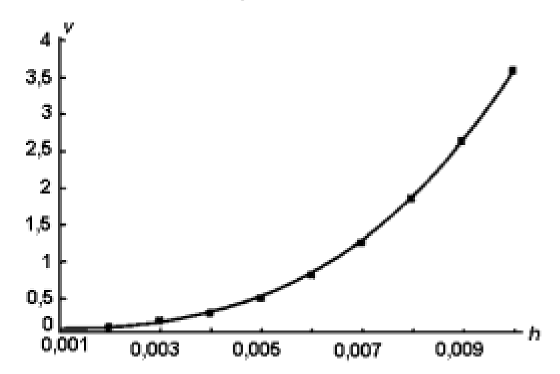


Fig. 5.9. *Dependence of the critical flutter velocity on the plate thickness (plate with an epitrochoid outer contour (e = 0,1, n = 4) and clamped edge, the air velocity vector was directed along the axis Ox);* $v = a + bh^3$, $a = 0.10124565$; $b = 3511783$

All the above-mentioned calculations were carried out on the 9×15 grid. To check the accuracy, calculations were also performed with $h = 0.01$ on a 15×31 grid. For the round plate, the critical flutter velocity coincided, with all the decimal places presented. For the epitrochoid, a close value of 6.2310 (1) was obtained. Looking ahead, we note that for a rectangular plate (see section 5.3), the dependence $v = v(h)$ has the same form as in the calculations which has just been considered, albeit with different constants a and b. The result obtained has important practical implications. It is sufficient to calculate the critical flutter velocity for two values of the thickness, then determine a and b, after which the formula $v = a + bh^3$ can be applied. This enables one to save a substantial amount of computational time.

5.3. Flutter of Rectangular Plate

The panel flutter of rectangular plates, as a rule, has been studied in a partial formulation [3] with the flow velocity vector parallel to one of the plate sides (see review in [4]). In papers [5, 6], which are exception from the above formulation, there is no substantiation of the derivation of the equations used. In [7, 1], the problem of the panel flutter of shallow shells and plates is considered in the general form using the planar section approach of supersonic aerodynamics and formulations of new problems are given. Conventional methods of numerical solution of these problems (finite-difference and finite-element methods having saturation [8]) appear to be ineffective [9], the accuracy of the Bubnov—Galerkin method in the solution of these problems has not been studied.

In the present Section, the numerical-analytical non-saturating algorithm developed in Section 5.1 for the flutter of a plate with an arbitrary smooth contour is extended to the case of a rectangular plate with an arbitrarily oriented flow velocity vector. Calculation results are compared with the results obtained using the Bubnov-Galerkin method in an eight-term approximation, as well as with A.A.Movchan's results [10].

5.3.1 Statement of the problem

The problem of the flutter of a rectangular plate occupying a region K: $\{|x|\le 1, |y|\le b\}$ in the plane xy reduces to the determination of eigenfunctions of the system [1, 9]:

$$D\Delta^2\varphi - k\boldsymbol{n}v\text{grad}\varphi = \lambda\varphi,\ \varphi = \varphi(x,y),\ x,y \in K, \qquad (5.3.1)$$

$$\phi|_{\partial K} = 0, \qquad (5.3.2)$$

$$\left.\frac{\partial\phi}{\partial x}\right|_{|x|=1} = 0,\quad \left.\frac{\partial\phi}{\partial y}\right|_{|x|=b} = 0, \qquad (5.3.3)$$

$$\left.\frac{\partial^2\phi}{\partial x^2}\right|_{|x|=1} = 0,\quad \left.\frac{\partial^2\phi}{\partial y^2}\right|_{|x|=b} = 0. \qquad (5.3.4)$$

Here, $D = Eh^3/(12(1-\nu^2)p_0 a^3)$ is the dimensionless rigidity of the plate, E and ν are Young's modulus and Poisson's ratio of the plate material, h is the thickness, a is the half-length in the x-direction, k is the polytropic index of the gas, p_0 is the freeflow pressure, $\boldsymbol{V} = \{v\cos\theta, v\sin\theta\}$ is the flow velocity normalized by the speed of sound, $v = |\boldsymbol{V}|$, the vector $\boldsymbol{n} = \{\cos\theta, \sin\theta\}$ defines the direction $\boldsymbol{V}$. The function $\varphi = \varphi(x,y)$ is the deflection amplitude, $w = \varphi\, exp(\omega\, t)$; therefore λ in (5.3.1) ,is defined by the relation

$$\lambda = -\rho h\omega^2 - k\omega, \qquad (5.3.5)$$

where ρ is the dimensionless density of the plate material normalized by the parameter p_0 / c_0^2, and the thickness h is normalized by a. The boundary conditions (5.3.2) and (5.3.3) imply that the plate is clamped at its edge, whereas the boundary conditions (5.3.2) and (5.3.4) imply the simple support.

The plate oscillations are stable for $Re\omega < 0$ and unstable for $Re\omega > 0$. In the complex plane $\lambda = \alpha + \beta i$, the regions of stable and unstable oscillations according to (5.3.5) are separated by the stability parabola [10] $F(\alpha,\beta) = k^2\alpha - \rho h\beta^2 = 0$. Since $\alpha = \alpha(v,\theta)$ and $\beta = = \beta(v,\theta)$, the equation $F(\alpha(v,\theta), \beta(v,\theta)) \equiv f(v,\theta) = 0$ in the plane of the parameters v,θ defines the neutral curve separating the region of subcritical values.

The following common properties of the eigenvalues of problem (5.3.1)-(5.3.4) are known [9–11]: 1) $Re\lambda > 0$; 2) the oscillations corresponding to the real values of λ are stable; 3) for fixed θ, the eigenvalues sequentially pass into the complex region as v increases; for a given value of v, the number of complex values λ is finite. According to this, the following scheme of analysis is adopted:

a) a discrete analog of the problem (5.3.1)–(5.3.4) is developed;

b) for a fixed θ, the critical velocity is determined from the first eigenvalue;

c) with the critical velocity obtained, a stability analysis is performed for other complex eigenvalues;

d) if a complex value of λ is found outside the stability parabola, the critical velocity is evaluated from this eigenvalue;

e) the smallest value is chosen from all the critical velocities thus obtained.

5.3.2 Discretization

We shall construct a discrete Laplacian H with boundary condition (5.3.2) using the procedure described in Section 3.2.

In the plane (x,y), we choose a grid consisting of:

$$x_\nu = \cos((2\nu - 1)\pi/2n),\ \nu = 1,2,\ldots,n; \qquad (5.3.6)$$

$$y_\mu = b\cos((2\mu - 1)\pi/2m),\ \mu = 1,2,\ldots,m; \qquad (5.3.7)$$

Let A be the matrix of the discrete operator corresponding to the differential operator $\partial^2\varphi/\partial x^2$ with the boundary condition $\varphi(-1) = \varphi(1) = 0$ on the grid (5.3.6), and let B be the matrix of the discrete operator corresponding to the differential operator $\partial^2\varphi/\partial y^2$ with the boundary condition $\varphi(-b) = \varphi(b) = 0$ on the grid (5.3.7).
Then, the discrete Laplacian becomes:

$$H = I_m \otimes A + B\otimes I_n, \tag{5.3.8}$$

where I_n and I_m are unit matrices of size $n\times n$ and $m\times m$; the $\otimes$ sign denotes the Kronecker matrix product. The eigenvector of the matrix H has the form $u = w\otimes v$, where v is the eigenvector of the matrix A and w is the eigenvector of the matrix B. In this case, the grid nodes are numbered first on x and then on y (right to left and bottom to top). One can state that the matrix (5.3.8) inherits the variable separation property of the differential Laplacian (see more details in Chapter 3).
Discretization of operator $\partial^2\varphi/\partial x^2$ with the boundary condition $\varphi(a) = \varphi(b) = 0$ is performed as follows: a) on the grid (5.3.6) ($a = -1$, $b = 1$) or (5.3.7) ($a = -b$, $b = b$), the interpolation Lagrange formula satisfying the boundary conditions is written; b) the second derivatives at the grid nodes are evaluated by differentiating the interpolation formula. As a result, we have:

$$D_{ij} = \left(\frac{2}{b-a}\right)\frac{2}{k\sin^2\psi_j}\sum_{q=0}^{k-1}\cos(q\psi_j)[(2+q^2)\cos q\psi_i + 3q\cos\psi_i + \\ +3q\cos\psi_i\frac{\sin q\psi_i}{\sin\psi_i}],\ \psi_j = \frac{(2j-1)\pi}{2k},\ i, j = 1, 2, ..., k. \tag{5.3.9}$$

Here, $k = n$, $a = -1$, $b = 1$ for the matrix A; $k = m$; $a = -b$, $b = b$ for the matrix B.
Discretization of the derivatives $\partial\varphi/\partial x$ and $\partial\varphi/\partial y$ is performed similarly. The interpolation Lagrange polynomial is written on the corresponding grid (5.3.6) or (5.3.7), and the values of the derivatives at the grid nodes are obtained by differentiating this interpolation formula. As a result, we obtain the differentiation matrix

$$D_{\nu\mu} = \frac{4}{k(b-a)}\sum_{q=0}^{k-1}\frac{q\cos q\psi_m \sin q\psi_\nu}{\sin\psi_\nu},\ \psi_\nu = \frac{(2\nu-1)\pi}{2k}, \\ \nu, \mu = 1, 2, ..., k. \tag{5.3.10}$$

For $k = n$, $a = -1$, $b = 1$ we obtain the matrix D^x of differentiation with respect to x; for $k = m$, $a = -b$, $b = b$ we obtain the matrix D^y of differentiation with respect to y. To obtain the derivatives of the function φ at the grid nodes, it is necessary to multiply the matrix D by the vector of the values of the function φ at the grid nodes. A consequence of boundary conditions (5.3.2) and (5.3.4) is the condition

$$\Delta\phi\big|_{\partial G} = 0, \tag{5.3.11}$$

ln this case, the matrix of the biharmonic operator with boundary conditions (5.3.2) and (5.3.11) is H^2 because the matrix H^2 has the same eigenvectors as the matrix H and the eigenvalues $\lambda_i^2, i = 1, 2, .., N$, where λ_i are the eigenvalues of the matrix H of size $N \times N$ ($N = mn$).
Let us consider discretization of Eq. (5.3.1) with boundary conditions (5.3.2) and (5.3.3), i.e., a plate clamped along the contour.
For the function $\varphi = \varphi(x,y)$ in the rectangle, we write the interpolation formula:

$$\varphi(x,y) = \sum_{j=1}^{n}\sum_{i=1}^{m} M_{i0}(z)L_{j0}(x)\varphi(x_j, y_i), \tag{5.3.12}$$

$$y = bz,\ z \in [-1,1],\ x \in [-1,1].$$

$$L_{j0}(x) = \frac{l(x)}{l'(x_j)(x - x_j)},\ l(x) = (x^2 - 1)^2 T_n(x),$$

$$T_n(x) = \cos n \arccos x,$$

$$x_j = \cos\vartheta_j,\ \vartheta_j = (2j - 1)\pi/2/n,\ j = 1, 2, ..., n;$$

$$M_{i0}(z) = \frac{M(z)}{M'(z_i)(z - z_i)},\ M(z) = (z^2 - 1)^2 T_m(z),$$

$$z_i = \cos\vartheta_{i,}\ \vartheta_i = (2i - 1)\pi/2m,\ i = 1, 2, ..., m.$$

The interpolation formula (5.3.12) satisfies the clamped boundary conditions. To obtain the matrix of the discrete biharmonic operator H, it is necessary to apply the biharmonic operator to the interpolation formula (5.3.12); it is necessary to differentiate formula (5.3.12) with respect to x and y four times. As a result, we obtain an asymmetric matrix H of size $N\times N$, $N = mn$. Let us number the nodes in the rectangle (x_j,y_i) first along y and then along x, i.e., from top to bottom and from right to left. As a result, the expression $\Delta^2\varphi$; is approximated by the expression $H\varphi$, where φ is the vector of the values of the function $\varphi = \varphi(x,y)$ at the grid nodes. We note that the matrix H is asymmetric although the biharmonic operator considered is self-conjugate. Consequently, the matrix H can have complex eigenvalues. In the stability problems, the presence of complex eigenvalues (due to discretization errors) for the discrete biharmonic operator is undesirable. Therefore, the approach used should be modified. Instead of the matrix H, we consider the matrix $(H + H')/2$. This approach can be explained as follows. The original problem is self-conjugate (biharmonic equation with a clamped boundary condition) but discretization results in an asymmetric matrix H. Let us write H as

$$H = (H + H')/2 + (H - H')/2$$

and consider the asymmetric part as the discretization error. The perturbation thus introduced into the eigenvalues of the matrix H depends on how close are the resolvents of the matrices H and $(H + H')/2$ in the part of the complex plane of interest for the flow stability analysis. This perturbation can be estimated theoretically using the scheme described in Chapter 1; hereafter some results of numerical evaluation of this perturbation are given.

The matrix H (for $b = 1$) of size 361×361 (361 = 19 × 19) has the first eigenvalue $\sqrt{\lambda_1}/\pi^2$ = 2.4902; this value was compared with the one obtained in [12] $\sqrt{\lambda_1^*}/\pi^2$ = 2.489; the matrix $(H + H')/2$ has the eigenvalue $\sqrt{\lambda_1'}/\pi^2$ = 2.3961. Thus, the perturbation introduced into the eigenvalues of the matrix H by symmetrization is acceptable.

Discretization of $qrad\varphi$ in the boundary-value problem (5.3.1)–(5.3.3) was performed similarly.

5.3.3. Numerical results

In this Section, we consider calculation results for a simply supported plate with the same mechanical parameters as in Section 5.2.4. Variation was performed for the (relative) size *b*, thickness *h*, flow velocity *v*, and angle θ.

1. Test calculations were performed for a square plate (b = 1, h = 0.003). The following results were obtained: $v_{cr}.(0) = v_{cr}.(\pi /2) = 0.2103$, $v_{cr.}(\pi /4) = 0.2001$; in all cases v_{cr}. was determined from the first eigenvalue (hereafter, λ_k are numbered in the ascending order). The plots of $Re\varphi(x,0)$ and $Re\varphi(0,y)$ are identical.

2. Results obtained for a plate with dimensions b = 0.5 and h = 0.003 are presented in Table 5.1; the eigenvalue number is given in parentheses for each critical velocity.

Table 5.1. b = 0.5, h = 0.003

θ	**0**	**π/8**	**π/4**	**5π/16**	**3π/8**	**15π/32**	**π/2**
$V_{cr.}$	0.3546 (1)	0.3737(1)	0.4346(1)	0.4801(1)	0.5235(1)	0.5275(2)	0.5257(2)
V^*_{cr}	0.3042	0.3307	–	0.4207	–	0.4022	0.4121

We note the following circumstance, which may be important in the numerical analysis of flutter: the values $|\lambda_1|$ = 1.5658 and $|\lambda_2|$ = 1.56660 are close, but $\lambda_1 > 0$ is real-valued and does not generate unstable vibration modes. In the third row of the table, the values of v^*_{cr} obtained by the Bubnov—Galerkin method in an eight-term approximation. Evidently, this method gives substantially underestimated values (the capabilities of the Bubnov-Galerkin method in application to the current problem will be discussed later).

Two points are worth noting:

a) the critical velocity increases abruptly in the angle range $\theta \in (\pi/4, 3\pi/8)$ and varies smoothly for other values of the angles;

б) the maximum of the critical flutter velocity is near the point θ = 15π/32 (so-called stabilization effect of plate vibrations with respect to fluctuations in the velocity vector direction in the neighborhood of θ = π /2.

We note that in [13], this effect was obtained when solving the flutter problem for a strip. Figures 5.10–5.12 show the real parts of the eigenfunctions for different angles θ (π/4, 5π/16, 3π/8) and $v = v_{кр.}$.

Calculations were performed for an elongated plate with dimensions b = 0.25, h = 0.0015 (the ratio of thickness to the smaller side of the plate is the same as in the previous calculation). Calculated results are summarized in Table 5.2.

Table 5.2. b = 0.25; h = 0.0015

θ	**0**	**π /8**	**π /4**	**5π /16**
$V_{cr.}$	0.2655(3)	0.2832(3)	0.3453(1)	0.4014(1)
θ	3π/8	7π/16	15π/32	π/2
$V_{cr.}$	0.4803(1)	0.4912(2)	0.4867(3)	0.4851(4)

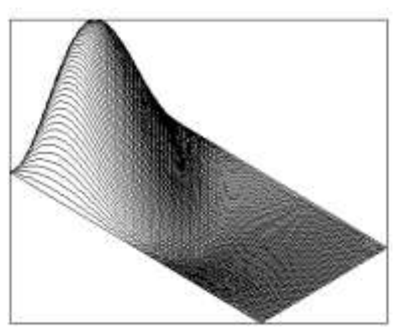


Fig. 5.10. *Rectangular plate (b = 0,5, h = 0,003), real part of the eigenfunction for angle* $\theta = \pi/4$ *and for* $v = v_{cr}$*;* $v = 0,4346$

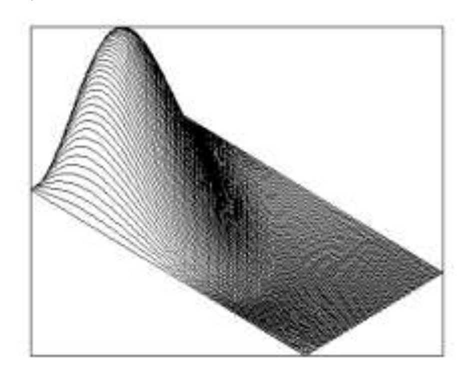


Fig. 5.11. *Rectangular plate (b = 0,5, h = 0,003), real part of the eigenfunction for angle* $\theta = 5\pi/16$ *and for* $v = v_{cr}$*;* $v = 0,4801$

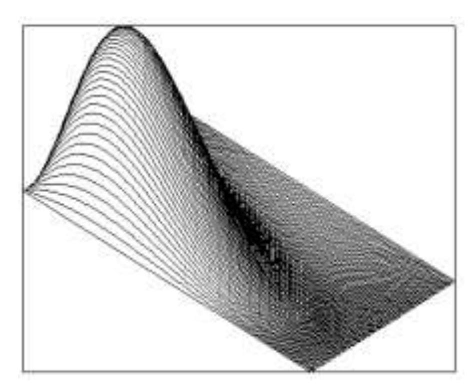


Fig. 5.12. *Rectangular plate (b = 0,5, h = 0,003), real part of the eigenfunction for angle* $\theta = 3\pi/8$ *and for* $v = v_{cr}$*;* $v = 0,5235$

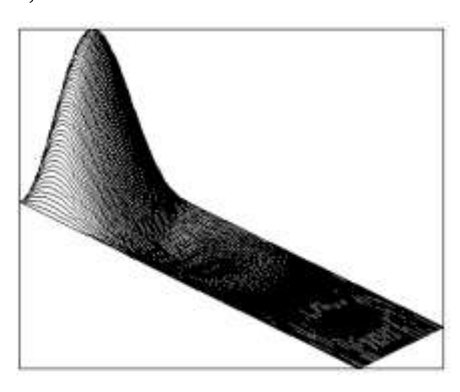


Fig. 5.13. *Rectangular plate (b = 0,25, h = 0,0015), real part of the eigenfunction for angle* $\theta = 0$ *and for* $v = v_{cr}$; $v = 0{,}2665$

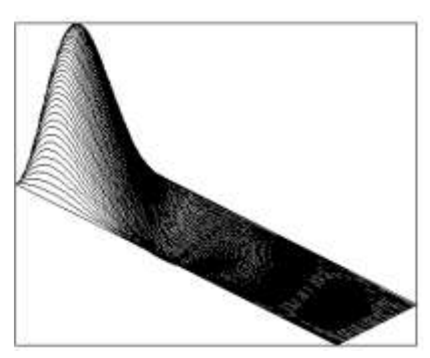


Fig. 5.14. *Rectangular plate (b = 0,25, h = 0,0015), действительная часть собственной функции при угле* $\theta = \pi/4$ *and for* $v = v_{cr}$; $v = 0{,}3541$

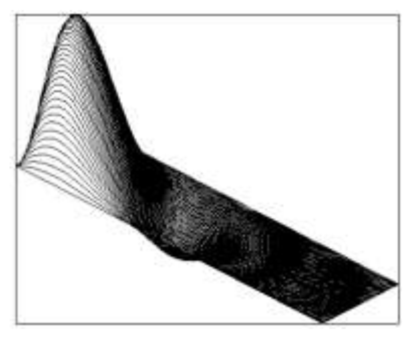


Fig. 5.15. *Rectangular plate (b = 0,25, h = 0,0015), real part of the eigenfunction for angle* $\theta = 5\pi/16$ *and for* $v = v_{cr}$; $v = 0{,}4014$

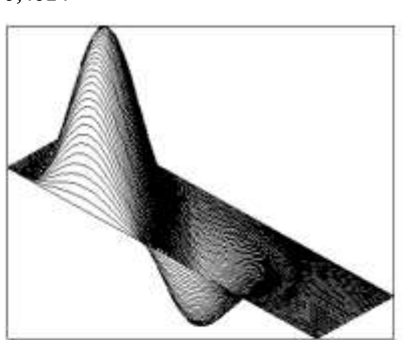


Fig. 5.16. *Rectangular plate (b = 0,25, h = 0,0015), real part of the eigenfunction for angle* $\theta = 3\pi/8$ *and for* $v = v_{cr}$; $v = 0{,}4803$

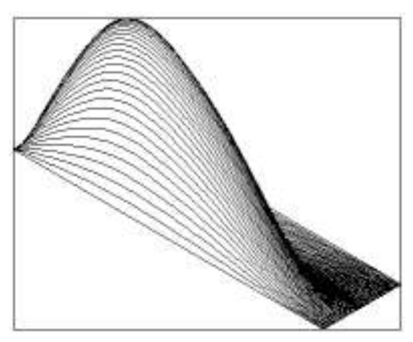


Fig. 5.17. *Rectangular plate (b = 0,25, h = 0,0015), real part of the eigenfunction for angle $\theta = 7\pi/16$ and for $v = v_{cr}$; v = 0,4912*

5.3.4. Bubnov-Galerkin (B-G) Method

It is assumed that in the rectangular plate flutter problem (in the traditional formulation $V = \{v_x, 0\}$) the Bubnov—Galerkin method gives a reasonable value of the critical velocity even in the two-term approximation. However, it is noted in [4] that in the case of a plate elongated in the streamwise direction, the effectiveness of the method decreases abruptly, and to reach some reasonable accuracy it is necessary to retain a considerable (generally speaking, unknown beforehand) number of terms in the approximating sum. Applicability of the Bubnov-Galerkin method to flutter problems for a plate in the general formulation has been studied insufficiently. The results given below fill in this gap to some extent. It follows from the figures presented that the characteristic dimension of perturbation is of the order of half the smaller side of the plate; therefore, an approximate solution was sought in the form $\varphi = c_{mn} sin m\pi y sin \beta\pi x$, $m = 1,2$; $n = 1,\ldots,4$ (the plate occupies the region $K = \{0 \le x \le \le 1/\beta, 0 \le y \le 1\}$). The standard procedure of the Bubnov—Galerkin method for solving Eq. (5.3.1) is reduced to the examination of the roots of the characteristic determinant of the eighth order, which is not written here because of its cumbersome form. It is necessary to determine the dependence $\lambda = \lambda(v,\theta)$. The calculated results are presented in the third column of Tables 5.2 and 5.3 for a plate with dimensions $b/a = 0.5$, $h/a = 0.003$.

Table 5.3. b = 0.5, h = 0.003, θ = 0; $v_{cr.}$ = 0.3546, $v^*_{cr.}$ = 0.3041

	Reλ	***Imλ***
0.2	0.3054; 0 0.6758; 0	0.2933; 0 0.6723; 0
0.5	0.6381; 0.0666 1.7361; 0	0.5159; 0 0.6522; 0
0.8	0.9426; 0.3118 1.6468; 0	0.7525; 0.2822 1.9168; 0
1.0	1.2452; 0.5275 (*) 1.5355; 0	0.8601; 0.4384 (*) 2.5660; 0.4498
2.0	3.1764; 0.7483 2.6887; 2.0591 (*) 4.9558; 0.1886 6.8751; 0	1.0475; 1.1202 (*) 2.3787; 3.0369 (*) 4.2831; 0.5942 7.8906; 1.7927

Table 5.4. $\theta = \pi/4$; $v_{cr.} = 0.4346$; $v^*_{cr} = 0.4121$

	Reλ	*Imλ*
0.5	0.7066; 0.02435 1.8095; 0	0.6499; 0 0.7027; 0
1.0	1.5252; 0.5838 (*) 1.8760; 0	1.3085; 0.5407 (*) 2.7396; 0.3776
2.0	3.4437; 2.5618 (*) 4.0025; 1.6035 (*) 4.8677; 0.3876 7.1122; 0	2.8552; 0.1886 2.3907; 2.3365 (*) 3.3375; 3.2750 (*) 7.0163; 1.1392

The first column is *Reλ*, the second one is *Imλ*, the (*) sign denotes the values of λ on the stability parabola or beyond it. The relative flow velocity $v/v^*_{cr.}$ is presented in the first columns of the tables. The second column of the tables contains the eigenvalues obtained by the method described here for the relative velocity $v/v_{cr.}$. An analysis of the results allows the following conclusions to be drawn:

(a) the Bubnov-Galerkin method gives satisfactory estimates for values of v^*_{cr} if the number of terms in the formula for φ is not less than N~$4a/b$ (two "half-waves" along the smaller side and $2a/b$ "half-waves" along the larger side);

(b) in the determination of the dependence $\lambda = \lambda(v,\theta)$, and consequently, the vibration modes, the Bubnov—Galerkin method gives an error that increases with the increase in the flow velocity and leads to the deterioration of qualitative results.

These conclusions are not final; investigation for plates of different geometries and different combinations of boundary conditions is required.

5.3.5 Comparison with results by A. A. Movchan

In 1955, A. A. Movchan published the calculations of the critical flutter velocity for a simply supported square plate in the particular case where the flow velocity vector is parallel to the side of the plate [10]. At that time, it was impossible to solve the above transcendental equation determining the critical flutter velocity. A. A. Movchan looked for the conditions at which a complex-valued eigenvalue appears in the spectral problem. However, he did not consider what velocity increment is necessary for the eigenvalue to reach the stability parabola. In this subsection, we present the results obtained by the approach proposed above, and compare them with those obtained by A. A. Movchan. The calculations were carried out for the following parameters: $p_0 = 1.0333$ kg/cm^2, $\rho_0 = 1.2283$ kg/m^3, $\nu = 0.3$, $k = 1.4$, $E = 0.2039 \cdot 10^7$ kg/cm^2, $\rho = 7.8\ 10^3$ kg/m^3. The plate thickness was variable. The results obtained are summarized in Table 5.5.

Table 5.5

h	*A.A.Movchan*	*9×9*	*19×19*
5.0000 E-3	1.0000	1.0615 (1)	1.0615 (1)
6.3091 E-3	2.0029	2.0991 (1)	2.0991 (1)
7.2202 E-3	3.0029	3.1325 (1)	3.1324 (1)
7.9365 E-3	4.0029	4.1523 (1)	4.1523 (1)
8.5470 E-3	5.0059	5.1806 (1)	5.1805 (1)
9.0909 E-3	6.0059	6.2296 (1)	6.2295 (1)
9.5694 E-3	7.0059	7.2627 (1)	7.2626 (1)
1.0000 E-2	8.0088	8.2853 (1)	8.2851 (1)
1.0417 E-2	9.0088	9.3632 (1)	9.3630 (1)

Here, in the first column the relative thickness of a square plate is given (b = 1), with E-3 denoting the factor of 10^{-3} (as in FORTRAN standard notation). In the second column, the eigenvalue obtained by A.A.Movchan is given. In the third and fourth columns, the values computed by the current approach on 9×9 and 19×19 grids are presented, respectively. In the parentheses, the number of the eigenvalue by which the stability was determined, is shown. Evidently, the data given in the Table reveal very good agreement. Of course, this is attributed to the form of the stability parabola (5.2.6) for the given parameter values. The maximum relative error observed in the bottom row is 3.8 %.

5.3.6. Dependence of the critical flutter velocity on the plate thickness

Calculations were carried out for a rectangular plate with aspect ratio (1:2) and the same parameter values as in section 5.2.5. Three directions of the velocity vector (i.e., angle between this vector and the axis ox) were used: $\varphi = 0, 3\pi/8, \pi/2$. In all the cases studied, the dependence $v_{кр.} = a + bh^3$ was confirmed. The values of a and b are summarized in Table 5.6 (clamped plate), rows 1, 2, and 3 as well as in Table 5.7 (simply supported plate), rows 1, 2, and 3.

Table 5.6

No.	***a***	***b***
1	0.18086698	88565587
2	0.28562681	16948368
3	0.088122509	29134275

Table 5.7

No.	***a***	***b***
1	0.15705135	6172557.5
2	0.23725284	10966926
3	0.075931991	17242086

The graphs of this dependence are similar to those presented in section 5.2.4, therefore, they are not shown here.

5.3.7. Dependence of the critical flutter velocity on the altitude above sea level

As an example, consider a simply supported rectangular plate with the aspect ratio 1:2 (b = 0.5) and relative thickness 0.005. Let the flow velocity vector be directed along the x-axis. The air pressure and density, gravity acceleration, and speed of sound as functions of altitude above sea level are given in [14]. All other parameters are the same as were used in section 5.3.3. The critical flutter velocity was calculated in the range of altitudes from 0 to 11 kilometers above sea level with the step of 1 kilometer. As before, calculations were carried out on two grids of sizes 9×9 and 19×19. The results obtained coincided within the accuracy with which the roots of the transcendental stability equation were evaluated. In all the cases, stability was determined by the first eigenvalue. The following critical flutter velocities were obtained: 0.9322, 1.0181, 1.1203, 1.2416, 1.3853, 1.5556, 1.7577, 1.9997, 2.2836, 2.6249, 3.0340, 3.5261. Thus, the critical flutter velocity is increased with the altitude above sea level. The data obtained can be approximated by the analytical function v =

$(a + cx + ex^2 + gx^3 + ix^4 + kx^5)/(1 + bx + dx^2 + fx^3 + hx^4 + jx^5)$, where v is the flutter velocity, x is the altitude above sea level. Here, a = 0.93220144, b = -0.03922232, c = 0.041901991, d = -0.0019833293, e = 0.002180686, f = 0.0002874881, g = 0.00012557829, h = -2.2255284e-5, i = 2.7092604e-6, j = 6.2616321e-7, k = -9.2719828e-7. Evidently, this analytical function is cumbersome and does not give clear view of the growth of the critical flutter velocity. Therefore, a simpler analytical approximation to the calculated data was also used: $v = a + bx^c$, a = 1.0064589, b = 0.021827843, c = 1.9714133.This approximation has accuracy within several percent at the altitudes below one kilometer; at higher altitudes the accuracy of the approximation is even better. Thus, the dependence of the critical flutter velocity on the altitude is nearly quadratic.

5.4. Flutter of shallow shells

In this section, we study numerically the flutter of shallow shells. First, we consider the flutter of a round-in-plan shallow spherical shell. From computational experiments we obtain the dependence of the critical flutter velocity on the shell thickness. It is shown that this dependence has the form $v = a + bh^c$, where a, b, and c are constants dependent on the problem parameters.

Then, an arbitrary rectangular in plan shallow shell is considered.

In paper [2], a new statement of flutter problem for a shallow shell is proposed which assumes that the excess pressure onto the shell is determined from the law of planar sections of supersonic aerodynamics [1]. From the mathematical point of view, the problem is reduced to an eigenvalue problem for a system of two equations with biharmonic higher-order operators with respect to the deflection amplitude function φ and stress function F. For some types of boundary conditions, the stress function F can be (numerically) eliminated; the remaining equation for φ will contain two non-dimensional constants of the orders 10^{-3} and 10^2 (for the characteristic parameter values) at the high-order derivatives, which makes the problem ill-conditioned. On the other hand, the solution includes the boundary layer, which indicates the necessity to refine the grid towards the contour.

The above-mentioned computational difficulties can be very efficiently overcome by the non-saturating method by K.I.Babenko. It was successfully applied to the study of flutter of a plate having arbitrary shape in plan (see section 5.2). In this chapter, the method is generalized to panel flutter problems of rectangular in plan shallow shells. Calculations are performed in the particular cases of cylindrical and spherical shells.

5.4.1. Flutter of a round-in-plan shallow spherical shell

In sections 5.2.5 and 5.3.5, the critical flutter velocity for a plate of arbitrary shape in plane was studied as a function of the plate thickness. It was shown that this dependence takes the form $v = a + bh^3$, where a and b are constants determined by the plate parameters. In this section, we continue similar studies for a round-in-plan shallow spherical shell. It turns out that the dependence $v = v(h)$ takes more complex form $v = a + bh^c$, where a,b, and c are constants determined by the shell parameters. In particular, c depends on the edge fixation, i.e., on the boundary conditions. This is different from the case of a plate, where in all problems studied it was obtained that $c = 3$. The approach we take is a computational experiment. A number of numerical simulations is carried out, after which an analytical dependence is found in the above-mentioned functional form. The details of these numerical experiments are considered below.

5.4.2. Formulation and numerical algorithm

We study the vibrations of a round-in-plan shallow spherical shell by considering the equation [15]:

$$D\Delta^2 w + (Eh/R^2)w + (\kappa p_0/c_0)(V grad w + \partial w/\partial t) + \rho h \partial^2 w/\partial t^2 = 0, \quad (5.4.1)$$

where R is the radius of the sphere, E is Young's modulus of the shell material, D is the cylindrical rigidity, h is the shell thickness, k is the polytropic index of air, p_0 is the air pressure in the undisturbed flow, c_0 is the speed of sound in the undisturbed flow, ρ is the shell material density. We use the same scales as in (5.2.1) to non-dimensionalize the problem: $E = E'p_0$, $h = h'l$, $\rho = \rho' p_0/c_0^2$, $\omega = \omega' c_0/l$, $\mathbf{V} = \mathbf{V}'c_0$, $w = w'l$, $x = x'l$, $y = y'l$, $R = R'l$, $t = t'l/c_0$, where l is the radius of the planform circle. In what follows, we omit the primes denoting the non-dimensional quantities. Assume that $w = \varphi \cdot \exp(\omega t)$; then we obtain from (5.4.1) that

$$D\Delta^2\varphi + \kappa \mathbf{V} grad\varphi = \lambda\varphi, \quad (5.4.2)$$

$$\lambda = -\rho h\omega^2 - \kappa\omega - b,\ b = Eh/R^2 \quad (5.4.3)$$

Consider two types of boundary conditions:

1) rigidly clamped edges

$$(x,y)\in\Gamma,\ \varphi = 0,\ \partial\varphi/\partial n = 0, \quad (5.4.4)$$

2) simply supported edges

$$(x,y)\in\Gamma,\ \varphi = 0,\ \Delta\varphi - ((1-\sigma)/l)\partial\varphi/\partial n = 0 \quad (5.4.5)$$

Here, σ is Poisson's ratio of the plate material, Γ is the boundary of the planform disc, n is the outer normal to it. Equations (5.4.2) – (5.4.3), together with one of the groups of boundary conditions (5.4.4) or (5.4.5) constitute an eigenvalue problem.

Whether the plate vibrations are stable or not depends on whether $Re\omega < 0$ or $Re\omega > 0$; if $\lambda_1 = \alpha_1 + \beta_1 i$ is an eigenvalue, the above inequalities correspond to $F(\alpha_1, \beta_1) > 0$ or $F(\alpha_1, \beta_1) < 0$, where

$$F(\alpha_1, \beta_1) = \kappa(b + \alpha_1) - \rho h\beta_1^2. \quad (5.4.6)$$

Let λ_1 be the first eigenvalue satisfying the condition $F = 0$; in other words, zeroes of the function $F(\alpha_1(V),\beta_1(V))$ have to be found for the given direction of the flow velocity. Evidently, the eigenvalue problems for a shallow shell and for a plate coincide, however, the stability parabola for the shell, according to (5.4.6), is shifted to the left by the value b: $\kappa(b + Re\lambda) = \rho h(Im\lambda)^2$. This entails some qualitatively new results which are studied in detail in the following sections.

5.4.3. Numerical experiments

Calculations were performed with the same parameter values as in section 5.2.1. The linear scale was taken equal to the radius of the planform circle. The relative plate thickness was varied in the range from 0.003 to 0.01 with the step of 0.001; also, the sphere radius R was varied. The computational method is considered in detail in Chapter 5. Note here its main features: the algorithm is non-saturating, i.e., it adjusts automatically to the smoothness of the problem being considered, so that its convergence rate is the higher, the stricter the smoothness conditions that the solution satisfies. Since the solutions of linear elliptic equations are smooth functions, the proposed approach is very efficient and enables acceptable accuracy to be obtained on rather coarse grids.

The first calculation was performed for a sphere of the radius of 2.6, which corresponds to the shell height of 0.2. Computations were carried out in the following sequence: on a coarse 11×19 grid (with 11 circular lines, each containing 19 nodes) the velocity V was incremented with the step 0.01 to detect the change of sign of the stability function (5.4.6) with respect to the first twenty eigenvalues. After finding out the interval at the ends of which the stability function for some eigenvalue number n has different signs, the procedure for the determination of the root of non-linear equation $F(\alpha_n(V),\beta_n(V)) = 0$ was started. The root was obtained by the bisection method in combination with the secant method. Then, for the sake of control, calculations for the same eigenvalue number n were performed on the same interval using the fine 15×31 grid. If the stability function on the fine grid did not have different signs at the ends of the interval, calculations for this interval were continued for all twenty eigenfunctions. If for all other eigenvalues the stability function did not have different signs at the ends of the interval, the search for the root of nonlinear equation $F = 0$ was continued to the left and right of the interval found (although, this was never required in practical calculations). In the example being considered, the critical flutter velocity determined on the two grids coincided up to four decimal places (this was the accuracy with which the root of non-linear equation was obtained). For the boundary-value problem of the first kind (clamping) and h varying in the above-mentioned interval, the critical flutter velocity obtained was: 1.5949(5), 2.1364(2), 2.7418(2), 3.4898(1), 4.3639(1), 5.2117(1), 6.2067(1), 7.5282(1). Here, the number of the eigenvalue which is the first to reach the stability parabola is given in the parentheses. The critical flutter velocities thus obtained were fitted by an analytical function $V = V(h)$. It turned out that this function is of the form $V = a + bh^c$ (Fig. 5.18). In this Figure, the calculated critical velocities are shown by the points; the parameters a, b, and c are also given in Fig. 5.18.

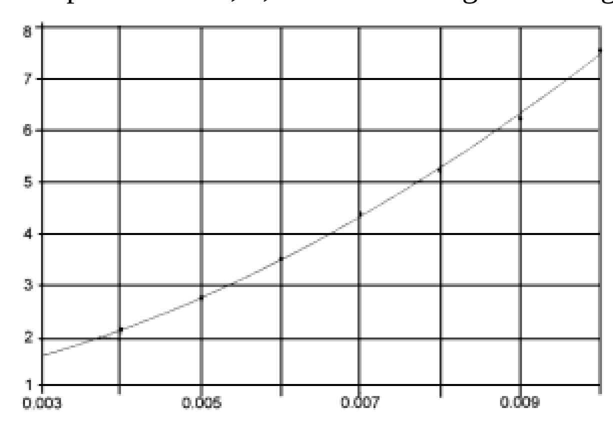


Fig. 5.18. *Fitting by analytical function $V = a + bh^c$, $a = 0.9073437$, $b = 31296.665$, $c = 1.839571$ of the critical flutter velocity for a round-in-plan shallow spherical shell with clamped edges*

The second calculation was performed with the same parameters for the boundary-value problem of the second kind (simply supported edges). The following critical flutter velocities were obtained: 1.5672(7), 2.0654(4), 2.6274(2), 3.1994(3), 3.9113(2), 4.7885(1), 5.5826(1), 6.3013(1). The dependence $V = V(h)$ turned out to be the same as for the boundary-value problem of the first kind, albeit with different parameter values (Fig. 5.19).

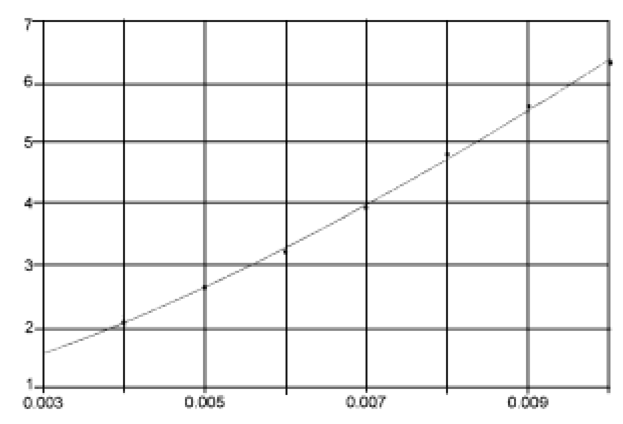


Fig. 5.19. *Fitting by analytical function* $V = a + bh^c$, *a = 0.65753604, b = 6759.6866, c = 1.5366793 of the critical flutter velocity for a round-in-plan shallow spherical shell with simply supported edges*

To clarify the question of how general is the obtained dependence of the critical flutter velocity on the shell thickness, the third calculation was carried out. We set $R = 2$, which corresponds to the shell height 0.2679. Boundary-value problem of the second kind was considered, the calculations were carried out on the 13×21 and 15×31 grids. The values of critical flutter velocity obtained on these grids coincided within the accuracy of the determination of the root of the non-linear equation. The following critical flutter velocities were obtained: 1.8782(9), 2.4620(6), 3.0935(4), 3.7760(3), 4.5015(2), 5.4443(1), 6.4914(1), 7.3992(1). The dependence $V = V(h)$ turned out to be the same as above (Fig. 5.20), albeit with different values of the parameters *a*, *b*, and *c*.

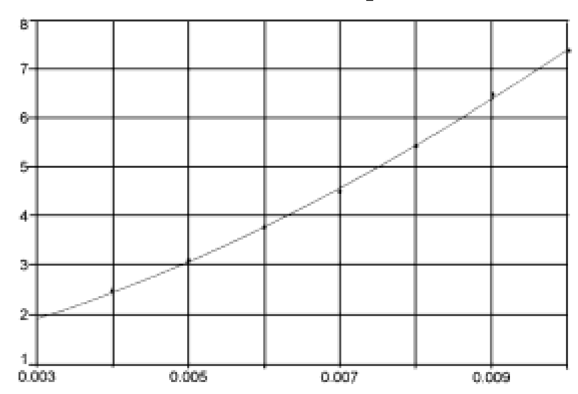


Fig. 5.20. *Fitting by analytical function* $V = a + bh^c$, *a = 1.0363245, b = 13385.075, c = 1.6602728 of the critical flutter velocity for a round-in-plan, shallow spherical shell with simply supported edges (R = 2)*

Note an interesting fact which does not occur for a plate. In Fig. 5.21, the functions $Re\varphi(x,0)$ and $Re\varphi(0,y)$ are shown for $V = 2.4620(6)$ corresponding to $h = 0.004$ in the third calculation. Evidently, the curves have quite a complicated shape.

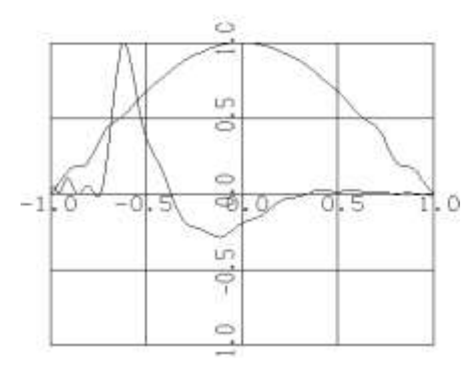


Fig. 5.21. *Functions Reφ(x,0) and Reφ(0,y) for flow velocity V = 2.4620(6), corresponding to h = 0.004 in the third calculation (R = 2)*

For h = 0.005, similar graphs are shown in Fig. 5.22 (V = 3.0935(4)). The shape of the curves has changed substantially and became similar to that in the case of a plate. Thus, for small thickness h, shell instability develops due to the higher modes (for a plate, the instability develops, as a rule, due to the first mode). Similar results are obtained in the other two calculations, but with h = 0.003.

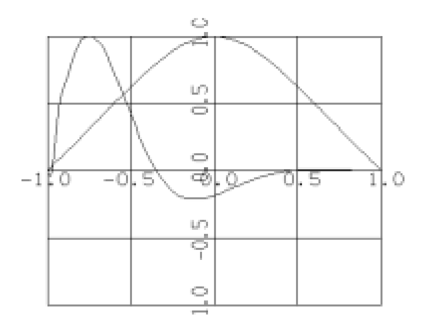


Fig. 5.22. *Functions Reφ(x,0) and Reφ(0,y) for flow velocity V = 3.0935(4), corresponding to h = 0.005 in the third calculation (R = 2)*

5.4.4. Conclusions

Numerous calculations confirmed that the dependence of critical flutter velocity on the shell thickness is expressed by a simple power-law dependence $V = a + bh^c$, where the coefficients a, b, and c are specific to the boundary condition type and problem parameters. Note that, for a plate, the dependence $V = V(h)$ has the same functional form, but with $c = 3$. For shells, the calculations gave $c < 3$. Thus, the critical flutter velocity for a round-in-plan shallow spherical shell is increased with the shell thickness slower than for a round plate with the same problem parameters; however, the critical velocity itself for a shell is higher than for a plate of the same thickness.

The result obtained has important practical implications: to obtain the dependence of the critical flutter velocity for a round-in-plan shallow spherical shell on the shell thickness, it is sufficient to find out three parameters a, b, and c. The latter dependence can be recovered if the critical flutter velocity is found just for three shell thicknesses.

5.4.5. Numerical study of shallow shell flutter

We consider the stability problem for the oscillations of a rectangular-in-plan shallow shell in the gas flow with an arbitrarily directed velocity vector. It will be shown that, from the mathematical point of view, the problem is reduced to an ill-conditioned numerical problem. To solve this problem, a non-saturating computational algorithm is proposed which enabled a solution to be obtained with acceptable accuracy on a grid with 169 = 13 × 13 nodes. In the particular cases of cylindrical and spherical shallow shells, new mechanical effects concerning the vibration modes and dependence of the critical flutter velocity on the direction of the velocity vector are obtained.

5.4.6. Statement of the problem

In the non-dimensional form, the initial system of differential equations is written as [2]:

$$D\Delta^2\varphi - hL(F) - k(\mathbf{v}, grad\,\varphi) = \lambda\varphi \qquad (5.4.7)$$

$$\Delta^2 F + EL(\varphi) = 0 \qquad (5.4.8)$$

$$\lambda = -\rho h\omega^2 - k\omega, \qquad (5.4.9)$$

$$L(f) = k_y\frac{\partial^2 f}{\partial x^2} + k_x\frac{\partial^2 f}{\partial y^2}, \qquad (5.4.10)$$

where $D = Eh^3/12(1-\nu^2)$ is the flexural rigidity, E is Young's modulus, ν is Poisson's ratio, k is the polytropic index, $\mathbf{v}$ is the air flow velocity, h is the shell thickness, ρ is the density of shell material, ω is the complex frequency of vibrations; k_x and k_y are the principal curvatures (the lines of principal curvatures coincide with the coordinate lines); $\varphi = \varphi(x,y)$ is the shell deflection, $F = F(x,y)$ is the stress function. All the above-mentioned quantities are dimensionless. Nondimensionalization was performed in the same way as in Section 5.1.

The above equations are considered on the domain $G = \{-1 \le x \le 1, -b \le y \le b\}$, i.e., on a rectangle; the lines of the principal curvatures of the shell coincide with the coordinate lines.

We solve Eqs. (5.4.7) – (5.4.9) for two types of boundary conditions:

1) hinged (simply supported) edges:

$$x = 1,-1: \varphi = 0, \frac{\partial^2\varphi}{\partial x^2} = 0, \frac{\partial^2 F}{\partial y^2} = 0, \frac{\partial^2 F}{\partial x\partial y} = 0. \qquad (5.4.11)$$

$$y = b,-b: \varphi = 0, \frac{\partial^2\varphi}{\partial y^2} = 0, \frac{\partial^2 F}{\partial x^2} = 0, \frac{\partial^2 F}{\partial x\partial y} = 0. \qquad (5.4.12)$$

2) clamped edges with slip:

$$x = 1,-1: \varphi = 0, \frac{\partial\varphi}{\partial x} = 0, \frac{\partial^2 F}{\partial y^2} = 0, \frac{\partial^2 F}{\partial x\partial y} = 0. \qquad (5.4.13)$$

$$y = b,-b: \varphi = 0, \frac{\partial\varphi}{\partial y} = 0, \frac{\partial^2 F}{\partial x^2} = 0, \frac{\partial^2 F}{\partial x\partial y} = 0. \qquad (5.4.14)$$

It can be shown easily that the boundary conditions imposed on the stress function F can be replaced, without loss of generality, by the equivalent conditions [16]:

$$(x,y) \in \partial G,\ F = 0,\ \frac{\partial F}{\partial n} = 0, \qquad (5.4.15)$$

where n is the vector of outward normal to the contour of the shell.

Whether the shell vibrations are stable or unstable depends on whether $Re\omega < 0$ or $Re\omega > 0$. If $\lambda = \alpha + i\beta$ is the eigenvalue of the formulated problem, in view of (2.3) the inequalities imply that $f(\alpha,\beta) > 0$ or $f(\alpha,\beta) < 0$, where $f(\alpha,\beta) = \alpha k^2 - \rho h\beta^2$. Since $\alpha = \alpha(v_x,v_y)$ and $\beta = \beta(v_x,v_y)$, where $v_x = v\cos\theta$, $v_y = v\sin\theta$, $v = |\mathbf{v}|$, the equation $f(\alpha,\beta) = 0$ determines the neutral curve (stability parabola) in the complex plane λ and the corresponding critical flutter velocity v for a specified θ.

If $v = 0$, all eigenvalues are real-valued; as the flow velocity increases, some eigenvalues enter the complex plane. Consequently, the problem is to find (for a given θ) the first complex eigenvalue that crosses the stability parabola. As a result, the critical velocity and the corresponding vibration mode (eigenfunction) are determined. It follows that, to solve the problem correctly, it is necessary to determine a sufficiently long initial part of the spectrum.

Thus, to determine the root of equation $f(\alpha,\beta) = 0$, on each iteration one has to solve the complete eigenvalue problem for a $N\times N$ nonsymmetric matrix, where N is the number of grid nodes. The difficulties are overcome by the saturation-free method, which provides good accuracy for smooth solutions even on relatively coarse grids. The eigenvalues of the matrix were calculated by the QR algorithm (implemented in EISPACK software package).

5.4.7. Discretization.

To discretize the boundary-value problems described above, it is necessary to discretize the biharmonic operators $\Delta^2\varphi$ and $\Delta^2 F$ with the boundary conditions of simple support (clamping) and clamping, respectively. Also, the operator $L(f)$ and the terms containing first-order derivatives $k(\mathbf{v},grad\,\varphi)$ should be discretized.

We assume that k_x and k_y are constants. We have $k_x = 0, k_y = 1/R$ for a cylindrical shell and $k_x = k_y = 1/R$ for a spherical shell (R is the radius of the shell). Therefore, discretization of the operator $L(f)$ under the homogeneous Dirichlet boundary condition is needed. This discretization is performed according to Chapter 3. The terms with the first-order derivatives $k(\mathbf{v},grad\,\varphi)$ is also discretized in a similar way. It should be noted that since $L(f)$ is a second-order operator, it suffices to satisfy only one boundary condition, namely, $f = 0$ on ∂G, to discretize this operator. Since there are no nodes on the boundary, an interpolation formula that does not satisfy (compulsorily) the boundary condition $\varphi = 0$ на ∂G was used for discretizing the terms with the first-order derivatives. In the discretization of biharmonic operators, both boundary conditions were satisfied. Calculations show that the solution obtained for φ satisfies the boundary conditions.

Discretization of the biharmonic operator under the boundary conditions of simple support or clamping (5.4.15) is described in Section 5.2.2. For the function $F = F(x,y)$ in a rectangle we use the interpolation formula:

$$F(x,y) = \sum_{j=1}^{n} \sum_{i=1}^{m} M_{i0}(z) L_{j0}(x) F(x_j, y_i), \qquad (5.4.16)$$

$$y = bz,\ z \in [-1,1], x \in [-1,1] .$$

$$L_{j0}(x) = \frac{l(x)}{l'(x_j)(x - x_j)}, l(x) = (x^2 - 1)^2 T_n(x),$$

$$x_j = \cos\vartheta_j, \vartheta_j = (2j-1)\pi/2/n, j = 1,2,...,n;$$
$$M_{i0}(z) = \frac{M(z)}{M'(z_i)(z-z_i)}, M(z) = (z^2-1)^2 T_m(z),$$
$$z_i = \cos\vartheta_{i,}\vartheta_i = (2i-1)\pi/2m, i = 1,2,...,m.$$

The interpolation formula (5.4.16) satisfies the boundary conditions (5.4.15). We enumerate the nodes in the rectangle (x_j, y_i) first along y, and then along x, i.e., from top to bottom and from right to left, and substitute (5.4.16) into (5.4.7), (5.4.8). As a result, we obtain:

$$H\varphi - hL^h F = \lambda\varphi \tag{5.4.17}$$
$$H_3 F + EL^h\varphi = 0 \tag{5.4.18}$$

Here, H is a $N\times N$ matrix of the discrete problem for the plate, where $N = mn$. Its construction for the case of simple support is described in Section 5.2.1. Resolving (5.4.18) with respect to F and substituting it into relation (5.4.17), we obtain:

$$(H = hL^h H_3^{-1} L^h)\varphi = \lambda\varphi \tag{5.4.19}$$

In Eq. (5.4.19), φ is a vector containing approximate values of the deflection of the shell at the grid nodes; λ is an approximate eigenvalue; L^h and H_3 are $N\times N$ matrices, resulting from the discretization of operators L (see (5.4.10)) and $\Delta^2 F$.
Further analysis was carried out using the finite-dimensional eigenvalue problem (5.4.19). As was mentioned in the Introduction, this problem contains a large parameter hE (of the order of 10^2 for the data used in calculations). This parameter is multiplied by a matrix which is nonsymmetric and can, therefore, have complex eigenvalues for the flow velocity $\boldsymbol{v}$ = 0, which was established in practical calculations. Therefore, the applied approach was updated. The matrix H_3 in (5.4.19) was replaced by the matrix $H_3 = 0.5(H_3 + H_3')$, where the prime denotes a transposed matrix. This operation can be interpreted in the same way as in Section 5.3.2.
Similar symmetrization was applied to the matrices L^h and H_0 (here, H_0 is the matrix of discrete biharmonic operator for the deflection φ). As a result, the matrix $L^h H_3^{-1} L^h$ became symmetric with an accuracy of 10^{-6}. This, however, was insufficient, since the discrete problem still had complex eigenvalues for $\boldsymbol{v}$ = 0. After the repeated symmetrization of the matrix $L^h H_3^{-1} L^h$, the eigenvalues of the discrete problem for $\boldsymbol{v}$ = 0 became real and positive. In calculating the critical velocity, convergence was observed.

5.4.8. Numerical results

Calculations were performed with the same values of parameters as in Section 5.2.1. The relative thickness and dimensionless radius of the shell were taken to be $3\cdot10^{-3}$ and 2.5, respectively. Preliminary calculations on 9×9, 13×13, and 19×19 grids showed that the results for the 13×13 and 19×19 grids are close. Below, we give the critical velocities obtained for on the 19×19 grid.
Calculations for a square-in-plan spherical shallow shell can be regarded as test ones. For the angles θ = 0, $\pi/8$, $\pi/4$, $3\pi/8$, and $\pi/2$ the following critical velocities were obtained 1.4263 (20), 1.4924 (18), 1.5813 (18), 1.4924 (18), and 1.4263 (20). The bracketed numbers indicate the first eigenvalue that enters the stability parabola. As was expected from the symmetry of the problem, the critical velocities are symmetric about the straight line θ =

$\pi/4$. This supports the correctness of the method and its program implementation. Furthermore, to control the calculations, the following two diagrams were plotted: the deflection function $Re\varphi(x, 0)$ and $Re\varphi(0, y)$ and the two-dimensional function $Re\varphi(x, y)$. For $\theta = \pi/4$ the curves $Re\varphi(x, 0)$ and $Re\varphi(0, y)$ coincide, which confirms the validity of calculations. The eigenfunctions $Re\varphi(x, y)$ are also identical at the angles $\theta = 0$ and $\theta = \pi/2$. This all shows that the calculations are correct.

For a clamped spherical shallow shell, for the same directions of flow velocity vector, the following critical velocities were obtained: 1.6424 (20), 1.7038 (16), 1.6876 (17), 1.7038 (16), 1.62384 (20). Generally, the results are similar to those obtained in the previous case.

Calculations for a rectangular-in-plan ($b = 0.5$) spherical shallow shell were performed. For the case of simple support, the following critical velocities were obtained for the same values of angle θ: 1.7752 (9), 1.8787 (9), 1.8414 (5), 1.8558 (4), 1.7469 (4). For the boundary conditions of clamping, we obtained, respectively: 1.6138 (9), 1.6902 (9), 1.8935 (5), 1.7335 (5), 1.6602 (5).

Further calculations were performed for a square-in-plan cylindrical, simply supported shell. For the same values of angle θ we obtained the following critical velocities: 2.7654 (7), 0.5606 (1), 0.3004 (1), 0.2205 (1), 0.2120 (1). The principal difference is seen between these and the previous results: the velocity decreases abruptly for θ close to $\pi/2$. We note that, for a square plate, the critical velocity is equal to 0.2103 at $\theta = 0$ and $\pi/2$. Thus, the critical flutter velocity for the flow along the generatrix of the cylindrical shell is an order of magnitude higher than that across the generatrix. This effect can be explained easily: the bending rigidity of a cylindrical shell along the generatrix is much higher than that across the generatrix. The evolution of the eigenforms is shown in Figs. 5.23–5.27.

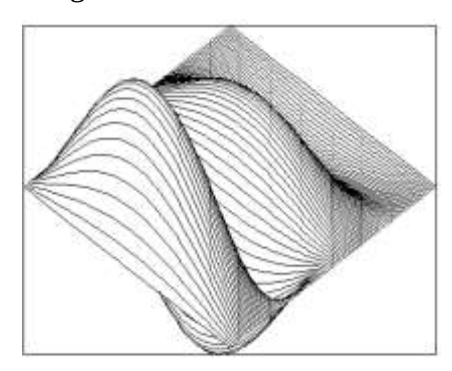


Fig. 5.23. *Calculations for a square-in-plan cylindrical simply supported shell,* $\theta = \pi/2$, $v = 0{,}2120$

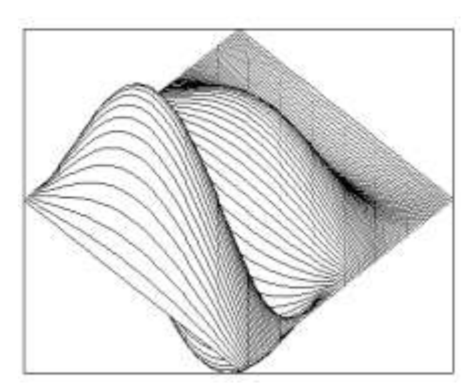


Fig. 5.24. *Calculations for a square-in-plan cylindrical simply supported shell,* $\theta = 3\pi/8$, $\nu = 0{,}2295$

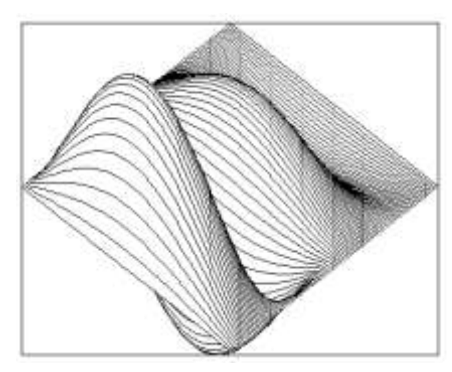


Fig. 5.25. *Calculations for a square-in-plan cylindrical simply supported shell,* $\theta = \pi/4$, $\nu = 0{,}3004$

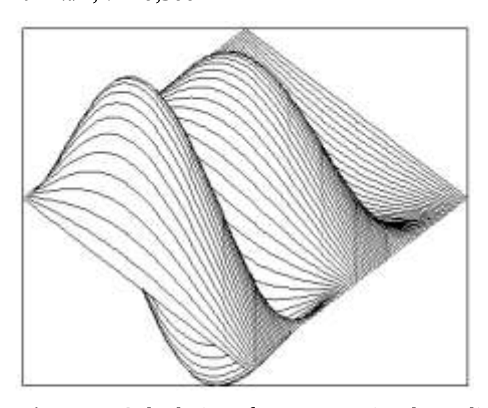


Fig. 5.26. *Calculations for a square-in-plan cylindrical simply supported shell,* $\theta = \pi/8$, $\nu = 0{,}5606$

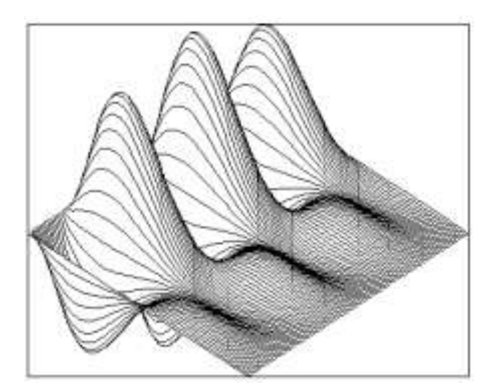


Fig. 5.27. *Calculations for a square-in-plan cylindrical simply supported shell, $\theta = 0$, $v = 2,7654$*

In addition, calculations were performed for cylindrical shells with the radii of 10 and 40 and for the same directions of the flow velocity vector. The critical velocity values obtained for the radius equal to 10 are 0.8216 (14), 0.4629 (1), 0.2287 (1), 0.1727 (1), and 0.1591 (1), and those obtained for the radius 40 are 0.3378 (6), 0.3439 (1), 0.2433 (1), 0.1673 (1), and 0.1514 (1). Thus, as $R \rightarrow \infty$, the critical flutter velocity decreases for the flows directed both along and across the generatrix. This conclusion is very important, since small initial convexity of the shell in a transverse flow (for a radius equal to 40, the shell rise is 0.0125) leads to the decrease in the critical flutter velocity.

5.4.9. Conclusions

An experimental algorithm for the complex computational problem of calculation of the critical flutter velocity of a shallow shell has been described. The calculations show good accuracy for a grid containing 169 = 13×13 nodes. The results were obtained by Babenko’s non-saturating discretization method. All the results concerning the mechanics of solids are new. Flutter of a spherical shallow shell was studied previously by the Bubnov-Galerkin method [17]. As is well known, this method underestimates the critical flutter velocity. A new mechanical effect for a cylindrical panel has been found, namely, the abrupt change in the critical velocity as the angle θ is varied.

References

1. A. A. Ilyushin. The law of planar sections in aerodynamics of high supersonic velocities. Prikl. Mat. Mekh. (1956). V. 20. No. 6. pp. 733–755.
2. A. A. Ilyushin, I. A. Kiyko New formulation of the shallow shell flutter problem Prikl. Mat. Mekh. (1994) V. 58. No. 3. pp. 167–171.
3. A. A. Movchan, “Oscillations of a plate moving in a gas.” Prikl. Mat. Mech., V. 20. No. 2, pp. 231-243 (1956).
4. Novichkov Yu. N. Flutter of plates and shells. Itogi Nauki Tekhniki, Mekh. Deform. Tverdogo Tela. Moscow, VINITI, 1978. p. 67–122.
5. Ya. A. Metsaaver, "Flutter of clamped plates.” Izv. Akad. Nauk SSSR, Mekh. Tverd. Tela, 4, pp. 179 -180 (1969).

6. J. G. Eisley, D. Luessen. Flutter of thin plates under combined shear and normal edge forces. AIAA Journal, 1963, V. 1, No. 3, pp. 620-626.
7. A. A. Izmailov. On the determination of critical velocities for asymmetric supersonic gas flow past plates and shells. Vestnik MGU. Mathematics and Mechanics. 1969. No. 5. pp. 73-76.
8. Babenko K. I. Foundations of numerical analysis. Moscow, Nauka, 1986, 744 p.; 2nd-Ed. (revised): A. D. Bruno (Ed.), Moscow, Izhevsk, RChD, 2002, 847 p.
9. S. D. Algazin, I. A. Kiyko. Numerical and analytical study on the flutter of a plate of arbitrary shape in plan. Prikl. Mat. Mech., V. 60. No. 1, pp. 171-174 (1997).
10. A. A. Movchan. Some problems of oscillations of a plate moving in a gas. Proc. Institute of Mechanics Acad. Sci. SSSR, 1955. No. 1. p. 34.
11. S. D. Algazin, I. A. Kiyko Eigenvalues of the operator in the panel flutter problems. Izv. Ross. Akad. Nauk, Mekh. Tverd. Tela, No. 1, pp. 170 -176 (1999).
12. E. G. Goloskov, V. V. Dmitrienko. On the problem of unsteady panel flutter. In: Dynamics and strength of machines, 1972. Issue. 16. p. 17-23.
13. A. A. Izmailov. Some problems of stability of plates and shells in supersonic gas flow. Elasticity and inelasticity. Moscow, 1971. No. 1. p. 265.
14. Standard Atmosphere. GOST 4401-81. USSR State Standards. Moscow, 1981.
15. V. Z. Vlasov, N. N. Leontiev Beams, plates and beams on elastic foundation. Moscow, Fizmatgiz, 1960, 491 pp.
16. Handbook on elasticity. P.M.Varvak and A.F.Ryabov (Eds.). Kiev, Budivel'nik, 1971.
17. P. M. Ogibalov and M. A. Koltunov Shells and Plates [in Russian], Izd. Mosk. Univ., Moscow (1969). 695 p.

Data on the author: Algazin Sergey Dmitrievich, the leading research assistant of Institute of problems of mechanics of the Russian Academy of Sciences, 119526, Moscow, Vernadsky's 101-1 prospectus, Russia, an e-mail: algazinsd@mail.ru, Ph. +7 (916) 408-05-52. Correspondence the request to conduct to the electronic address.

ISBN 978-5-91741-068-5



Алгазин Сергей Дмитриевич. Численные алгоритмы классической матфизики. XXXIX. Numerical algorithms of classical mathematical physics.

Подписано к печати 21.01.2013. Заказ № 1-2013. Тираж 50 экз.

Отпечатано на ризографе Института проблем механики
РАН 119526, Москва, пр-т Вернадского, 101